Summer 8-3-2010

EXPERIMENTAL INVESTIGATION OF FOLDED PLATE GIRDERS AND SLAB JOINTS USED IN MODULAR CONSTRUCTION

Kyle A. Burner
University of Nebraska, kburner1@gmail.com

EXPERIMENTAL INVESTIGATION OF FOLDED PLATE GIRDERS AND SLAB JOINTS USED IN MODULAR CONSTRUCTION

By

Kyle A. Burner

A THESIS

Presented to the Faculty of

The Graduate College at the University of Nebraska

In Partial Fulfillment of the Requirements

For the Degree of Master of Science

Major: Civil Engineering

Under the Supervision of Professor Atorod Azizinamini

Lincoln, Nebraska

August 2010

EXPERIMENTAL INVESTIGATION OF FOLDED PLATE GIRDERS AND SLAB JOINTS USED IN MODULAR CONSTRUCTION

Kyle A. Burner, M.S.

University of Nebraska, 2010

Advisor: Atorod Azizinamini

The folded plate girder, a newly proposed bridge girder, is investigated through this thesis. The folded plate girder is cold bent out of a single sheet of steel. The cold bending eliminates the costly and inconsistent shop welds found in traditional girders. The folded plate girder is meant for application in short span bridges. The girder was subjected to an equivalent 75 year lifetime loading to investigate the fatigue performance.

The rebar detail used in the closure region between adjacent slabs has been investigated in the past by the NCHRP 12-68 project. This thesis will proposes a hooked rebar detail as a cost effective alternative to the previously recommended headed rebar detail. The proposed hooked rebar detail looks to improve upon the headed bar detail by increasing the clear cover, and reducing the cost of fabrication and shipment of the rebar. Six specimens containing closure regions are subjected to both positive and negative moment loading in order to investigate their behavior and failure modes under ultimate load.

ACKNOWLEDGEMENTS

I would like to thank the University of Nebraska and my advisor, Dr. Azizinamini, for the opportunity to perform this research. Without their help I would not have been able to receive my Masters Degree.

I would like to thank Dr. Aaron Yakel for his continuing support throughout my time at the University. His advice and was an integral part in my success at the University.

For all the long hours in the structures laboratory and the hard work in test construction I thank Peter Hilsabeck.

I wish to thank all the graduate students at NaBRO for your support both academically and otherwise during my time as a masters student. I would specifically like to thank Luke Glaser, through undergraduate and graduate work I was lucky enough to have someone to study with.

Thank you to all of my friends who supported me through the last two years and encouraged me.

Lastly I would like to thank my parents, for their love and support. I have been blessed with parents who love me and have supported me every day of my life. Without you guys I know that I would not be where I am today.

Table of Contents

List of Figures

List of Tables

1 INTRODUCTION

Today there are over 216,000 single span bridges in the United States, 70% of which have a span length less than 60ft. As these bridges approach their intended design life, most can be expected to require complete replacement. Relative to the shear number of ailing bridges as well as the current political and economic climates, increasing importance is being stressed upon costs and the speed of construction. Research performed by the National Bridge Research Organization (NaBRO) and the University of Nebraska, Lincoln (UNL) will significantly aid in the development of new bridge system designs that will provide safe and cost effective alternatives to current practices.

The folded plate girder is a girder detail being developed by the University of Nebraska. This thesis is part of an ongoing research project. The table below outlines each of the

specimens which have been tested to date. The specimen and test included in this thesis are outlined in red.

TABLE 1-1: FOLDED PLATE RESEARCH SPECIMENS

		Height	Width	Top Flange	Bottom Flange	Thick-ness	Side Length	Opening	Trap Height	Trap width	Ridge Height	Angle	Bend Radius	Yield Stress
	Units	in	in	in	in	in	in	in	in	in	in	degree	in	ksi
	Label	A	B	C	D	E	F	G	H	J	K	L	R	
Specimen	A	24.75	45.47	30	10	0.375	20.7	20.72	24.38	46.42	0*	75	2	65
	B	24.75	45.47	30	10	0.375	20.7	20.72	24.38	46.42	0*	75	2	65
	C	24.75	45.47	30	10	0.375	20.7	20.72	24.38	46.42	0*	75	2	65
	D	25.88	43.85	43.85	11.8	0.375	21.87	16.50	24.50	44.50	1.0	75	1.5	50
	E	25.88	43.85	43.85	11.8	0.375	21.87	16.50	24.50	44.50	1.0	75	1.5	50

* No ridge in top flange

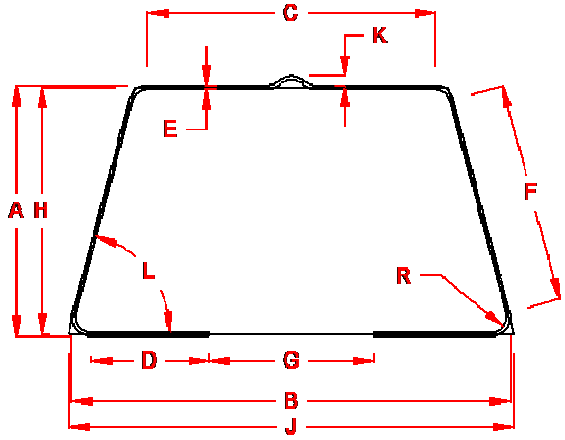

FIGURE 1-1: DIMENSION LABELS FOR TABLE 1-1

TABLE 1-2: TESTING DESCRIPTION FOR ALL FOLDED PLATE SPECIMENS

		Tests				
ID	Specimen	Length*	Type	Stiffener @ load point	Deck	Comments
A1	A	41’	Constructability	No	No	
B1	B	41’	Constructability	Yes	No	
C1	C	41’	Fatigue	No	Yes	
C2	C	41’	Ultimate	No	Yes	
D1	D	46’	Constructability	Yes	No	
E1	E	46’	Ultimate	No	Yes	Galv.
E2	E	22’	Shear	No	Yes	Galv.
E3	E	22’	Shear	No	No	Galv.
E4	E	22’	Shear	Yes	No	Galv.

* Length specifies the span length from centerline of support to centerline of support

The FPG detail, generally intended for short span bridge applications, improves upon typical I-beam and box girder details. Fabricated from a single piece of steel, the FPG is cold bent to the specified shape. Cold bending the girder eliminates the high cost and inconsistencies of shop welds.

The FPG is considered ideal for use in modular bridge construction. Modular bridge construction has provided a very cost effective alternative to traditional bridge construction. Through modular bridge construction the time and cost of forming cast in place decks has been greatly reduced. The girder/slab sections used may be formed and casted in an off-site plant, or an on-site staging area. Once cast, these girder slab sections may be placed side-by-side with a small closure region between. With all components in place the longitudinal closure regions may be filled with cast in place concrete.

The FPG in combination with modular bridge construction alleviates many of the common concerns experienced with construction and routine maintenance of short span bridges. This is done through accomplishing the following:

- Elimination of intermediate braces used to provide horizontal stability
- Elimination of costly and inconsistent shop welds
- Reducing costs and speeding up construction by reducing the quantity of forms required over roadways

1.1 Research Objectives

The objective of this research is to evaluate the fatigue resistance of the composite FPG system, and to analyze multiple rebar details used in the closure region between adjacent slabs as seen in modular bridge construction. The specific research objectives related to the FPG and closure regions are as follows:

- Apply the equivalent of 75 years of cycles to the FPG
- Analyze the strains and deflections of the FPG system throughout cyclic loading
- Analyze the effect of varying rebar details on the strength of slab specimens
- Analyze the failure mechanisms as they relate to each rebar detail
- Determine which rebar detail best simulates the behavior of a traditional bridge deck with straight rebar.

1.2 Thesis Content

This thesis will outline and detail the construction, testing, and monitoring of the composite FPG specimen and closure region tests. Chapter 1 is an introductory chapter which includes the research objectives. Chapter 2 describes the test specimen and testing procedures for folded plate specimen. Chapter 2 also includes the data acquisition systems and sensors used during testing. Chapter 3 describes the material tests performed for the folded plate specimen. Chapter 4 discusses the test results from the cyclic testing of the folded plate girder. Chapter 5 explains the background of the closure region tests. Chapter 6 describes the test specimens along with the testing

procedures. Chapter 7 includes the material testing of the concrete and rebar used in the closure region tests. Chapter 8 discusses the results from testing of the closure region specimens. Finally, chapter 9 contains conclusions from all tests performed.

2 FOLDED PLATE TEST SPECIMEN & PROCEDURES

This chapter describes the tests specimen and procedures for test C1 as found in Table 1-2. C1 is the fatigue testing of the composite FPG.

2.1 DESCRIPTION OF COMPOSITE FOLDED PLATE TEST SPECIMEN

The Composite FPG specimen was delivered to the structures laboratory and constructed using typical construction practices in order to obtain a final specimen which would represent a bridge system found in application.

A prototype bridge is used to determine the specific geometry of the test specimen. Figure 2-1 shows the Prototype Bridge. The shaded regions in Figure 2-1 are the

longitudinal joints between adjacent slabs which are cast once all girders are in place. For fatigue testing the center section was chosen, and constructed in the lab.

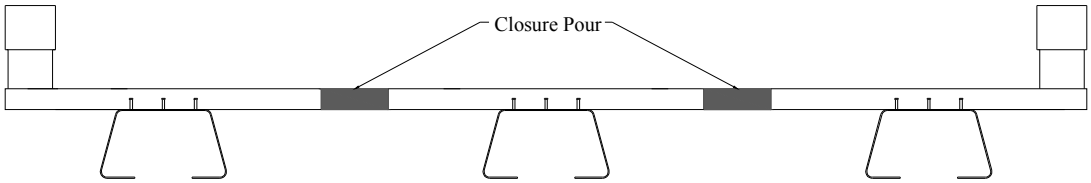

FIGURE 2-1: PROTOTYPE BRIDGE USED FOR COMPOSITE FPG SPECIMEN

The final dimensions of the composite deck are 9.5’ wide, 42’ long, and 7.5” thick. For testing purposes the deck will be cast once the girder is placed on the testing supports. The composite deck poured in the field would be cast in a staging area, and then the girder would be lifted into place on the supports.

2.1.1 GIRDER FABRICATION

The FPG was fabricated in Kansas using equipment and methods used in the fabrication of utility poles. The primary limitation in using this fabrication process is the span length. Span length will be limited to the length of the hydraulic bed used in fabrication. A large hydraulic press is used to form all the bends in the girder out of a single steel plate. By cold bending the girder the time required for fabrication can be reduced from the hours it would take to roll a beam, or weld a plate girder, to just minutes to bend the FPG. The idea behind this process is that the fabricator would have various

thicknesses of steel plate on hand so that a FPG could be fabricated in a moment's notice. Figure 2-2 shows the bending schedule for the folded plate girder.

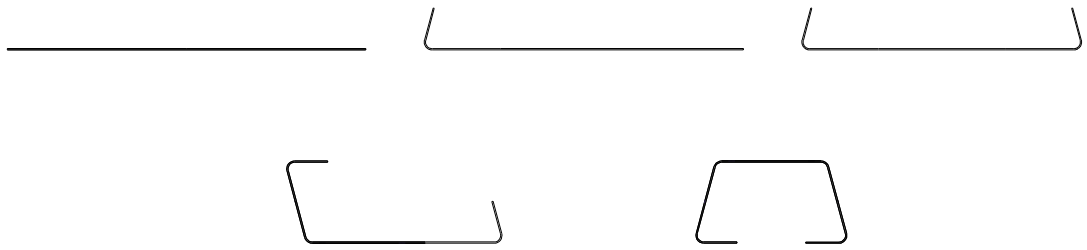

FIGURE 2-2: FABRICATION PROCESS SHOWING BEND SCHEDULE

2.1.2 FPG SPECIFICATIONS

Using the fabrication process discussed in the previous section the FPG is fabricated per the specifications shown in Figure 2-3. The FPG bears a similarity to an inverted box girder with inclined webs. The purpose of the inclined webs in the application of the FPG is to provide increased lateral stiffness. This is one of the major advantages over typical I-beam systems. The increased lateral stiffness of the FPG eliminates the need for cross braces between girders. Tie plates between the bottom flanges were used to limit movement of the bottom flanges. Tie plates were attached using a single bolt line consisting of 2 bolts on each flange.

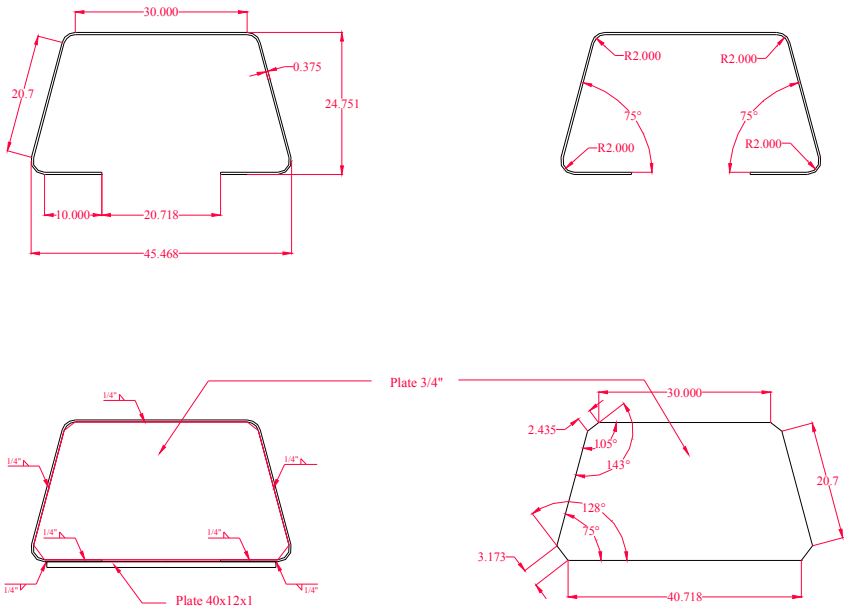

Bearing Stiffener

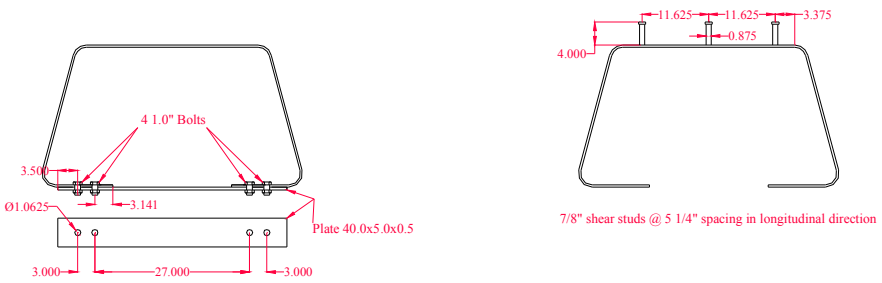

Tie Plates and Bolts

Shear Studs

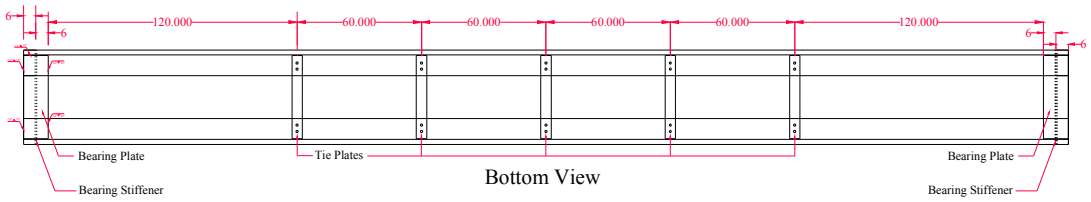

Bottom View

FIGURE 2-3: STEEL GIRDER DETAILS

FIBERLAST bearing pads were used at each of the supports. These bearing pads were placed under steel bearing plates at each support. The bearing pads are made to accommodate the high cyclic loading the system will experience. Figure 2-4 shows the FIBERLAST bearing pad. The setup results in a simply supported beam with a span length of 41'.

FIGURE 2-4: END SPAN SHOWING FIBERLAST BEARING PAD BETWEEN GIRDER AND SUPPORT

2.1.3 Preparation and Construction of Full Depth Composite Deck

The formwork was constructed on the concrete supports using plywood and 2x4 framing materials. The composite concrete deck was 7.5" thick and 9.5' wide, spanning the entire length of the girder. Figure 2-5 shows the cross section of the FPG composite specimen.

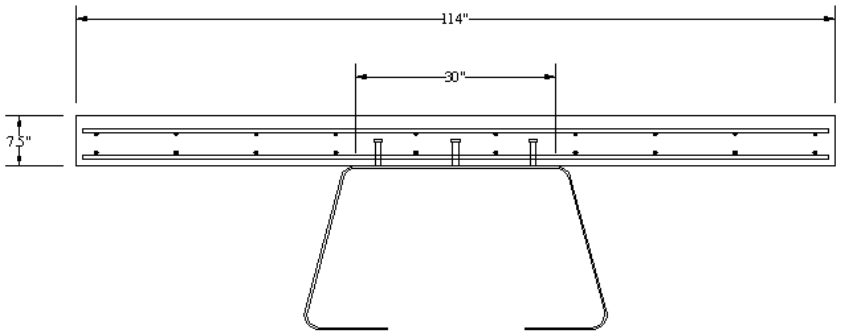

FIGURE 2-5: COMPOSITE SPECIMENT CROSS SECTION

Knee braces were used to transfer the load of the wet concrete to the girder. Knee braces on either side of the girder are connected by a 2x4 which runs beneath the girder. The braces are fastened to the shear studs by a metal clamp.

FIGURE 2-6: KNEE BRACES USED TO SUPPORT WET CONCRETE

The rebar schedule was designed according to the provisions given by AASHTO 9.7.2, empirical deck design. The main discrepancy with the requirements for usage of empirical deck design is lack of lateral bracing. However, the lateral stiffness of the FPG

is such that lateral bracing may be ignored and empirical deck design assumed valid. Figure 2-7 shows a cross section of the rebar used in the composite deck.

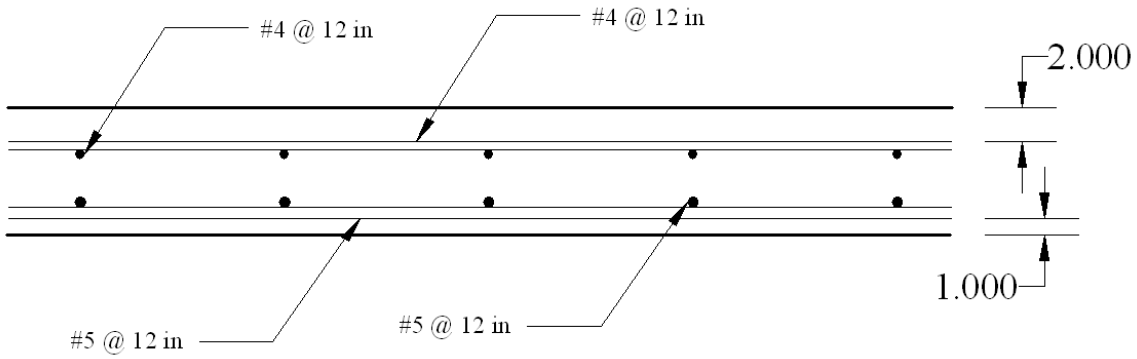

FIGURE 2-7: REBAR SCHEDULE FOR COMPOSITE DECK

FIGURE 2-8: PICTURES SHOWING REBAR CAGE

As is typical in bridge deck construction, 47BD concrete with a maximum aggregate size of ½ in was used. The specified 28-day strength of the concrete was 4,000 psi. The concrete required to cast the concrete deck and 6 test cylinders was 9.5 yd^3. Using a 1.5yd^3 bucket and an overhead crane the concrete was placed in the forms. The surface of the deck was finished by hand.

FIGURE 2-9: CONCRETE POURING PROCESS

2.2 Data Acquisition and Sensors

2.2.1 Data Acquisition Systems

Two data acquisition systems were used for the fatigue loading of the FPG; the MTS system and the MEGADAC system. The hydraulic actuators used in the cyclic testing of the FPG were connected to the MTS computer which controls the displacement and force in the rams. Data is graphed in real time so that adjustments may be made to obtain optimum results.

Strains in the FPG system are monitored through the use of smaller steel strain gages, and larger vibrating wire strain gages which are used on the concrete surface. These gages are wired to the MEGADAC 3407DC data acquisition system, developed by Optim Electronics. The potentiometers which are used to measure deflections in both the FPG system and the slab tests are also wired to the MEGADAC system.

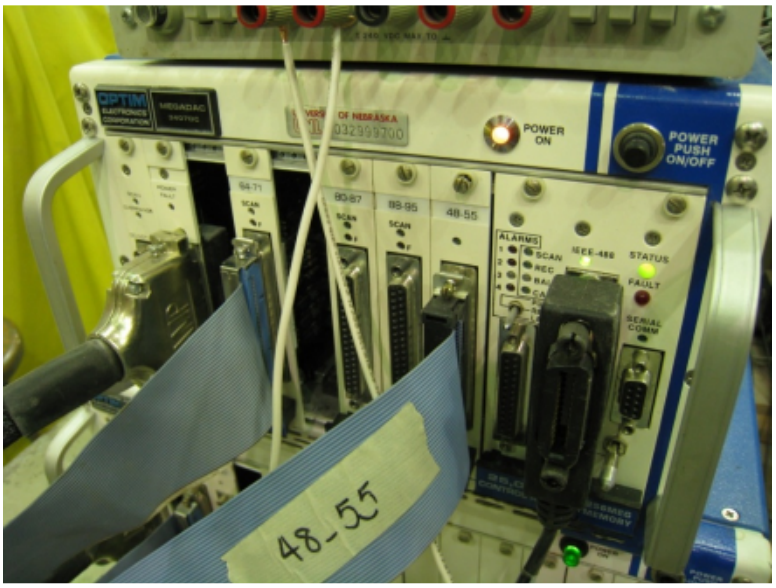

FIGURE 2-10: DETAIMEGADAC DATA ACQUISITION SYSTEM

The MTS and MEGADAC systems both require an external computer to fully analyze the data gathered. The data must be downloaded periodically from each system and transferred to an external computer to avoid filling the small amount of on board memory.

2.2.2 Folded Plate Gages

Three different gage types were used in the testing of the FPG. These gages have previously been mentioned in the data acquisition section and are as follows: steel strain gages, concrete surface gages, and linear potentiometers. The wires from each of the gages are run to the monitoring station, and positioned a safe distance away from the test. At the monitoring station the wires are connected to a module containing 8 inputs. It is these modules which are subsequently connected to the MEGADAC system for data acquisition.

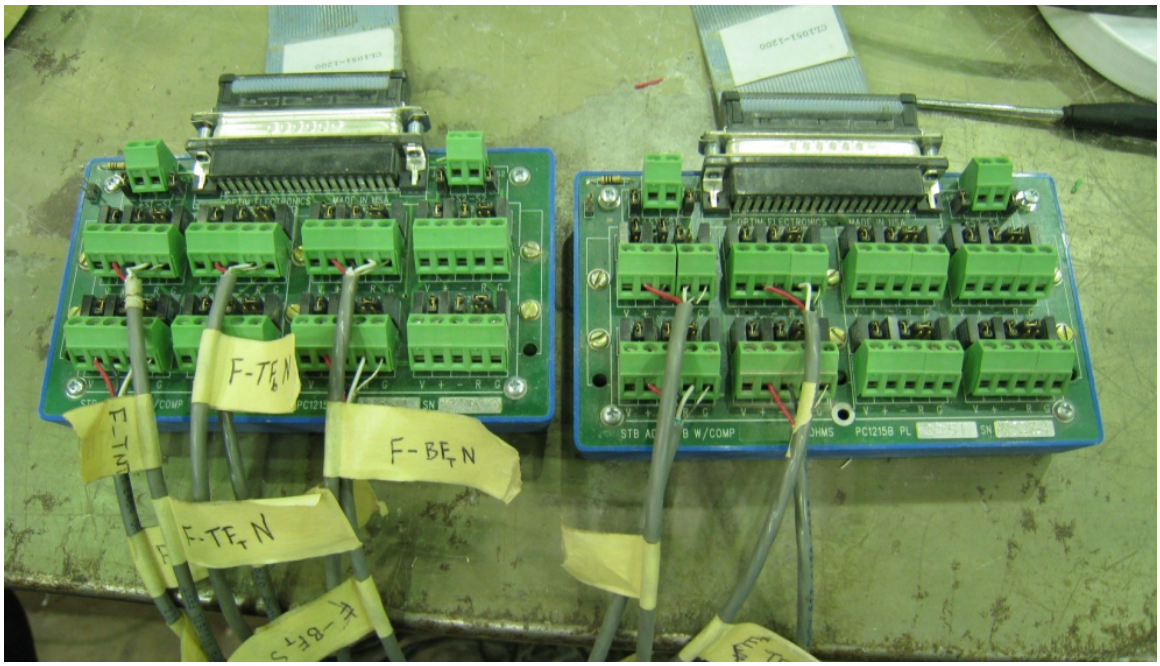

FIGURE 2-11: DATA COLLECTION MODULES

2.2.2.1 STEEL STRAIN GAGES

General purpose linear strain gages were used on the girder surface. Larger numbers of gages were used near the mid-span of the girder in order to more accurately capture the behavior in the region of highest moment. General Purpose rosettes were used to monitor the behavior of the bend at the bottom flange. The rosettes consist of three gages, the center being horizontal and the two outer gages positioned at 45°. The rosettes are used in order to gather extensive data on the cold bends in the steel plate. The bends are of particular concern due to the high stress in this area of the girder plus the residual stress from the cold bending process. Pictures of the gages used are shown in Figure 2-12.

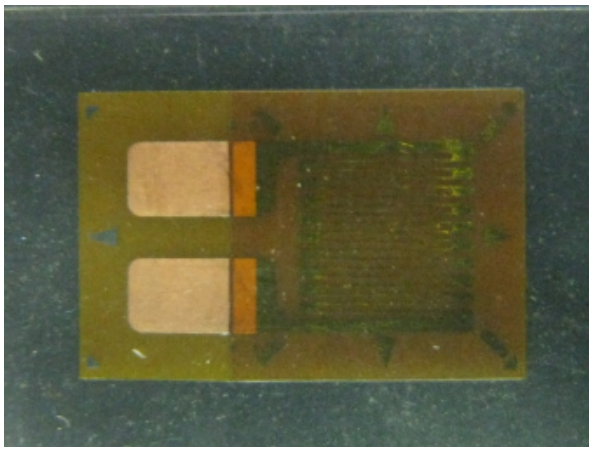

LINEAR STRAIN GAGE

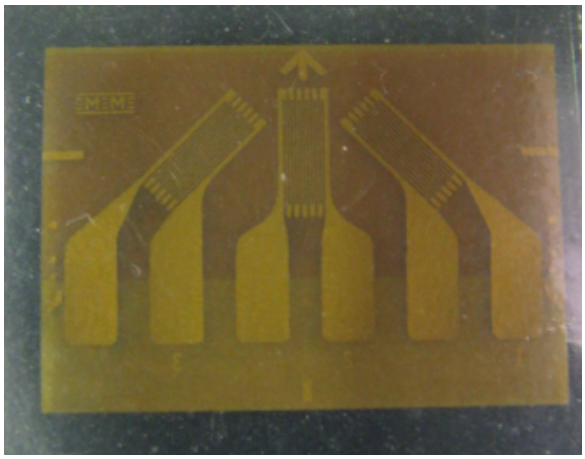

STEEL ROSETTE

FIGURE 2-12: GENERAL PUPROSE STRAIN GAGES

Gages are named based on the girder section and cross section location. The section designations are shown in Figure 2-13. The cross sectional location of each of the gages is shown in Figure 2-14. The cross-sections are labeled with their section designation.

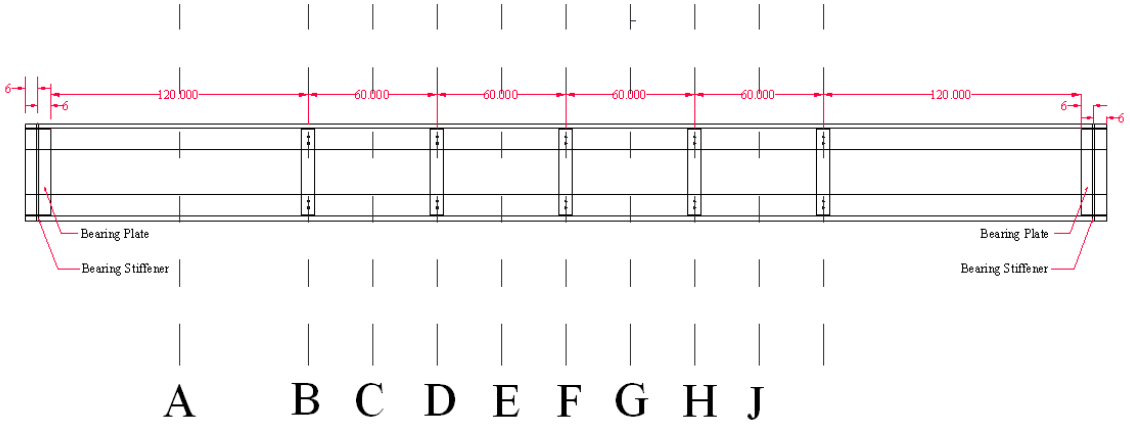

FIGURE 2-13: GIRDER SECTIONS

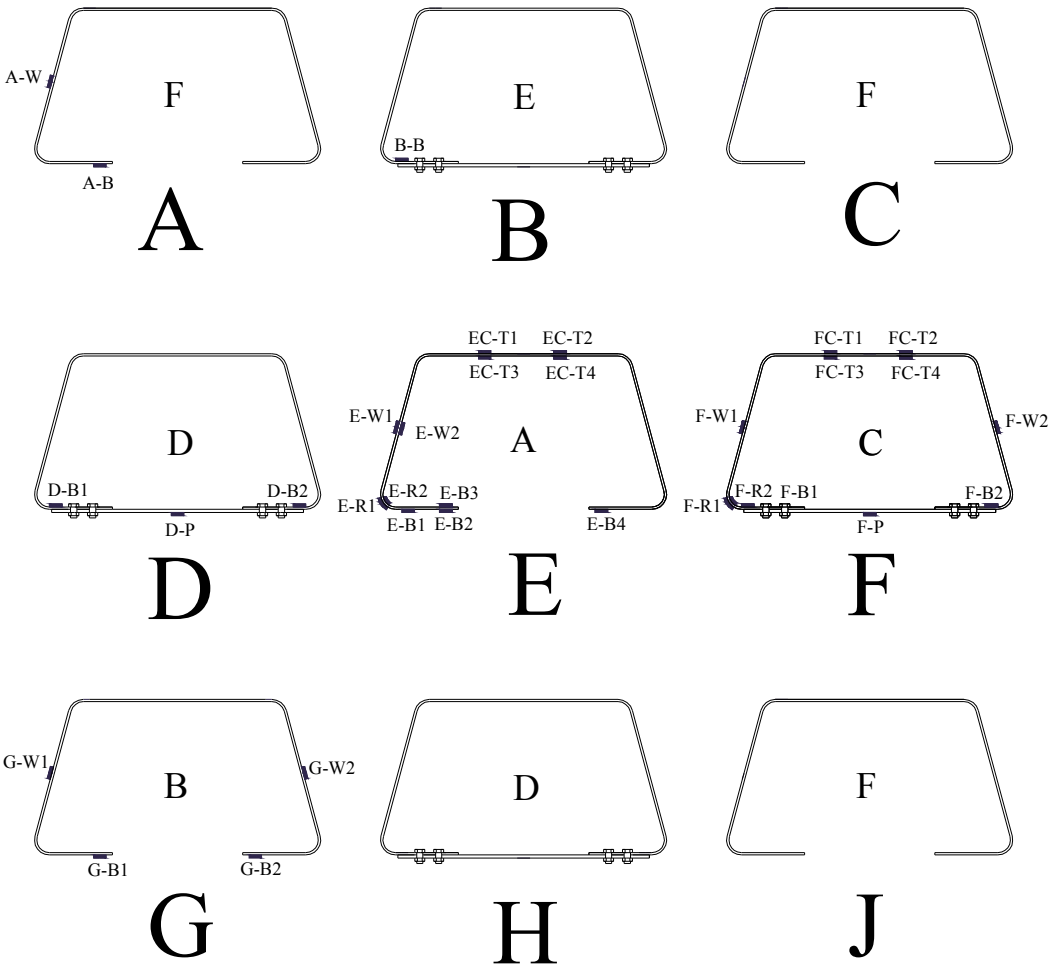

FIGURE 2-14: CROSS-SECTIONAL GAGE LOCATION

2.2.3 Concrete Surface Gages

Concrete surface gages were used on both the top and bottom surfaces of the composite deck to evaluate the strains throughout the composite specimen. Figure 2-15 shows the concrete surface gages used during testing. Seven surface gages were placed at the centerline of the bridge at the locations shown in Figure 2-16.

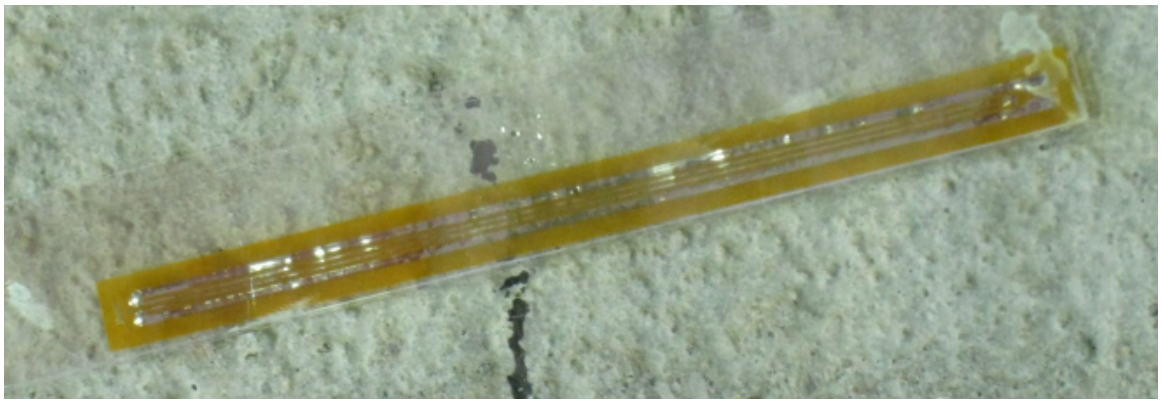

FIGURE 2-15: TYPICAL CONCRETE SURFACE GAGE USED DURING TESTING

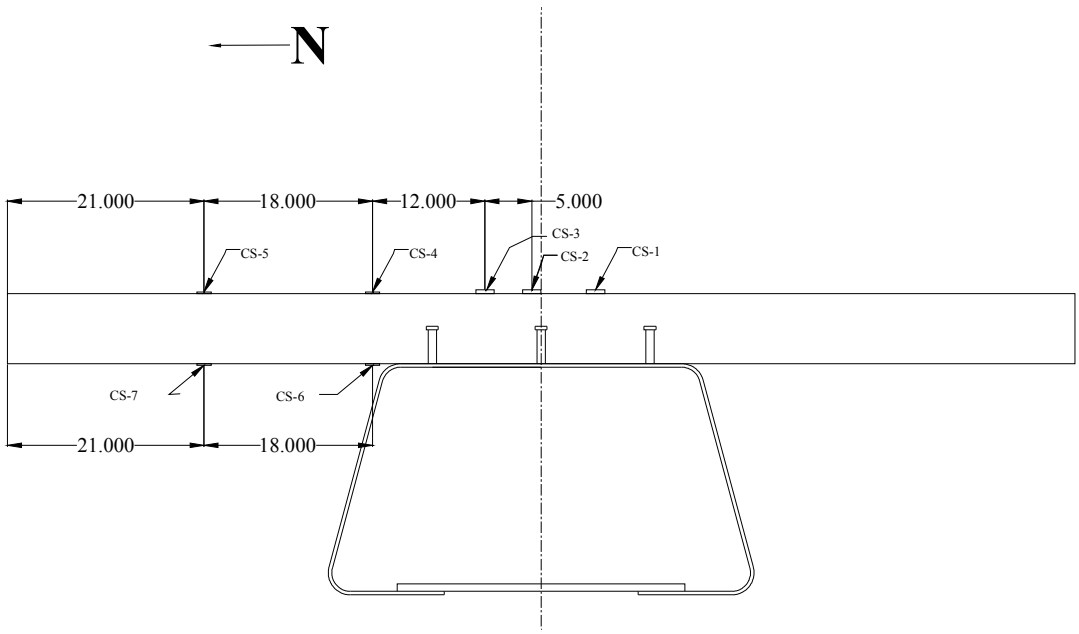

FIGURE 2-16: CONCRETE SURFACE GAGE LOCATIONS

2.2.4 POTENTIOMETER

During cyclic testing the deflection will be measured though a single potentiometer (pot) located at the mid-span of the bridge. More potentiometers were not used due to the damage that they would experience from the high cycle loading. The Potentiometer was attached to a wooden base, which was attached to the floor in order to eliminate any movement. The deflection measured by the potentiometer may be compared to the deflections recorded in the MTS rams.

2.3 TEST SETUP FOR CYCLIC LOADING OF FPG

Two MTS Series 244 rams were used to apply cyclic load, simulating 75 years of truck traffic. The Series 244 rams have a capacity of 220 kips each. The maximum stroke of 10" provides sufficient deflection limits for testing requirements. The test setup is shown in Figure 2-17, different setup components are labeled in the figure and described in Table 2-1.

TABLE 2-1: TEST SETUP DESCRIPTIONS

Part	Description
1.	Composite specimen resting on concrete supports
2.	Metal frames used to stabilize MTS rams during initial setup.
3.	MTS Rams used to apply load
4.	Spreader beams used to post tension the MTS rams to the floor
5.	Concrete filled spreader beam used to transfer load from MTS rams
6.	Steel I-beam spanning between the MTS rams. The spreader beam is post-tensioned to the MTS Rams.

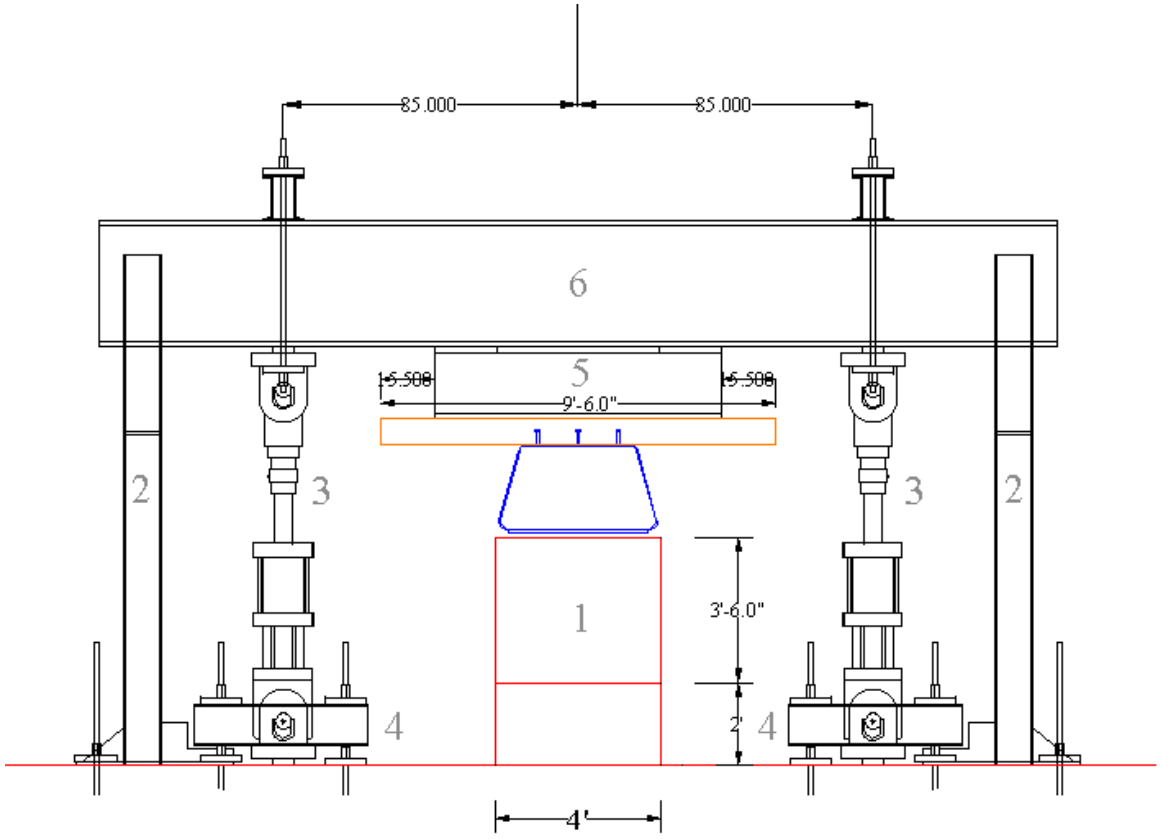

FIGURE 2-17: TEST SETUP USING MTS SERIES 244 RAMS

The Series 244 rams used for testing can be controlled through displacement or through loading. The use of displacement control will cause slight variations in load from cycle to cycle. These slight variations will be taken into account through the use of Miner's Rule when determining fatigue damage.

FIGURE 2-18: COMPOSITE TEST SETUP

2.4 Fatigue Testing Procedures

The use of interlocks as a safety allowed for 20-24 hours of testing each day. Each day began and ended with 5 slow cycles. The slow cycles allow for detailed data to be recorded from each of the gages. The data obtained from the slow cycles will be used for analysis throughout testing.

2.4.1 Determination of lifetime cycles

The calculation of lifetime cycles as outlined by AASHRO LRFD C.3.6.1.4.2 is calculated below. Rather than assuming values for average daily traffic (ADT), the physical limitation of 20,000 vehicles/day was used. Using the physical maximum ensures that

the lifetime cycles will in all probability be overestimated, resulting in a conservative analysis.

ADT x Traffic Factor x n=$ADTT_{SL}$

20,000 x 0.20 x 1.0 = 4,000 Trucks

Where

ADT= Physical limit of vehicles to cross bridge in a day

Traffic Factor= Table C3.6.1.4.2-1 (AASHTO LRFD)Fraction of Trucks in Traffic

n= Factor for number of lanes available to trucks

$ADTT_{SL}$= Average Daily Truck Traffic for a single lane loaded

By combining the $ADTT_{SL}$ with a 75 year design life, and a factor for short span bridges, the lifetime cycles may be calculated.

$$N = Design\ Life \times n \times ADTT_{SL}$$

$$365 \times 75 \times 2 \times 4000 = 219{,}000{,}000\ cycles$$

The limit for the "n" value as determined by AASHTO LRFD Table 6.6.1.2.5-2 is 40ft. Being that the span length is only slightly over 40ft and a conservative value of lifetime cycles is desired, the higher value of 2 is used for "n".

2.4.2 Fatigue Loading

AASHTO LRFD 2009 splits fatigue into two categories, finite and infinite fatigue life. For the testing of finite fatigue life a factor of 0.75 is used. The maximum moment due to the AASHTO fatigue truck shown in Figure 2-19 is calculated using QCON Bridge and verified through hand calculations. Using 3D finite element analysis, the interior

distribution factor for the prototype bridge is 0.683. The non-factored fatigue moment is 413.161 kip-ft, with the 0.75 fatigue factor, and the appropriate distribution factor for the moment becomes 211.66 kip-ft.

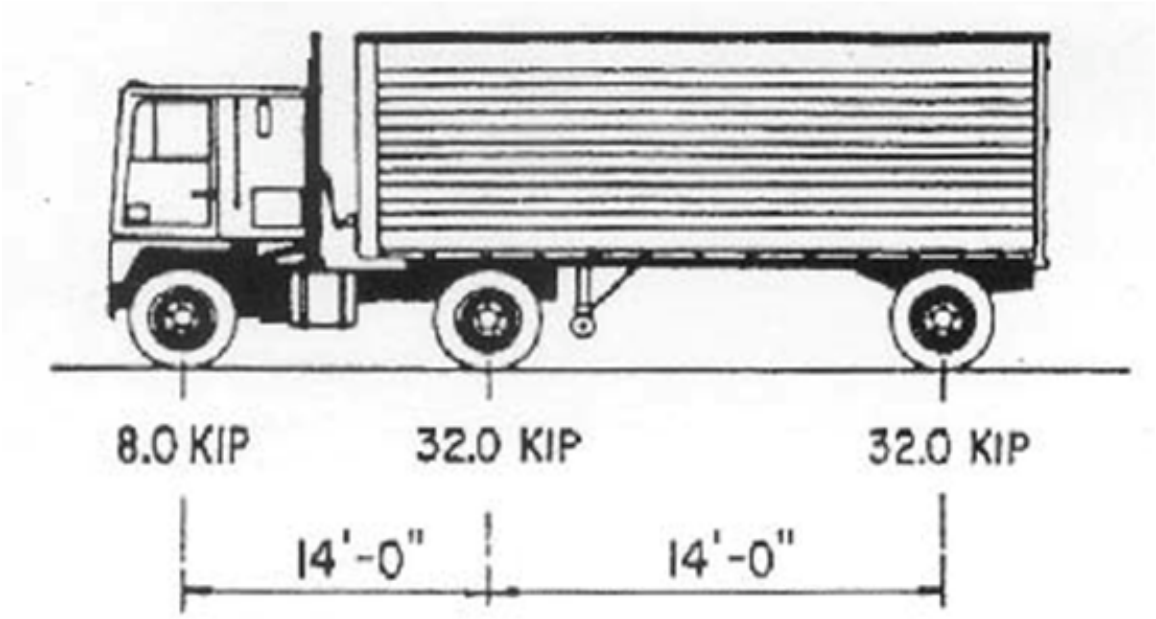

FIGURE 2-19: AASHTO LRFD FATIGUE TRUCK

The cyclic moment applied to the system throughout testing shall be 20-30% of the plastic moment capacity of the system. Figure 2-20 shows the deflection of the MTS rams for typical loading, when the graph becomes more linear as is shown the rams are not reaching the specified deflection and the speed of cycling must be reduced.

The system is controlled through deflection. The desired load is approximated and using the stiffness of the system a deflection may be calculated and entered into the MTS system. By having the system in deflection control it will keep the load within a close range and protect against any excessive deflections due to softening of the system.

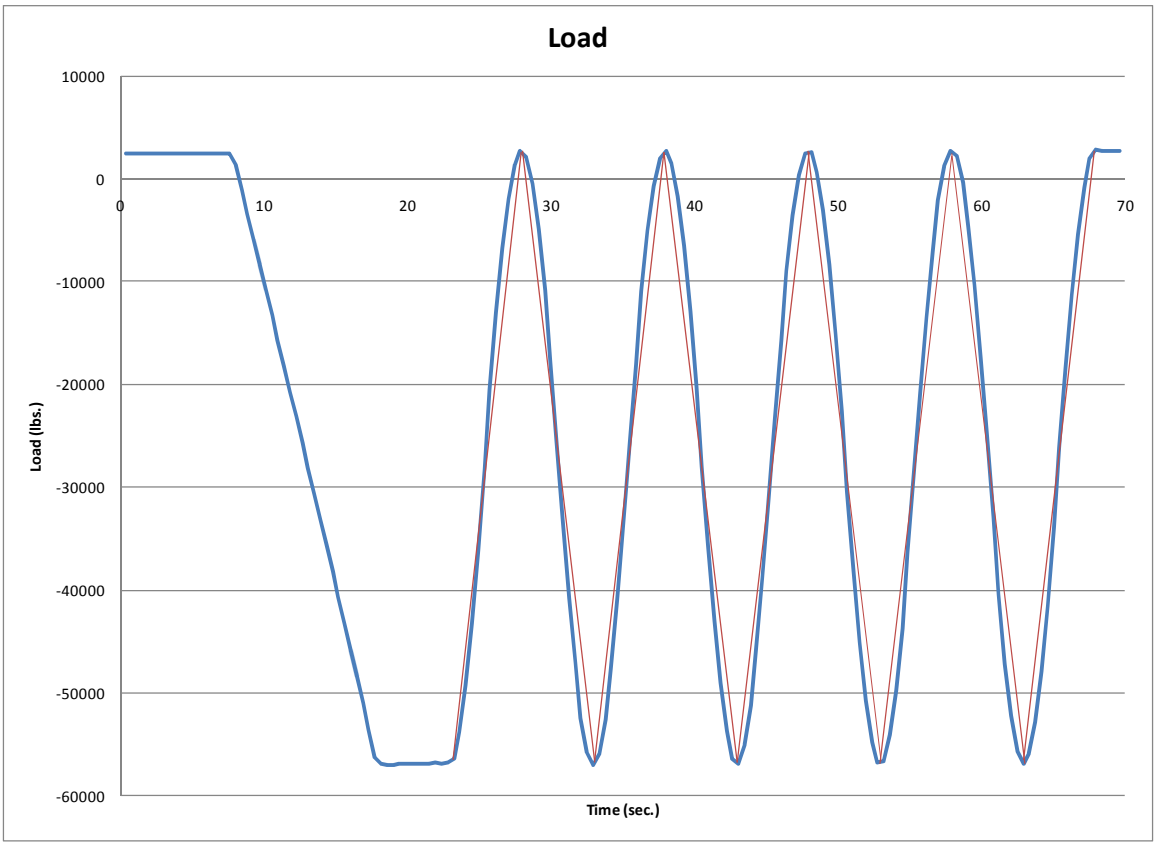

FIGURE 2-20: DEFLECTION FOR TYPICAL CYCLIC LOADING COMPARED TO CYCLIC LOADING AT EXCESSIVE SPEEDS

3 FOLDED PLATE MATERIAL TESTS

3.1 STEEL TENSILE TESTS

The specified steel strength for this FPG specimen was 65 ksi. Material testing was performed once testing was complete to determine the exact strength of steel used in the Sections were cut from either end of the girder and machined for material testing after testing was complete. These samples are taken in both directions along the girder and from both ends to obtain a representative sample of the steel plate. Four samples in each direction were machined for testing. The dimensions are shown in Figure 3-1.

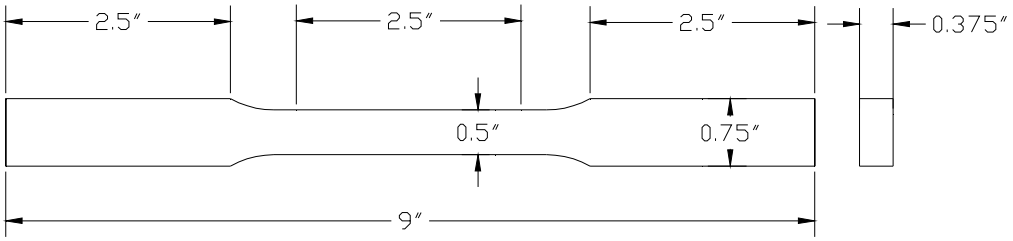

FIGURE 3-1: STEEL MATERIAL SAMPLE FROM FPG

The tensile testing apparatus was connected to the MTS computer for the steel material tests. An extensiometer is used to gathers strain data, while the MTS system gathers the load and deflection data for each of the tests. Using these tests, a stress vs. strain curve may be developed for the material. The cross sectional area for each of the specimens was measured in three different spots along the neck of the specimen, these measurements can be found in Table 3-1 and

Table 3-2. The average area was used in the formation of the stress vs. strain curves. The stress vs. strain diagrams for the transverse and longitudinal samples can be seen in Figure 3-2 and Figure 3-3.

TABLE 3-1: TRANSVERSE SPECIMEN DIMENSIONS AND CROSS SECTIONAL AREA

		1	2	3	4
Top	Width:	0.37”	0.3695”	0.3725”	0.3715”
	Thickness:	0.501”	0.4955”	0.4985”	0.4975”
Middle	Width:	0.3715”	0.3685”	0.3685”	0.3705”
	Thickness:	0.5005”	0.494”	0.4955”	0.4975”
Bot	Width:	0.3685”	0.368”	0.3705”	0.3695”

	Thickness:	0.499”	0.4955”	0.4945”	0.4975”
	Average Area:	0.185062 in ^{2}	0.18249 in ^{2}	0.183832 in ^{2}	0.184324 in ^{2}

TABLE 3-2: LONGITUDINAL TEST SPECIMEN DIMENSIONS AND CROSS SECTIONAL AREA

		1	2	3	4
Top	Width:	0.373”	0.3705”	0.3705”	0.3735”
	Thickness:	0.495”	0.4965”	0.498”	0.5”
Middle	Width:	0.377”	0.3715”	0.373”	0.375”
	Thickness:	0.497”	0.4945”	0.5”	0.4965”
Botto	Width:	0.372”	0.3675”	0.3715”	0.373”
	Thickness:	0.497”	0.497”	0.502”	0.4995”
	Average Area:	0.185629 in ^{2}	0.183436 in ^{2}	0.185834 in ^{2}	0.186417 in ^{2}

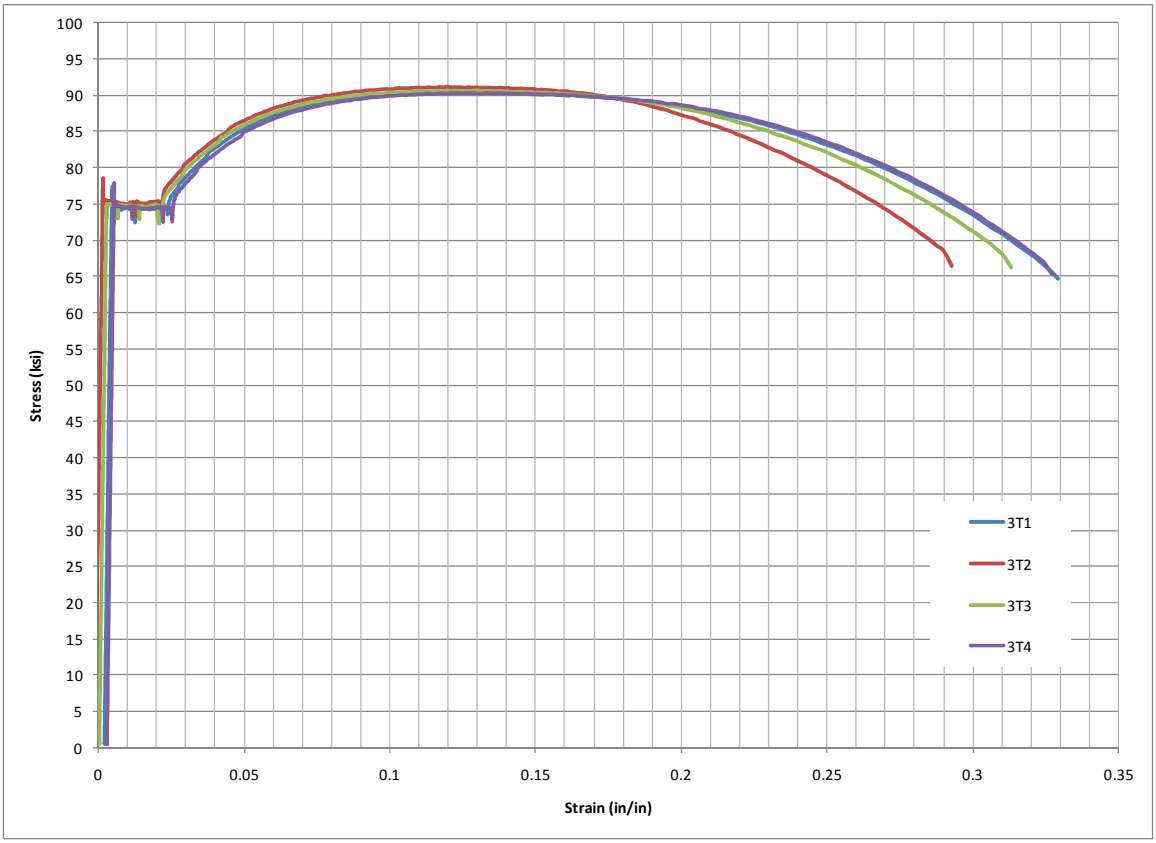

FIGURE 3-2: STRESS VS. STRAIN CURVE FOR TRANSVERSE SAMPLES

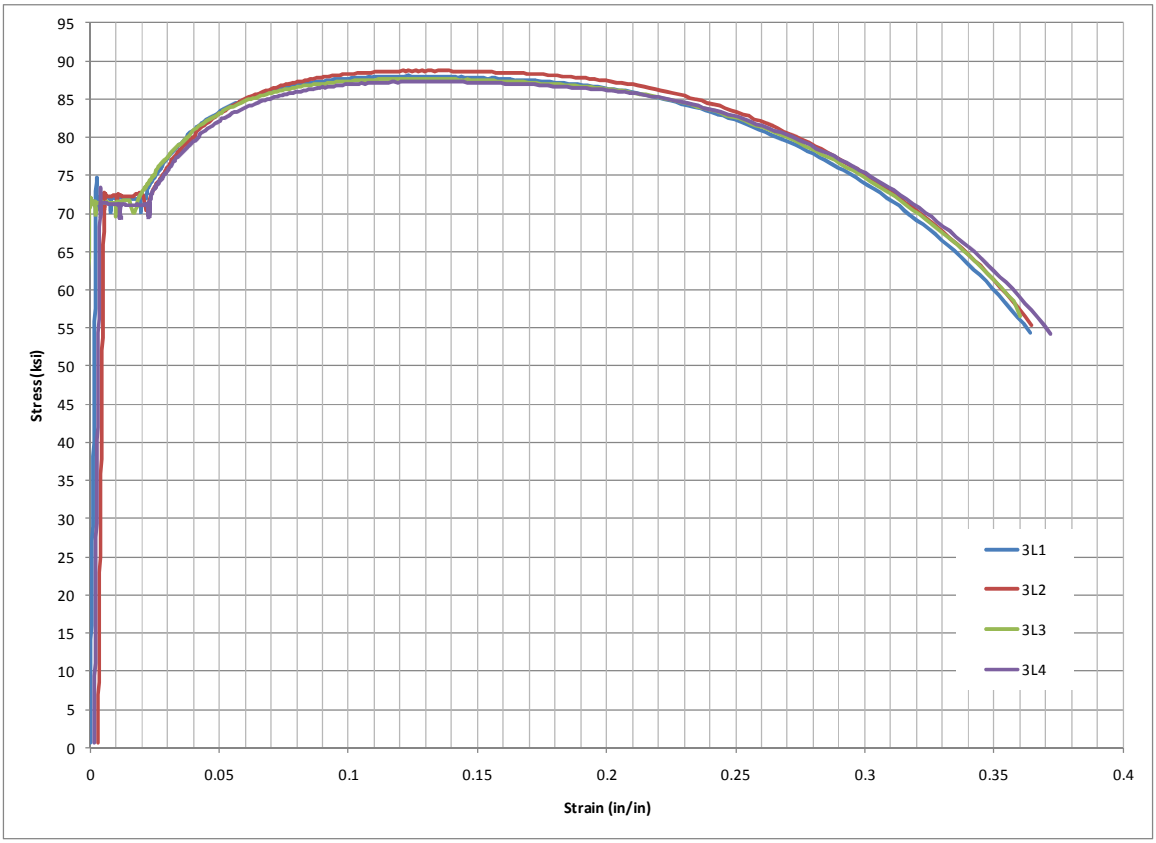

FIGURE 3-3: STRESS VS. STRAIN CURVE FOR LONGITUDINAL SAMPLES

The testing method used was developed by the Structural Stability Research Council (SSRC). By holding the load at three equally spaced times during the yielding region of the sample, the behavior becomes independent of strain rate. The initial strain rate for the tensile tests is .05 in/sec. When the specimen reaches the yield region, it is held as previously described. The dips in the stress vs. strain graph in the yielding region show where the load was held. Using these dips the yield strength of the material may be determined.

The determination of yield strength of the material is based on the assumptions that the stress will be linear with a slope of zero in the yielding region of the graph. At each point where the loading is held the material will begin to recover. When loading is resumed the stress vs. strain will follow the same slope as the recovery for a short while and then diverge and continue yielding. The second assumption which is made is that the point of divergence is the yield strength of the material. By using the three points where the loading was held an average yield stress may be found for the material. Figure 3-4 & Figure 3-5 show the yielding region of both the transverse and longitudinal samples. The straight lines represent the determined yield strength.

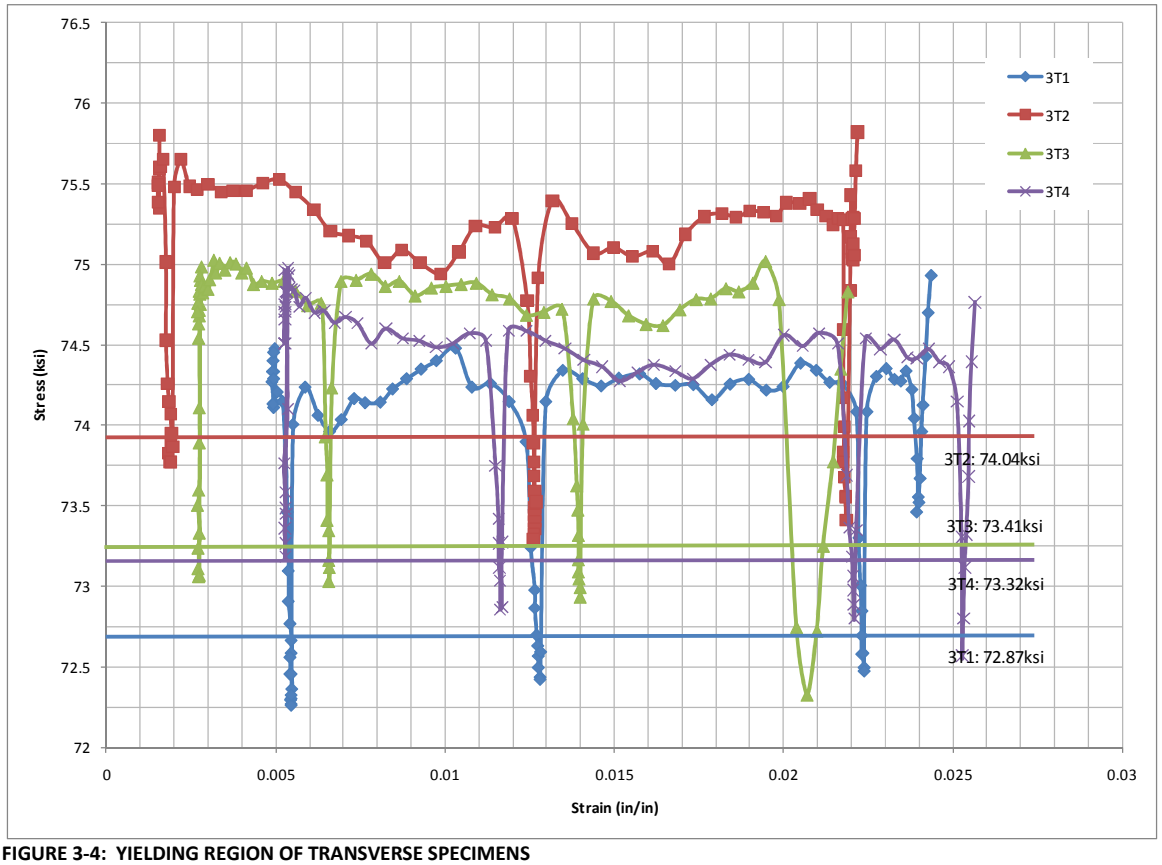

FIGURE 3-4: YIELDING REGION OF TRANSVERSE SPECIMENS

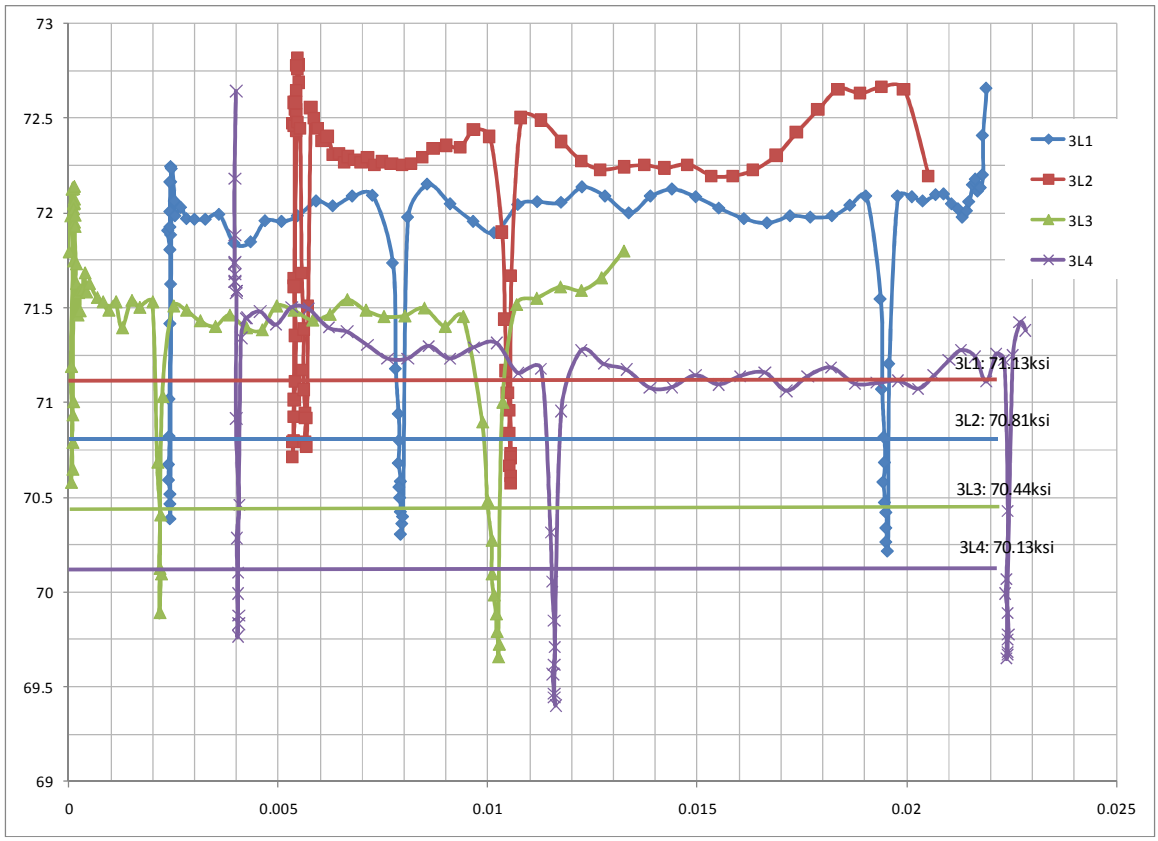

FIGURE 3-5: YIELDING REGION OF LONGITUDINAL SPECIMENS

TABLE 3-3: YIELD STRESS AVERAGES

	1(ksi)	2(ksi)	3(ksi)	4(ksi)	Average(ksi)
Transverse	74.04	73.41	73.32	72.87	73.41
Longitudinal	70.81	71.13	70.44	70.13	70.63

TABLE 3-4: ULTIMATE STRESS

	1(ksi)	2(ksi)	3(ksi)	4(ksi)	Average(ksi)
Transverse	90.41	91.18	90.68	90.26	90.63
Longitudinal	88.06	88.77	87.67	87.33	87.96

After the yielding region, when the material begins to experience strain hardening the strain rate was increased to 0.1 in/sec. The strain rate may once again be increased to 0.2 in/sec if desired. The ultimate stress in the material is as shown in Table 3-4.

3.2 FPG Concrete Tests

During the pouring of the composite concrete deck, ten 6”x12” concrete cylinders were made. Three cylinders were tested at 28 days, and three were tested at the end of cycling, equivalent 234 days. The remaining cylinders were kept in case further testing was needed. The ultimate strengths for both sets of tests cylinders are shown below in Table 3-5.

TABLE 3-5: COMPOSITE DECK CONCRETE COMPRESSIVE STRENGTH

	28-Day Compressive Strength (psi)	**234-Day Compressive Strength (psi)**
1	4462.2	4853.5
2	4703.1	5094.7
3	4446.4	4722.3
Average	4537	4890

4 TEST RESULTS AND DISCUSSION OF FPG SPECIMEN

4.1 CYCLIC LOADING CALCULATIONS & OBSERVATIONS

Damage is considered as the amount of cycles the specimen has experiences as compared to the previously calculated lifetime cycles. The cumulative damage is calculated through the use of Miner's Rule. Miner's Rule states that each stress range corresponds to an equivalent amount of fatigue cycles. The equivalent cycles for each stress range may be summed and compared to the previously calculated lifetime cycles to obtain a percentage of the calculated lifetime cycles.

$$\frac{M_1}{M_2} = \left(\frac{N_2}{N_1}\right)^{1/3}$$

Where:

M_1= Maximum moment due to fatigue truck

M_2= Moment applied to the system

N_1= Number of cycles experienced over the lifetime of the bridge

N_2= Number of cycles to failure at applied load

By using Miner's rule the slight load variations and increases in load are accounted for. The only effect that the increase in the load will have is a larger number of equivalent cycles for each stress range.

TABLE 4-1: SUMMARY OF LOAD STAGES

Load Stage	Cycle Range	Load (kips)	Cycle Rate (Hz)
1	0-302,797	60	1.4
2	302,7989-5,115,287	60	1.2
3	5,115,287-7,179,071	72	1.0

Table 4-1 summarizes the load history for the composite system. Since the system is under deflection control the load values will vary slightly from cycle to cycle. The loads reported in Table 4-1 are an average of the load throughout cycling.

The lifetime cycles determined for a 75 year bridge life was previously calculated as 219,000,000, and will be classified as a Miner's Value of 1.0. Using this scale the damage is classified as a Miner's Value from 0-1.0.

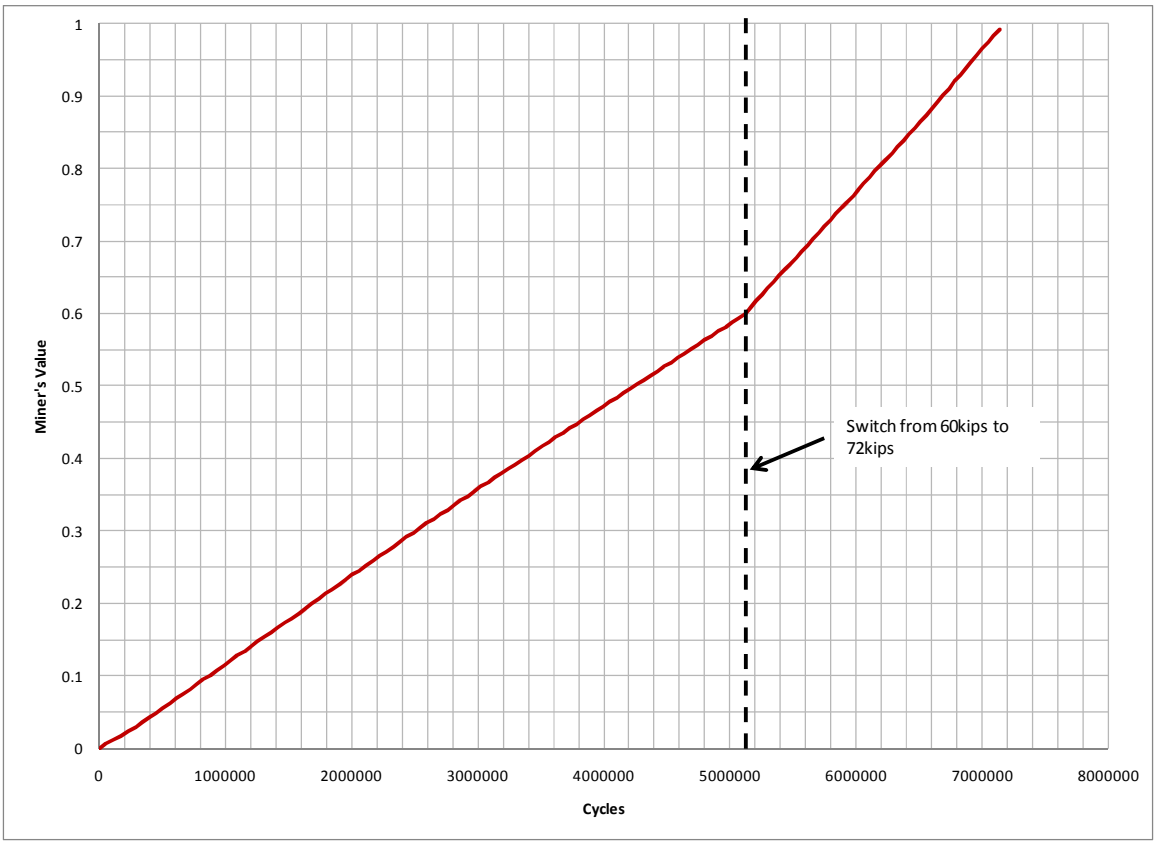

FIGURE 4-1: FATIGUE DAMAGE

Figure 4-1 shows the cumulative damage of the system on a scale from 0-1.0. Very small variations in slope exist due to the small changes in load. The drastic increase in slope at 5.1 million cycles is where the load was increased from an average of 60 kips to 72 kips.

Along with the speed of cycling, the deflection range of the rams must also be adjusted throughout testing. Lowering the deflection range as the test goes on ensures that the spreader beam connecting the two MTS rams never leaves contact with the smaller 6' spreader beam attached to the bridge deck. The spreader connecting the two MTS

rams weighs 5,681lbs. With the addition of the small spreader beams used to attach the larger spreader to the MTS rams, the uplift limit is approximately 6,000lbs.

The load in a single ram was never allowed to reach an uplift greater than 3 kips. Each time the deflection was reset, the system was allowed to begin to recover stiffness. The stiffness of the system can be calculated at any point during testing by dividing the load in the rams by the deflection. Using this method the stiffness is graphed and shown in Figure 4-2.

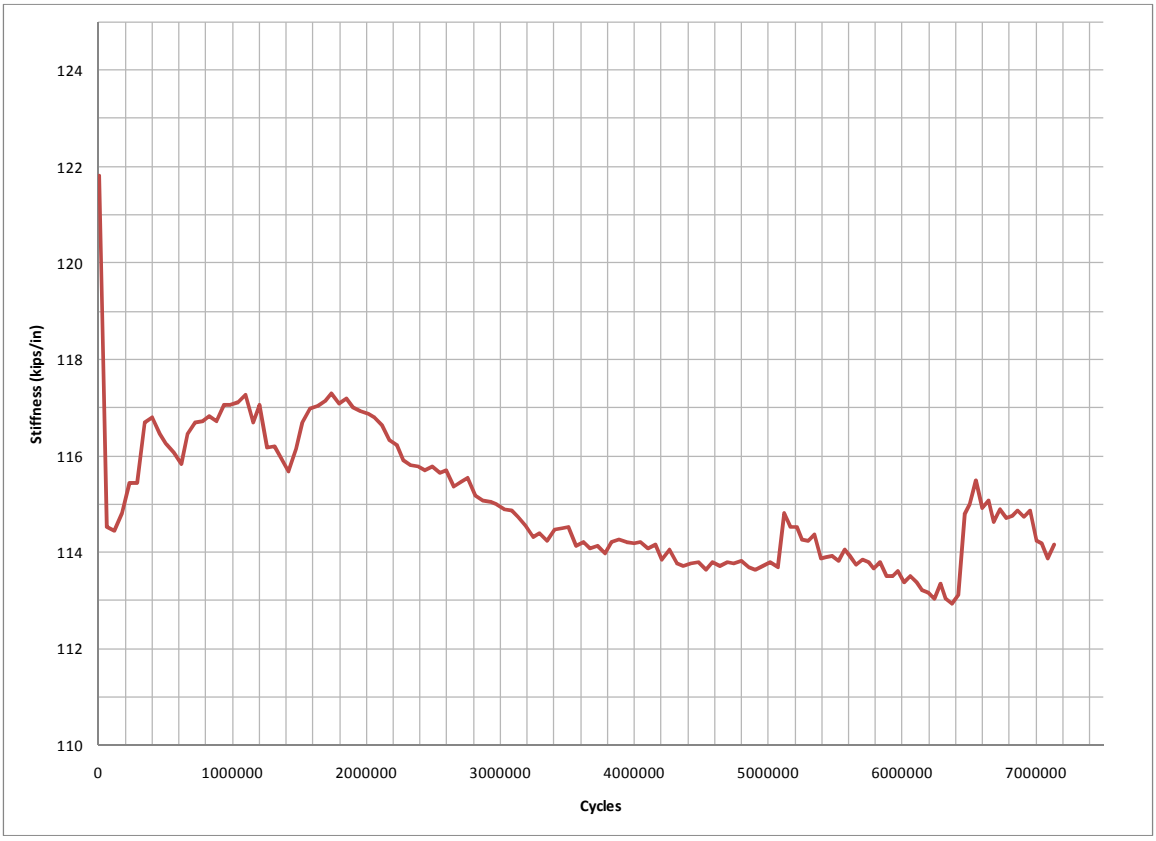

FIGURE 4-2: SYSTEM STIFFNESS

The stiffness graph shows the definite points of stiffness recovery. These points match up with the times that the system was adjusted to bring down the uplift.

TABLE 4-2: STIFFNESS AT 1/4 POINTS OF TEST

	Initial	**1,794,770**	**3,589,540**	**7,179,071 (final)**
Stiffness	116.1571kips/in	117.0952kips/in	114.1837kips/in	114.0183kips/in

When studying the initial stiffness compared to that recorded at the end of the test , a 1.9% difference can be observed.

4.2 Stress and Strain Analysis for FPG

The strain distribution at sections E & F are analyzed in order to verify that the system experienced no fatigue damage. The strain gages are "zeroed" to account for the weight of the concrete deck, spreader beam, and other components used in the test setup which add strain to the system. The strain distributions were formed by plotting the strain at a given point vs. the location of the gage above the bottom flange. The strain distribution at the beginning of testing is shown below in Figure 4-3 & Figure 4-4.

The data points in each figure represent the strain from testing. The lines represent the theoretical strain. The theoretical stress and strain were found using $\sigma=MC/I$. In order to use this method the concrete was converted into steel and section properties were found.

The figures below show that at the beginning of the test the strain distribution is linear, as expected, with the neutral axis lying right at the interface between steel and concrete. Figure 4-5 & Figure 4-6 show the strain distribution at the end of the test. In order to make a comparison between the strain at the beginning of the test and strain at the end, points with similar load were chosen.

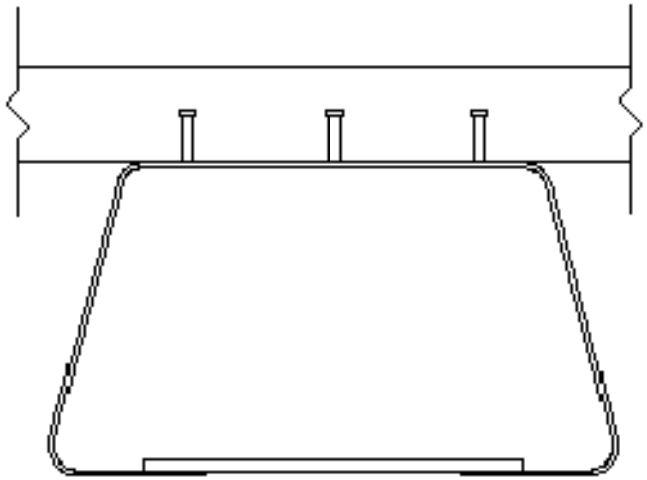

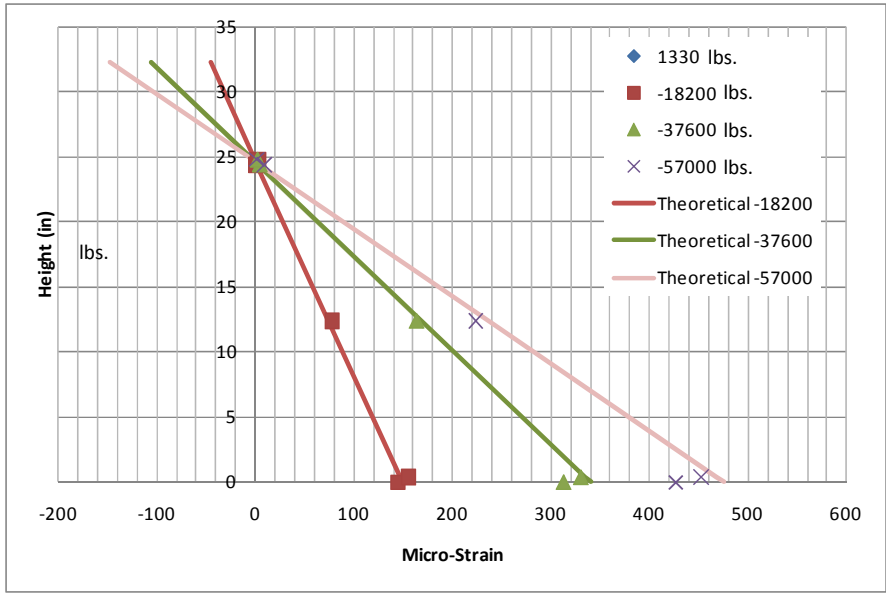

FIGURE 4-3: STRAIN FOR SECTION E AT THE BEGINNING OF THE TEST

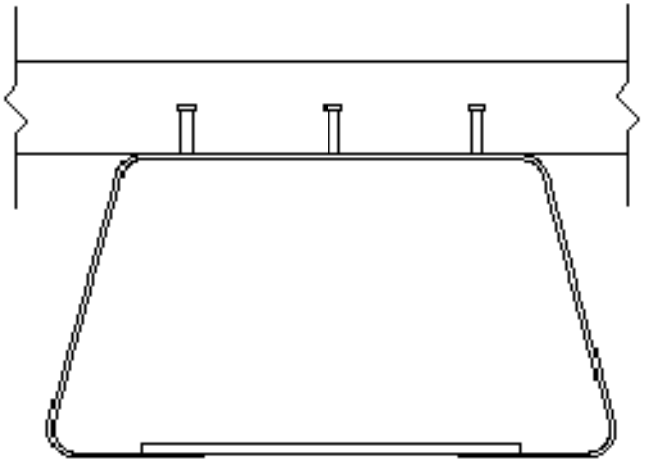

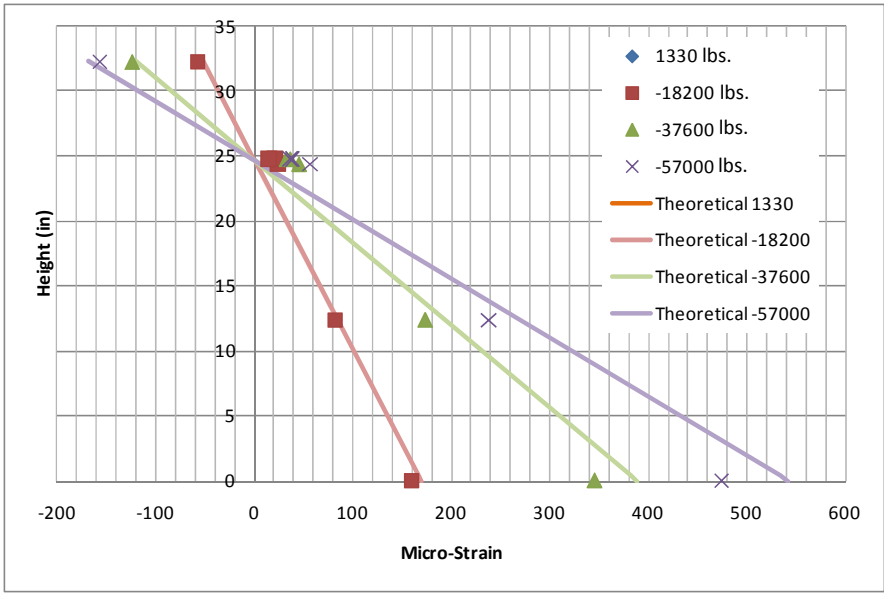

FIGURE 4-4: STRAIN FOR SECTION F AT THE BEGINNING OF THE TEST

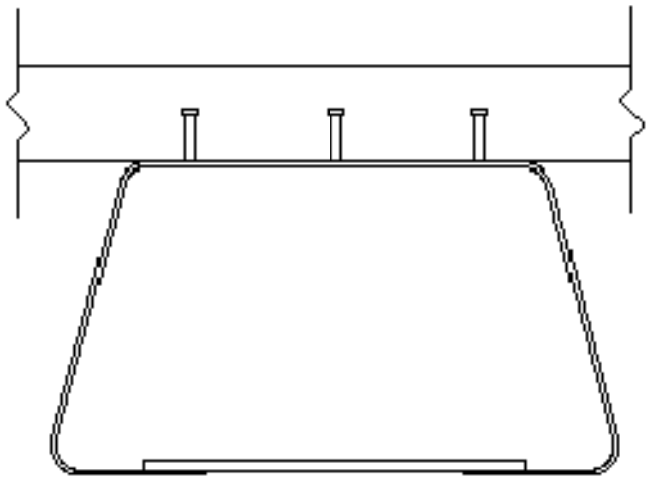

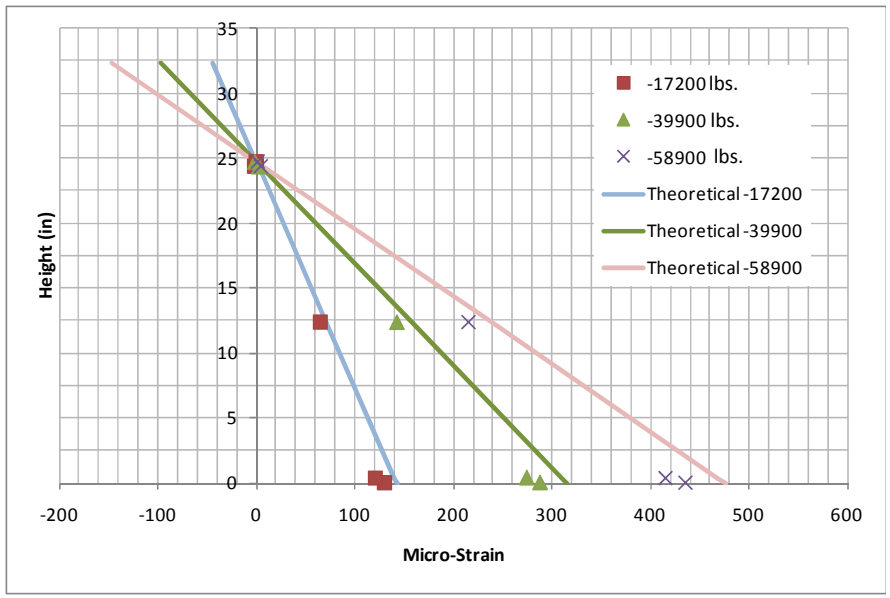

FIGURE 4-5: STRAIN FOR SECTION E AT THE END OF THE TEST

FIGURE 4-6: STRAIN FOR SECTION F AT THE END OF THE TEST

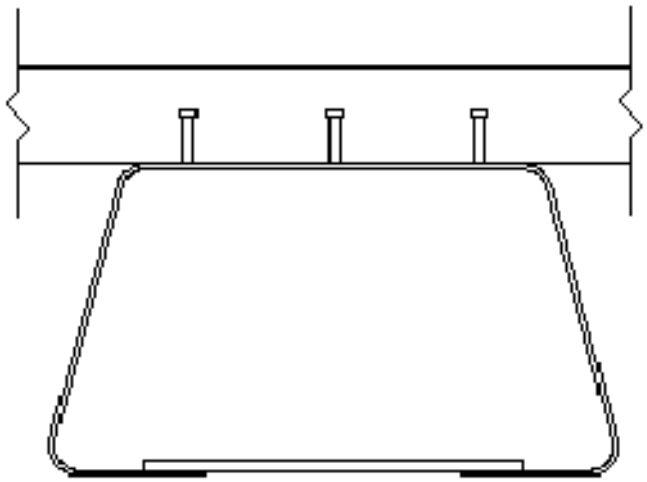

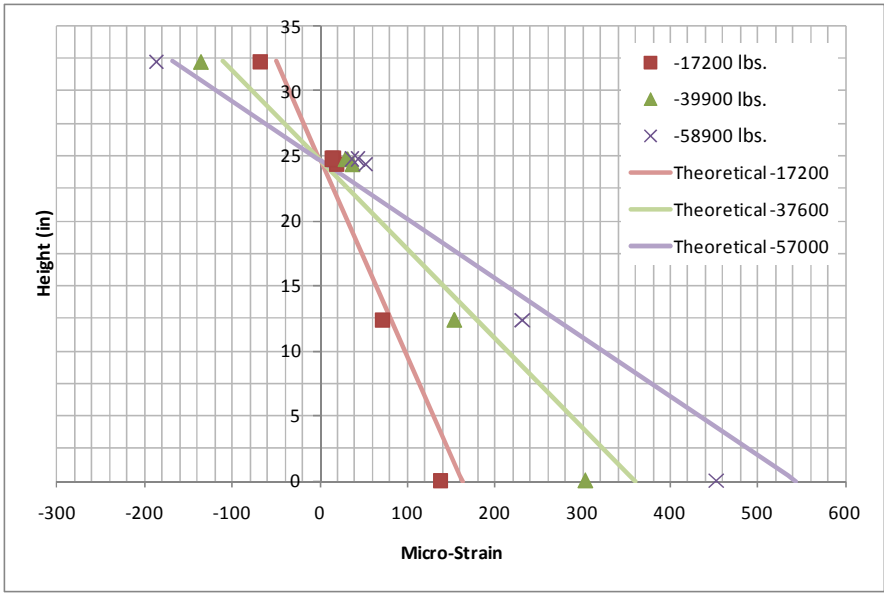

As the above figures show, the actual strain vs. theoretical strain loses accuracy as the load is increased. For the beginning and end of testing, as the load was increased, the theoretical strain consistently over estimated the actual strain. The consistency in strain readings from the beginning and end of the test indicate that no significant fatigue damage occurred during the test.

Rosettes were used at the bend points of the bottom flange in order to obtain detailed strain data in a region of great concern, because of the residual stressed due to cold bending. The graph below shows a slow cycle from the beginning and the end of testing. The graph shows that all the cycles are linear and follow the same path, indicating that, as expected, the strains experienced were linear. The graph also shows that the cycles from the beginning and the end of the test follow the same path, showing that no fatigue damage was experienced in the bends at the bottom flange.

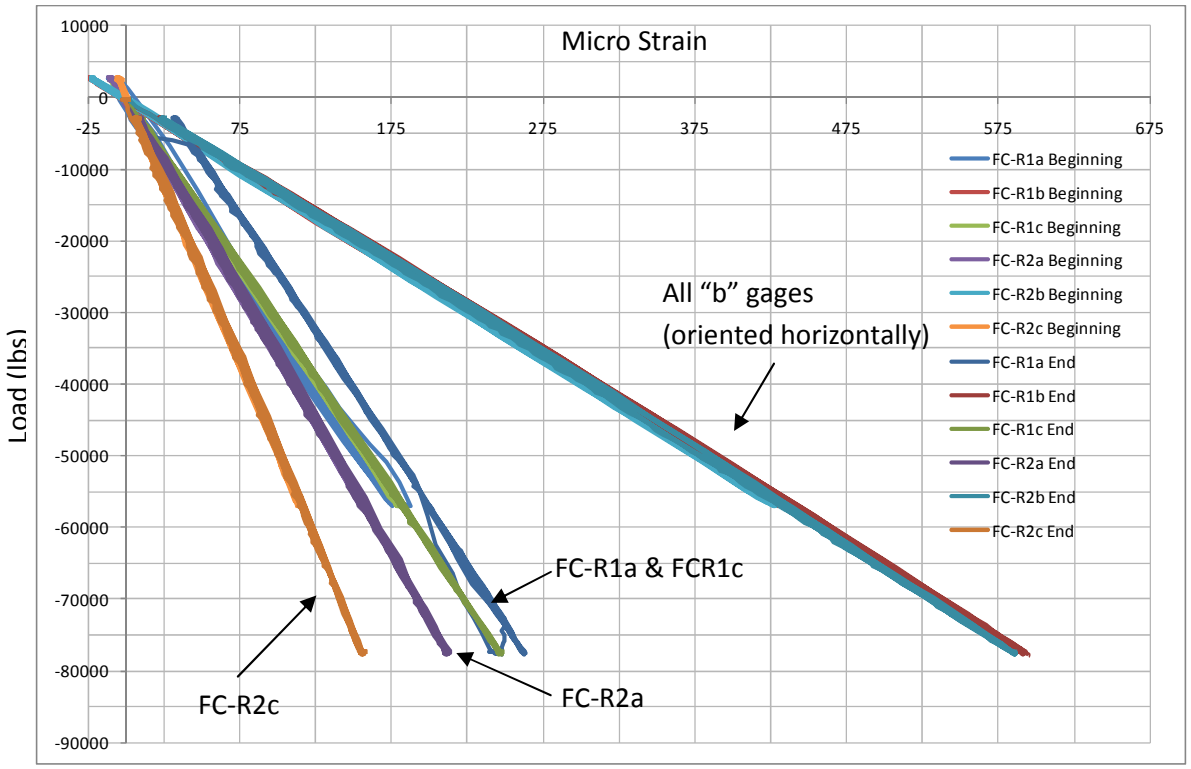

FIGURE 4-7: ROSETTE STRAINS

5 Background and Proposed Options for Rebar Details

With the increased popularity of modular bridge systems research has been funded to investigate areas of concern, and in particular the rebar detail which is to be used in the closure region between adjacent slabs. The University of Tennessee, Knoxville (UTK), as part of the ongoing NCHRP 12-69 project , is performing research on proposed rebar details for use in joints between adjacent slabs. The quality of given details were judged based on constructability and durability. As a part of the research performed by UTK a survey was sent to various bridge professionals. This survey was used to determine concerns with proposed rebar details. The primary concerns obtained from the survey were the overall width of the closure region, and constructability of each of the details.

Comments pertaining to the three different rebar details included in the survey are shown in Table 5-1.

TABLE 5-1: COMMENTS OBTAINED FROM SURVEY SENT OUT BY UTK

Rebar Detail	Comments
Spiral Wire	Complex construction will raise cost due to time consuming installation. Also the small amount of clearance could cause issues with concrete penetration into all voids
U Shaped Bar	Main concern is obtaining proper bend radius, while maintaining the clearance requirements.
Headed Bar	Was considered the most favorable option in the survey due to ease of installation.

The research at UTK, and NaBRO's experience in modular construction both show shortcomings in the rebar details outlined in Table 5-1. Each of these details is extensively examined in the following sections.

5.1.1 HEADED REBAR DETAIL

The headed bars, developed by the University of Texas, are currently used in many modular bridge systems. Although headed rebar was chosen by NCHRP 12-69 as the best alternative based on its constructability, the rebar often has to be bent for proper placement of the pre-top girders as shown in Figure 5-1.

FIGURE 5-1: HEADED REBAR IN LONGITUDINAL JOINT

The shortcomings of this detail are as follows

- They are expensive, and subject to availability from specialized distributors.
- Small misalignments as shown in Figure 5-1 can cause considerable construction delays.
- The increased size of the head at the tips can cause issues with concrete cover, and in some cases cause the clear cover on the bottom of the slab to be less than 1 inch.

5.1.2 U Shaped Bar Detail

The details shown in Figure 5-2, obtained from the study performed by UTK, show the U-Bar detail. This option provides a solution to the clearance problems experienced with the headed rebar. U-bars do, however, create many issues that must be dealt with before they are used. These issues include, but are not limited to the following.

- The top and bottom layer of reinforcement must be the same size; this is typically not the situation for bridge decks and empirical deck design.
- In order to meet bent bar requirements as outlined in 7.1 and 7.2 of the ACI code, the thickness of the deck needs to be greater than 9.5", but is typically less than 8.5".

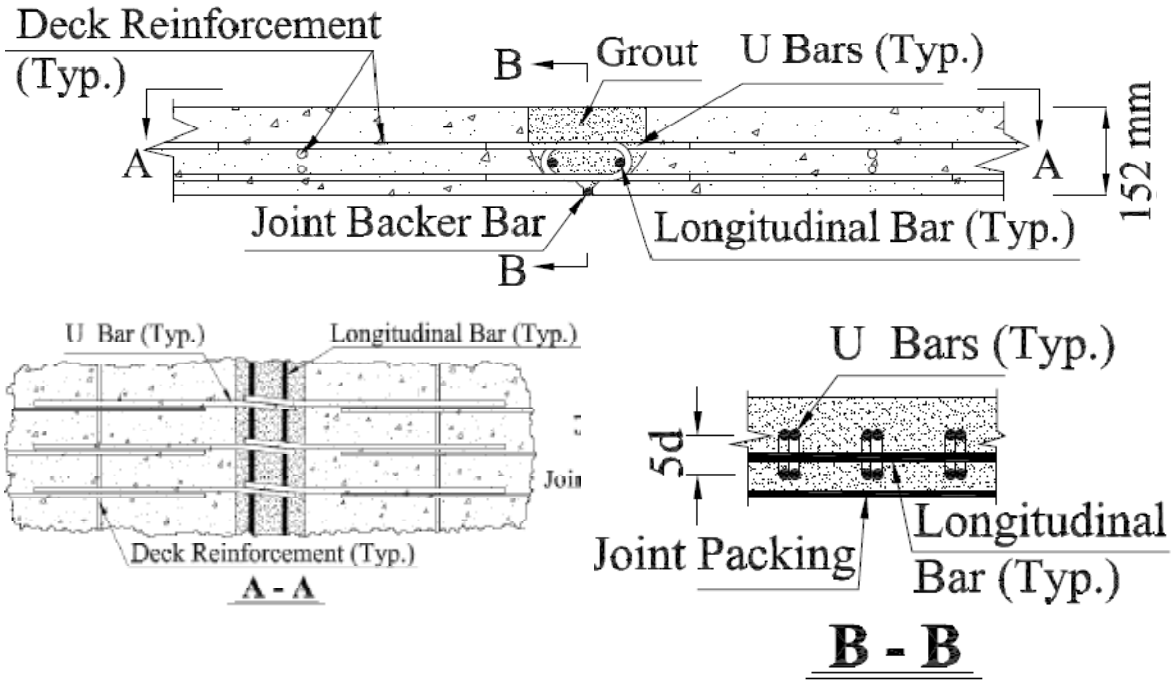

FIGURE 5-2: U-BAR DEATILS AS USED IN CLOSURE REGIONS

5.1.3 Spiral Reinforcement Detail

The spiral reinforcement detail allows for the use of typical straight bars wound in spiral reinforcement throughout the closure region. The major concern with this detail is the amount of work required to install the spiral reinforcement and the congestion created by the spirals. The difficulties related to constructability make this detail the least popular of the three previously outlined.

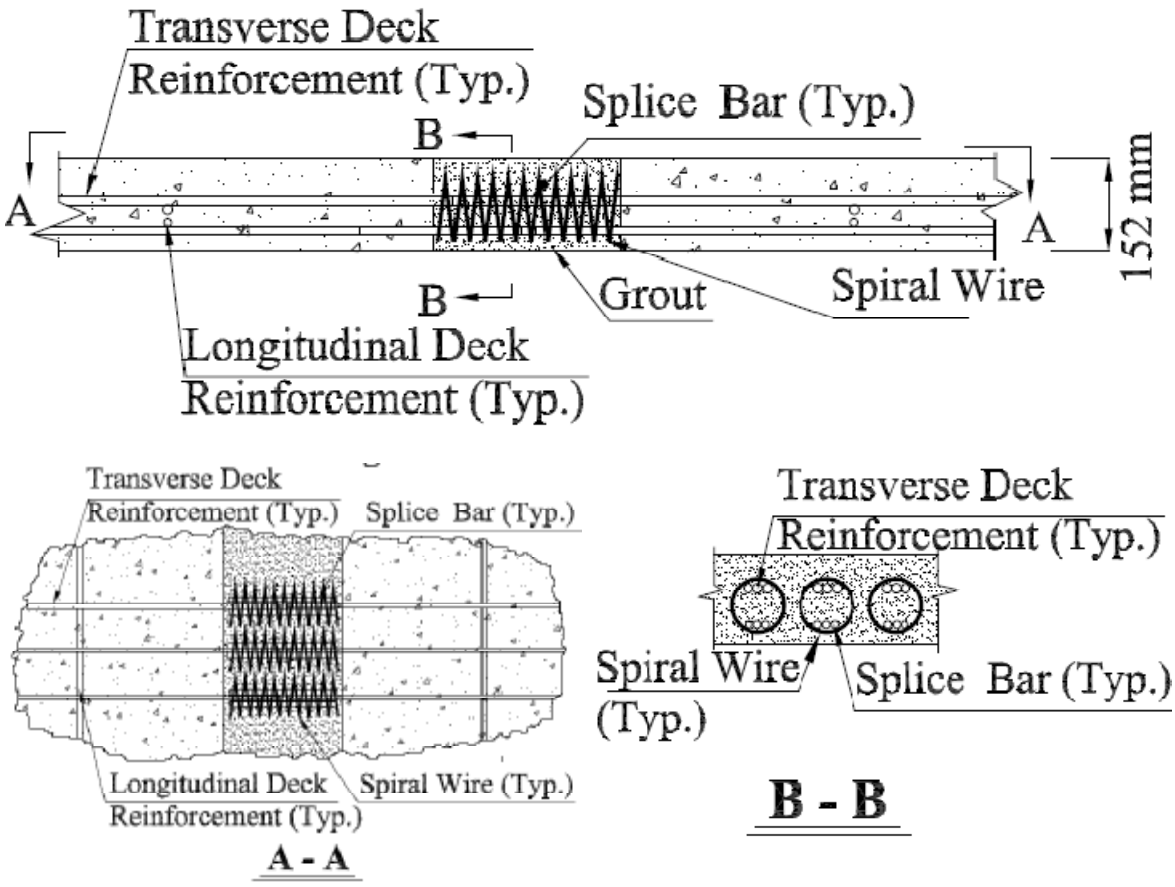

FIGURE 5-3: USING SPIRAL REINFORCEMENT TO DEVELOP TRADITIONAL STRAIGHT BARS IN THE CLOSURE REGION

5.1.4 Hooked Rebar Detail

The shortcomings of the three previously discussed rebar options demonstrate that a new detail is essential. This detail needs to be cost effective and comparatively easy to

install. The hooked bar detail could be such a detail. The hooked rebar can be obtained from any local steel manufacturer and provides the ease of construction seen with the headed bar detail.

6 DESCRIPTION OF SLAB SPECIMENS

The second set of testing consisted of 6 slab specimens, 4 of which contained a closure region between adjacent slabs, used to analyze different rebar details. The two remaining specimens were straight slabs used as control specimens.

Six slab specimens were constructed to investigate the closure region behavior. Figure 6-1 shows the section which is to be tested. The specimens were 8’ wide and 3.5’ long. The six test specimens consisted of three sets, with two straight slabs, which were used as a control group. The two remaining test sets contained headed rebar and hooked rebar. The headed rebar was obtained from HRC, a company that specializes in the fabrication of headed rebar. The hooked bars were obtained from a local steel

fabricator. The hooked bar is the proposed solution to the issues which have been experienced using the headed bars.

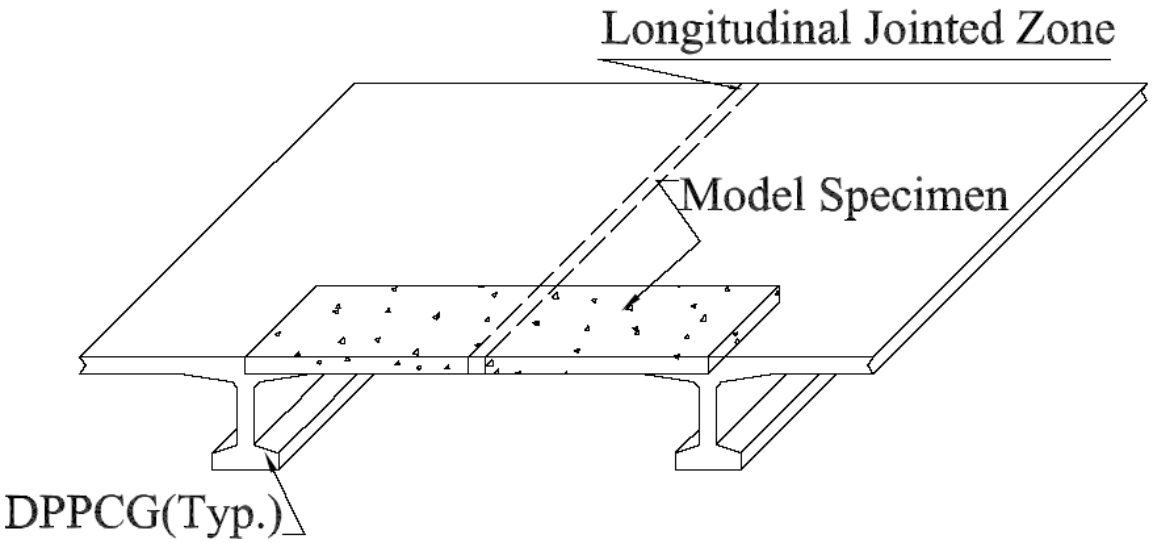

FIGURE 6-1: SLAB SECTION FROM ADJACENT SLABS

The total width of the closure region for the slabs is 12". To avoid constructability issues the rebar is staggered. The slabs were cast in two stages, the first stage being a 6.5" pour on only the outside sections. Cast one month later, the second stage includes the closure regions and a 2" topping.

The following table outlines each of the specimens with important dimensions and aspects of each.

TABLE 6-1: SLAB SPECIMEN SUMMARY

Specimen	Closure Region (Y/N)	Rebar Type	Moment Applied	Concrete Cover at Tension Face	Concrete Cover at Compression Face
S1	N	Straight	Negative	3”	1.5”
S2	N	Straight	Positive	1.5”	3”
HD1	Y	Headed	Negative	3”	1.5”
HD2	Y	Headed	Positive	1.5”	3”
H1	Y	Hooked	Negative	3”	1.5”
H2	Y	Hooked	Positive	1.5”	3”

6.1.1 SLAB DETAIL WITH STRAIGHT BARS

Two slab specimens were built as a control group. These slabs did not have the closure region and used straight rebar as would typically be seen in bridge construction.

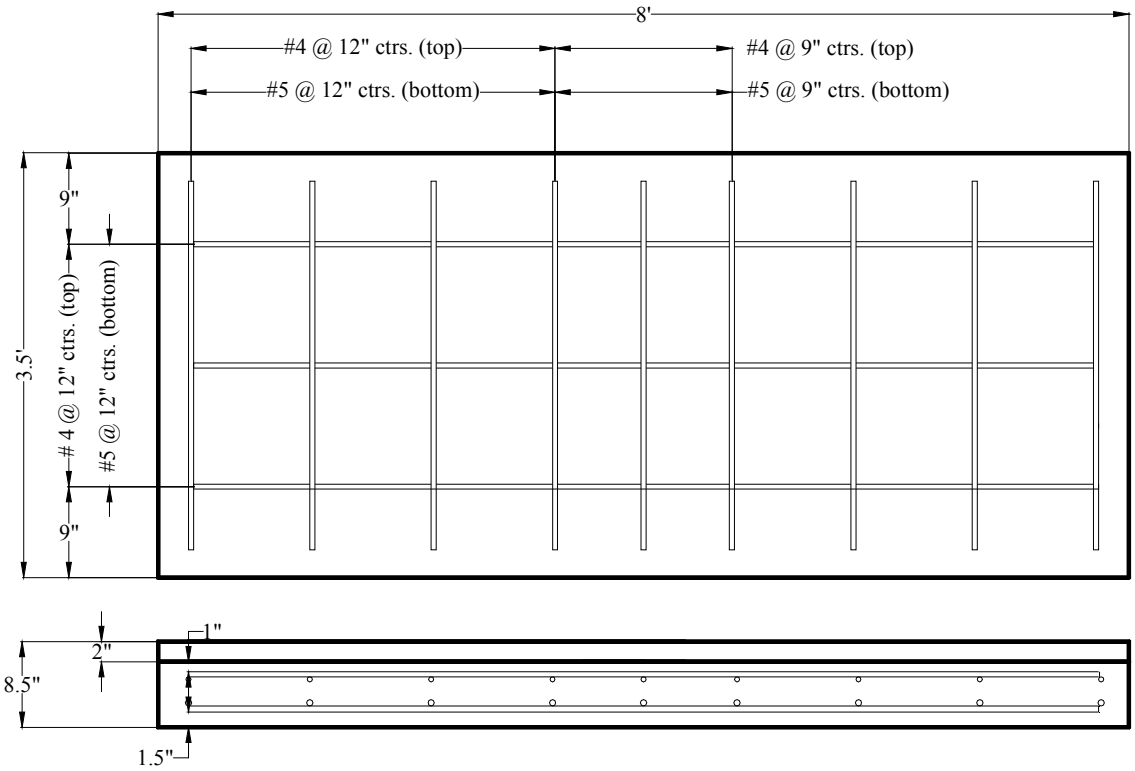

FIGURE 6-2: SLAB DETAIL FOR STRAIGHT BARS

6.1.2 Slab Detail with Headed Bars

Two headed bar test specimens were formed. The heads at the end of the rebar come in multiple shapes and sizes. Test performed at HRC showed that the circular heads provided better connection to the rebar, and had a higher ultimate strength when compared to the rectangular heads. For this reason circular heads were used for testing. . Figure 6-3, obtained from the HRC, shows the fabrication details for the #4 and #5 headed bars. Confinement rebar were used to prevent the vertical punch-out of any of the headed bars confinement rebar were used. Confinement bars were used on either side of the slab.

TYPE 220

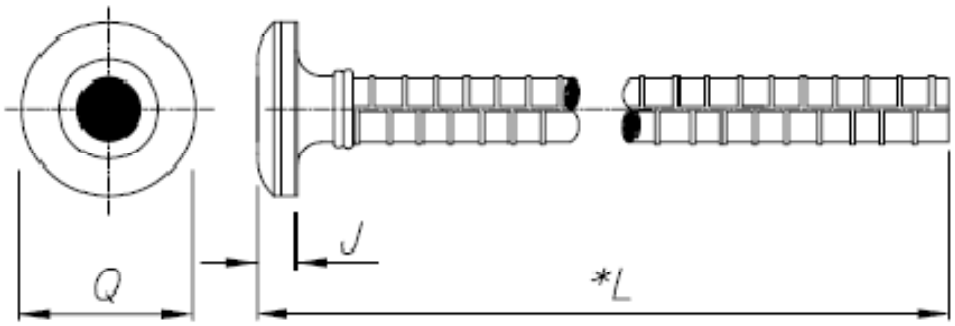

Properties ASTM 706 Standard					Head / Thread Dimensions														
Bar Size	Dia. in	A in^2	Strength lb/in Yield	Tensile	A Inch	B Inch	C Inch	D Inch	E Inch	F Inch	G Inch	H Inch	I Inch	J Inch	K Inch	M (mm)	N Inch	P Inch	Q Inch
#4	0.500	0.20	–	–	2.00	1.00	0.50	---	---	---	---	---	---	0.41	---	---	---	----	1.750
#5	0.625	0.31	18600	24800	2.50	1.25	0.50	2.00	0.500	---	---	---	1.98	0.50	3.75	M18	0.750	2.000	2.000
#6	0.750	0.44	26400	35200	3.00	1.50	0.75	2.25	0.625	3.00	1.52	.612	2.37	0.56	3.75	M24	1.000	2.375	2.375
#7	0.875	0.60	36000	48000	4.00	1.50	0.75	2.50	0.625	3.50	1.73	.625	2.77	0.63	3.75	M24	1.000	2.750	2.750
#8	1.000	0.79	47400	63200	4.00	2.00	.875	3.00	0.750	4.00	1.97	.687	3.20	0.63	3.00	M27	1.125	3.250	3.250

FIGURE 6-3: HEADED BAR FABRICATION SPECIFICATIONS

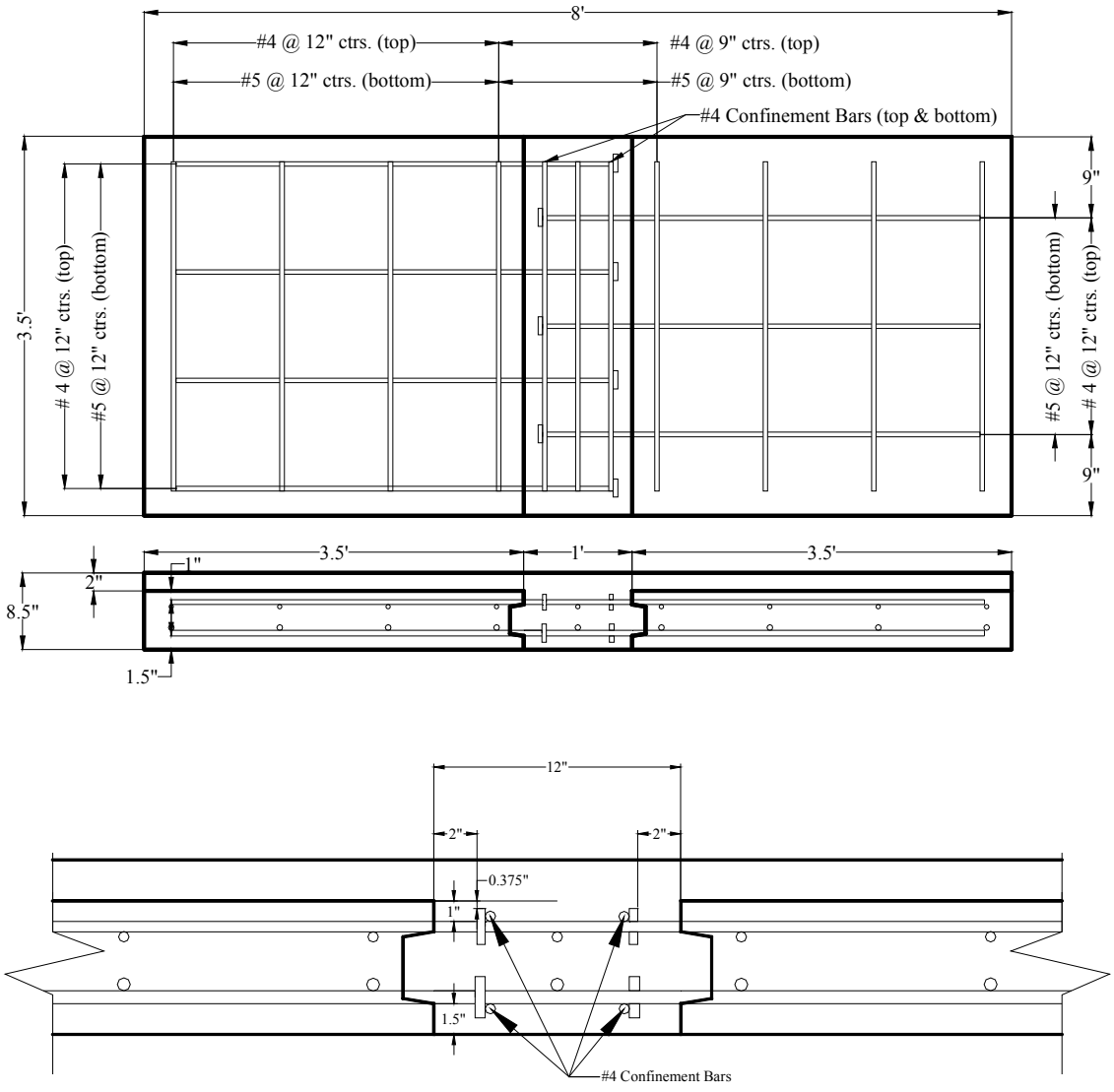

FIGURE 6-4: HEADED BAR CONSTRUCTION DETAILS

FIGURE 6-5: HEADED BAR LAB PICTURES

6.1.3 Slab Detail with Hooked Bars

As with the other rebar details, two specimens were formed using hooked bars. The hooked bars may be obtained from any local steel fabricator, greatly reducing the time and cost of fabrication and shipment to the work site. The hooked bar also provides greater clearance on both faces by eliminating the headed end treatment. As with the headed rebar, confinement bars were used with the hooked detail.

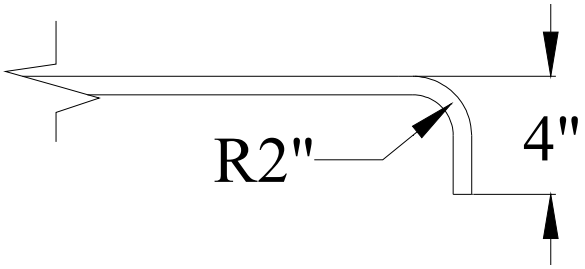

FIGURE 6-6: HOOKED BAR SPECIFICATIONS

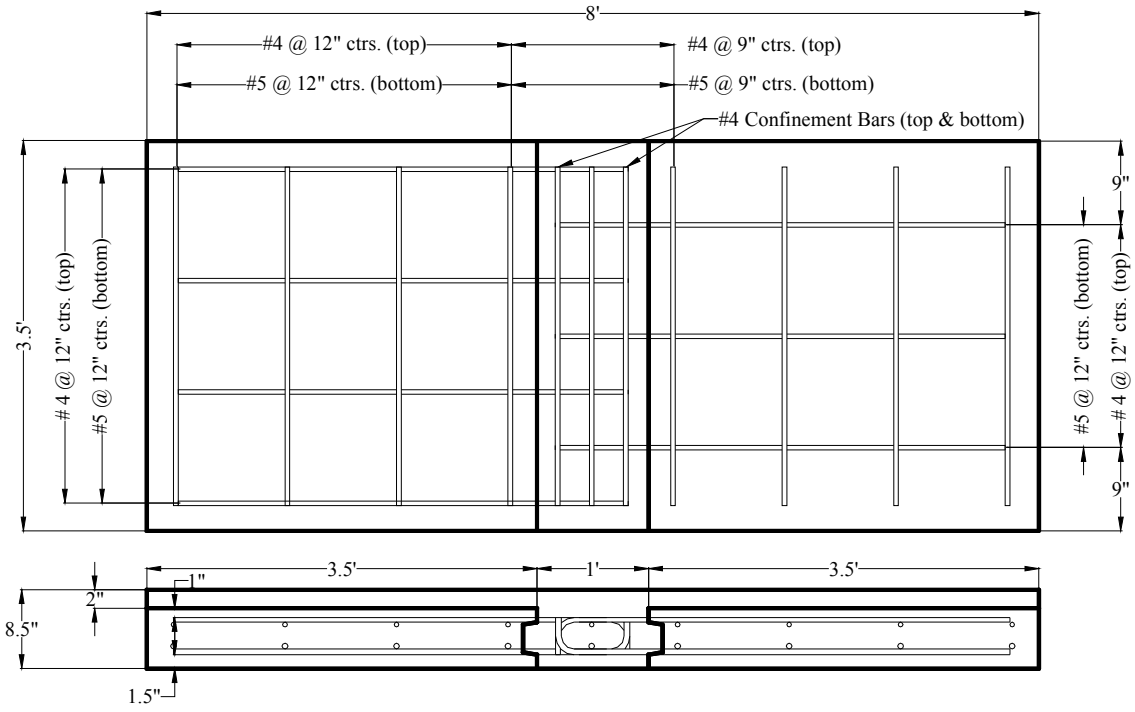

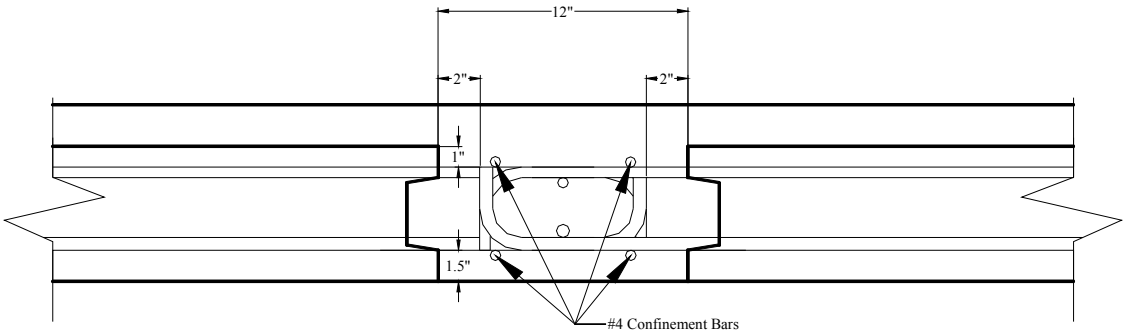

FIGURE 6-7: HOOKED BAR CONSTRUCTION DETAILS

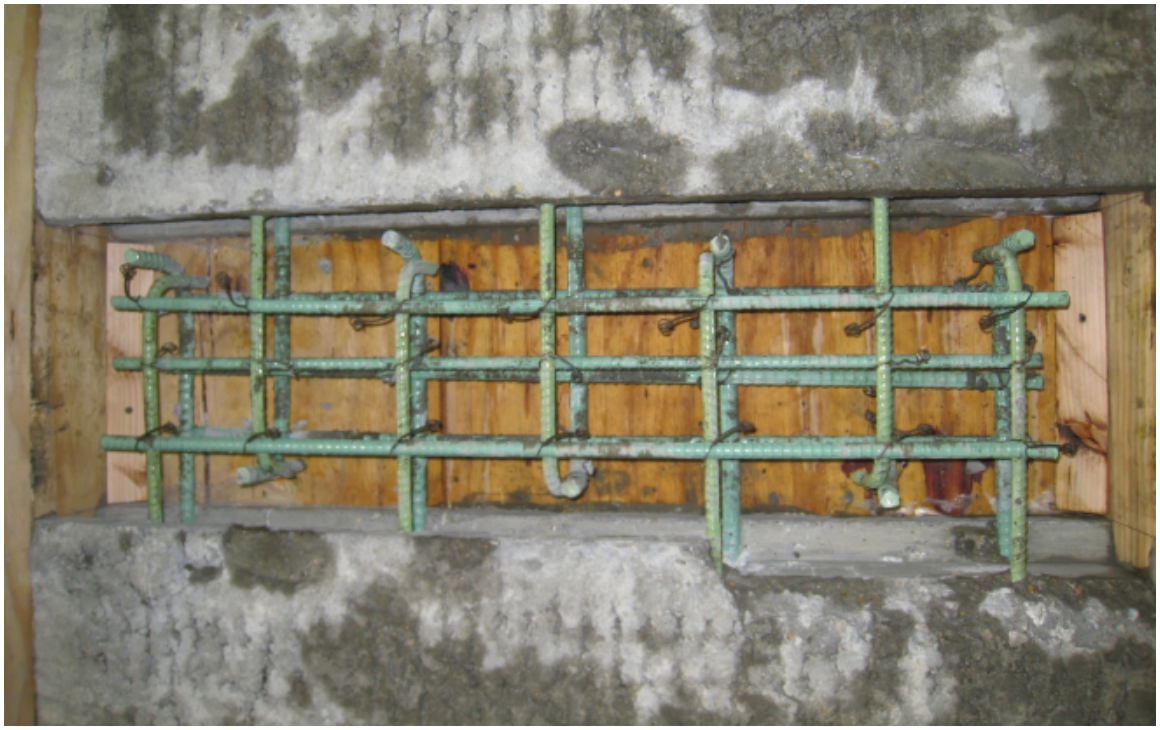

FIGURE 6-8: HOOKED BAR LAB PICTURES

6.1.4 Final Preparation of Slab Specimens

Each test specimen was painted white. The contrast between the white paint and the natural color of the concrete make it easier to recognize crack initiation and propagation. The location of the closure region and all longitudinal rebar was drawn on

each slab to better identify and understand where cracking occurs relative to rebar placement. Finally a grid is drawn on each slab as a reference for crack location.

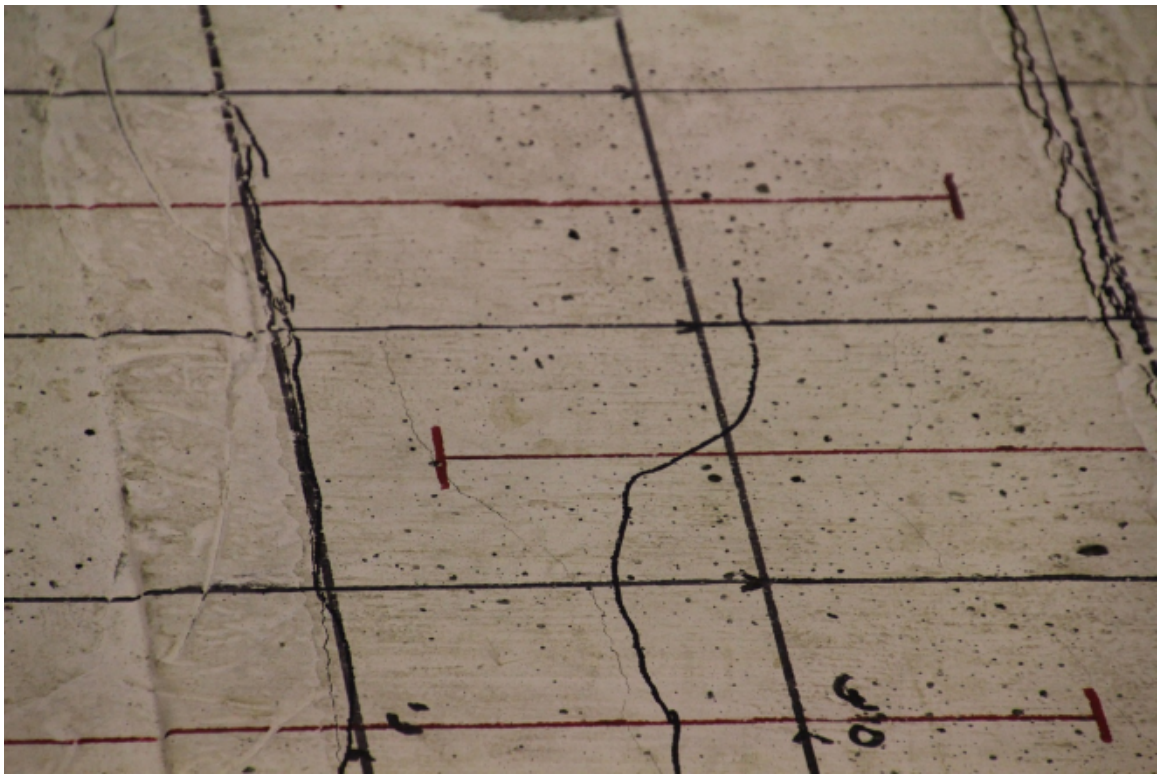

FIGURE 6-9: FINAL PREPARATION OF SLAB SPECIMENS

6.2 SLAB POTENTIOMETERS

The test monitoring of the slab specimens is done through the use of 9 potentiometers. These potentiometers are placed in three rows of three. A single row will be placed at mid-span, and a row on either edge will also be used. A diagram of the location and naming of these potentiometers may be seen in Figure 6-10.

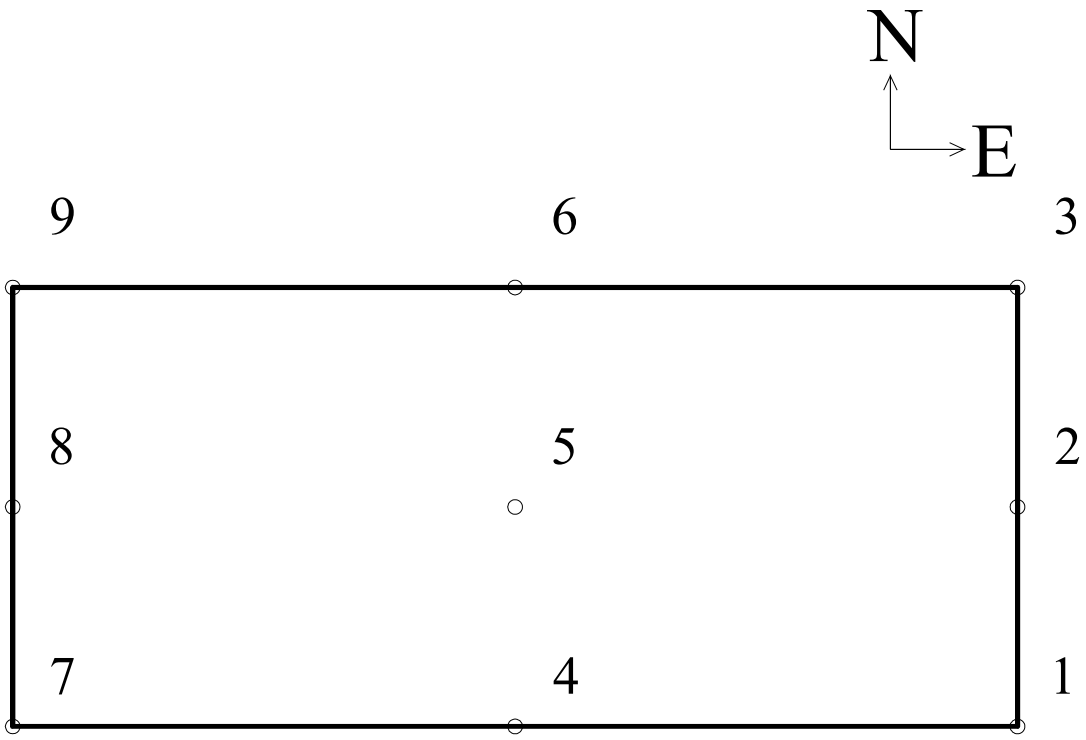

FIGURE 6-10: SLAB SPECIMEN POTENTIOMETER LOCATION AND NAMING

6.3 PROCEDURES FOR STRENGTH TESTING OF SLAB SPECIMENS

As a proof of concept test it is important to gain as much information as possible to form a basis for future tests. As previously stated, the specimens are cast in a two-stage pour, which does not allow for the topping to contribute to the overall strength of the system. Since the topping may not be counted on for additional strength the theoretical cover on the top is reduced to 3/8", and becomes the critical face of the slab. The test setup was designed to put the top face of the slab in tension. This setup will provide data on the effectiveness of the overlay in adding to the strength of the slab, and will

provide results which may be used in a comparison of the three different rebar details used.

Although the topping cannot necessarily be counted on to add strength to the system, if it is shown to do so then the clear cover of 1.125" in the bottom of the slab would be the critical cover. Accordingly, the slabs are tested for both positive and negative moment.

As shown in Figure 6-11, the slabs are supported 1.5' from the centerline and pulled down by a spreader beam attached to the load cells in the basement of the structures laboratory. Rockers are used between the slab and the supports to provide the necessary rotation of the slab. FIBERLAST Bearing Pads are used between the slab and the spreader, filling minor deviations in the concrete surface and providing a small amount of rotation.

Each specimen is loaded until failure. Load and deflection of the system is continuously monitored, and new cracks at each load stage are mapped and documented.

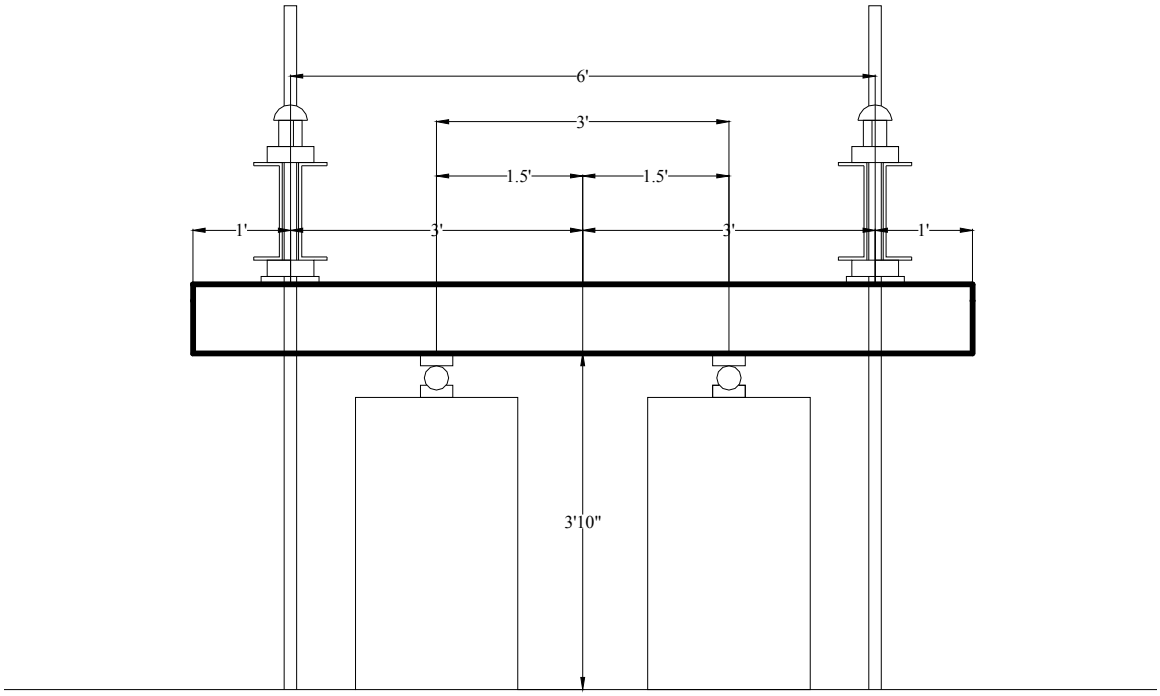

FIGURE 6-11: SLAB TEST SETUP

7 SLAB MATERIAL TESTS

7.1 SLAB REBAR TESTS

After the completion of all tests four rebar were extracted from each of the specimens. Two rebar from each side of the specimen were used in the tensile tests. These tests were performed in order to verify the strength of the rebar used in testing. Only valid data is shown in this section. The complete measurements and testing results are shown on the next two pages.

TABLE 7-1: REBAR MEASUREMENTS FOR TENSILE TESTS

Rebar Measurements

Rebar Designation:	Inner Diam. (in)	Outer Diam. (in)	Ridge Diam.	Ridges/in
S2- #1	0.47	0.57	0.05	4
S1- #1	0.59	0.7	0.03	3
S1- #2	0.59	0.72	0.04	3
S2- #2	0.47	0.54	0.02	4
H1- 3 rebar #1 (#4)	0.48	0.55	0.025	4
H1- 4 rebar #1 (#4)	0.48	0.56	0.025	4
H1- 3 rebar #2 (#4)	0.47	0.56	0.03	4
H1- 4 rebar #2 (#4)	0.47	0.54	0.025	4
H2- 3 rebar #1 (#5)	0.59	0.72	0.038	3
H2- 4 rebar #1 (#5)	0.6	0.68	0.04	3
H2- 3 rebar #2 (#5)	0.59	0.7	0.04	3
H2- 4 rebar #2 (#5)	0.59	0.7	0.04	3
HD1- 3 rebar #1 (#4)	0.47	0.6	0.04	4
HD1- 4 rebar #1 (#4)	0.49	0.56	0.04	4
HD1- 3 rebar #2 (#4)	0.48	0.58	0.04	4
HD1- 4 rebar #2 (#4)	0.49	0.5	0.035	4
HD2- 3 rebar #1 (#5)	0.61	0.68	0.04	3.5
HD2- 4 rebar #1 (#5)	0.6	0.68	0.038	3.5
HD2- 3 rebar #2 (#5)	0.6	0.71	0.036	3.5
HD2- 4 rebar #2 (#5)	0.6	0.7	0.04	3.5

*Inner dimension is the smallest diameter between ridges
*Outer Dimension is the diameter between the wide parts on each side
*ridge diameter is the diameter between the spiraling ridges

TABLE 7-2: COMPLETE RESULTS FROM REBAR TESTING

Test Measurements

Rebar Designation:	Test Length	Yield Strength	Ultimate Strength	Inner Dia.	Outer Dia.	
S2- #1	56.25	67000	108370	0.4	0.47	
S1- #1	59.625	63000	99780	0.5	0.6	
S1- #2	51.5	61000	97600	0.5	0.62	
S2- #2	52.875	63000	103560	0.43	0.5	
H1- 3 rebar #1 (#4)	33.5	?	43200	0.41	0.5	*Machine Error, requiring repair
H1- 4 rebar #1 (#4)	31.875	28000	64940	0.43	0.7	
H1- 3 rebar #2 (#4)	32.5	63000	103270	0.423	0.51	
H1- 4 rebar #2 (#4)	34.175	65000	103740	0.49	0.55	
H2- 3 rebar #1 (#5)	24.125	60700	98250	0.5	0.59	
H2- 4 rebar #1 (#5)	31	62500	103110	0.5	0.62	
H2- 3 rebar #2 (#5)	29	52000	89060	0.53	0.65	
H2- 4 rebar #2 (#5)	28	61500	97820	0.53	0.65	
HD1- 3 rebar #1 (#4)	37.375	68000	114610	0.42	0.51	
HD1- 4 rebar #1 (#4)	37.5	73000	102100	0.38	0.45	*slipped @ 4000 psi (Did not affect yeild or ultimate strength
HD1- 3 rebar #2 (#4)	36	-	59160	-	-	*lots of slipping, quit testing(never made it to yeilding)
HD1- 4 rebar #2 (#4)	33.875	70000	102640	0.41	0.49	
HD2- 3 rebar #1 (#5)	36.375	70000	98310	NA	NA	* Stopped short of failure (real ultimate is unknown)
HD2- 4 rebar #1 (#5)	32.875	72000	102450	0.41	0.5	
HD2- 3 rebar #2 (#5)	33.5	69000	98990	0.46	0.52	
HD2- 4 rebar #2 (#5)	33.25	73000	102700	0.44	0.51	

*Test Length is the length between the chucks once in the testing apparatus

*The inner and outer diameter for test measurements is at the smallest point after break.

The values were averaged in order to obtain yield and ultimate strengths used in modeling. The averages do not include values which were altered due to mechanical errors in testing equipment. This table shows that the rebar obtained from the local steel manufacturer, used in the straight specimens, and the hooked specimens were 60ksi steel, and the rebar used in the headed rebar specimens were 70ksi. The yield strength obtained will be used in the comparison of each of the specimens.

TABLE 7-3: REBAR TEST STRENGTHS

Test Specimen	Yield Strength(psi)	Ultimate Strength(psi)
S1- #1	63000	99780
S1- #2	61000	97600
Average:	**62000**	**98690**
S2- #2	63000	103560
S2- #1	67000	108370
Average:	**65000**	**102327.5**
H1- 3 rebar #2 (#4)	63000	103270
H1- 4 rebar #2 (#4)	65000	103740
Average:	**64000**	**103505**
H2- 3 rebar #1 (#5)	60700	98250
H2- 4 rebar #1 (#5)	62500	103110
H2- 3 rebar #2 (#5)	52000	89060
H2- 4 rebar #2 (#5)	61500	97820
Average:	**59175**	**97060**
HD1- 3 rebar #1 (#4)	68000	114610
HD1- 4 rebar #1 (#4)	73000	102100
HD1- 4 rebar #2 (#4)	70000	102640
Average:	**70333**	**106450**
HD2- 3 rebar #1 (#5)	70000	98310
HD2- 4 rebar #1 (#5)	72000	102450
HD2- 3 rebar #2 (#5)	69000	98990
HD2- 4 rebar #2 (#5)	73000	102700
Average:	**71000**	**100613**

7.2 Slab Concrete Tests

Concrete test cylinders were taken from each of the two pours for the closure slab specimens. The cylinders were tested at the conclusion of the slab test, which was 114 and 79 days respectively from the time of casting for the outer sections and the closure region respectively. The compressive strengths for all samples are shown in Table 4-6 and Table 7-5.

TABLE 7-4: COMPRESSIVE STRENGTH OF OUTER SECTIONS OF SLAB SPECIMENS

Sample #	Compressive Strength (psi)
1	2991.7*
2	7023.5
3	6702.2
4	7189
5	6237.5
6	5705.3
Average:	6571.5

**Note: This specimen is considered an outlier and not used in the average concrete strength due to issues with the capping of the cylinder.*

TABLE 7-5: COMPRESSIVE STRENGTH OF CLOSURE REGION OF SLAB SPECIMENS

Sample #	Compressive Strength (psi)
1	3999.4
2	4088.5
3	2089.2*
Average:	4044

*Note: This specimen is considered an outlier and not used in the average concrete strength.

8 Test Results and Discussion of Slab Specimens

A finite element model was created in order to predict the behavior of the slab specimens. Specimens S1 and S2 were modeled, and compared to experimental results

8.1 Finite Element Model of Straight Slabs

The finite element model was created in two 3D parts the first part being 8’ x 3.5’ x 6.5”, and the second being 8’ x 3.5’ x 2”. The two 3D parts represent the slab and the topping respectively. The topping was modeled with an 8 node linear brick element (C3D8). 1D parts measuring 90” and 36” were used to simulate the longitudinal and transverse reinforcement. The reinforcement was modeled using a 2 node linear truss element (T3D2). A 2.5” mesh was used for the faces of the model with a 1” mesh thickness.

Three different material models were created and assigned to the model parts. The three material models are concrete models with compressive strength of 4ksi and 6ksi, and a steel model with a yield stress of 65ksi. The different diameter of reinforcement was modeled by creating two distinct sections. The embedded region constraints were used to simulate the reinforcement embedded into the slab.

The loading was applied to the model by assigning a surface traction boundary condition to an area of 3.5 ft x 6 in. In addition, a gravity type of load was also used. Displacement type of boundary condition was used to simulate both pinned and roller supports.

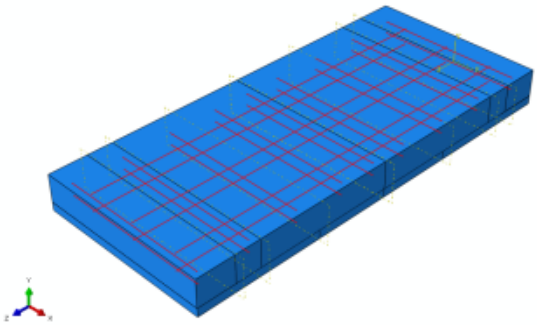

A) EMBEDDED TRUSS ELEMENT TO SIMULATE THE REINFORCEMENT

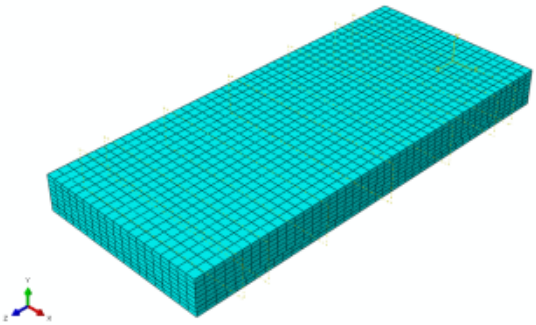

B) MESH OF FE MODEL

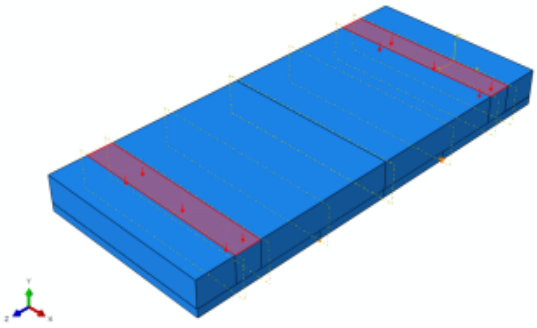

C) SURFACE TRACTION TYPE OF BOUNDARY CONDITION ASSIGNED TO THE MODEL

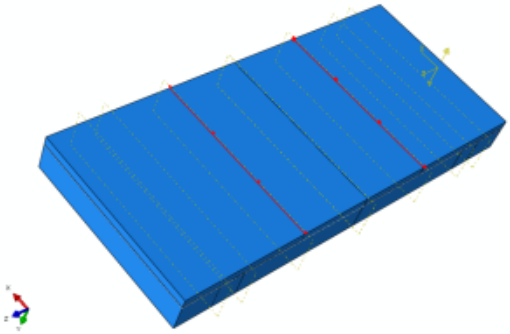

D) DISPLACEMENT TYPE OF BOUNDARY CONDITION ASSIGNED TO THE MODEL

FIGURE 8-1: FINITE ELEMENT MODEL DETAILS

A) PLASTIC STRAIN IN CONCRETE (PREDICTION OF CRACK PATTERN) AT MAXIMUM LOAD STAGE

B) STRESS IN CONCRETE EQUAL TO 6 KSI AT MAXIMUM LOAD STAGE

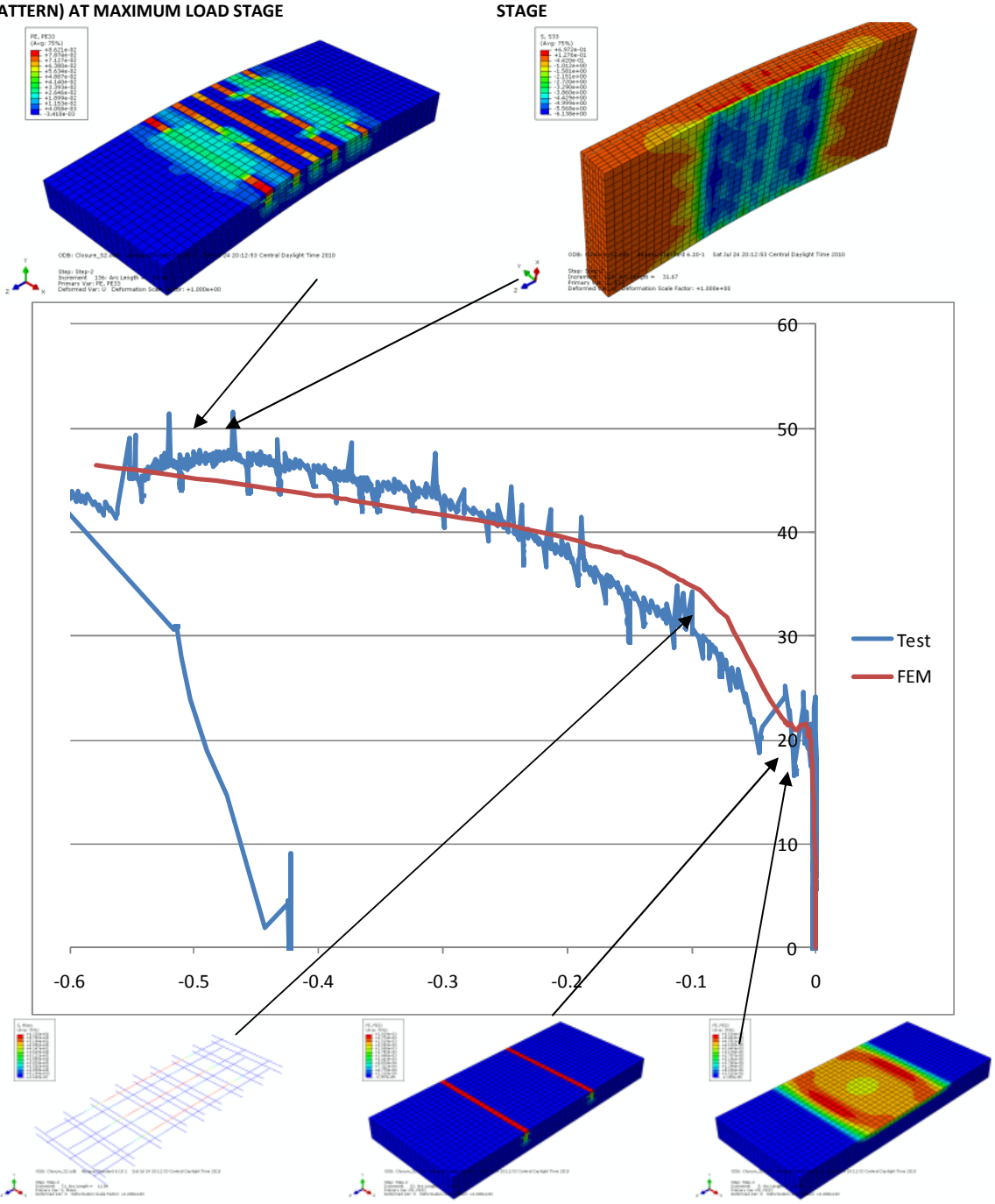

C) YIELDING OF TOP REINFORCEMENT AT 65 KSI

D) PLASTIC STRAIN IN CONCRETE (AGGRAVATION OF CRACKS AND PROPAGATION TO SLAB)

E) PLASTIC STRAIN IN CONCRETE (PREDICTION OF FIRST CRACKS) AT EARLIER LOAD STAGE

FIGURE 8-2: FINITE ELEMENT RESULTS FOR S2

A) PLASTIC STRAIN IN CONCRETE (PREDICTION OF CRACK PATTERN) AT MAXIMUM LOAD STAGE

B) STRESS IN CONCRETE EQUAL TO 6 KSI AT MAXIMUM LOAD STAGE

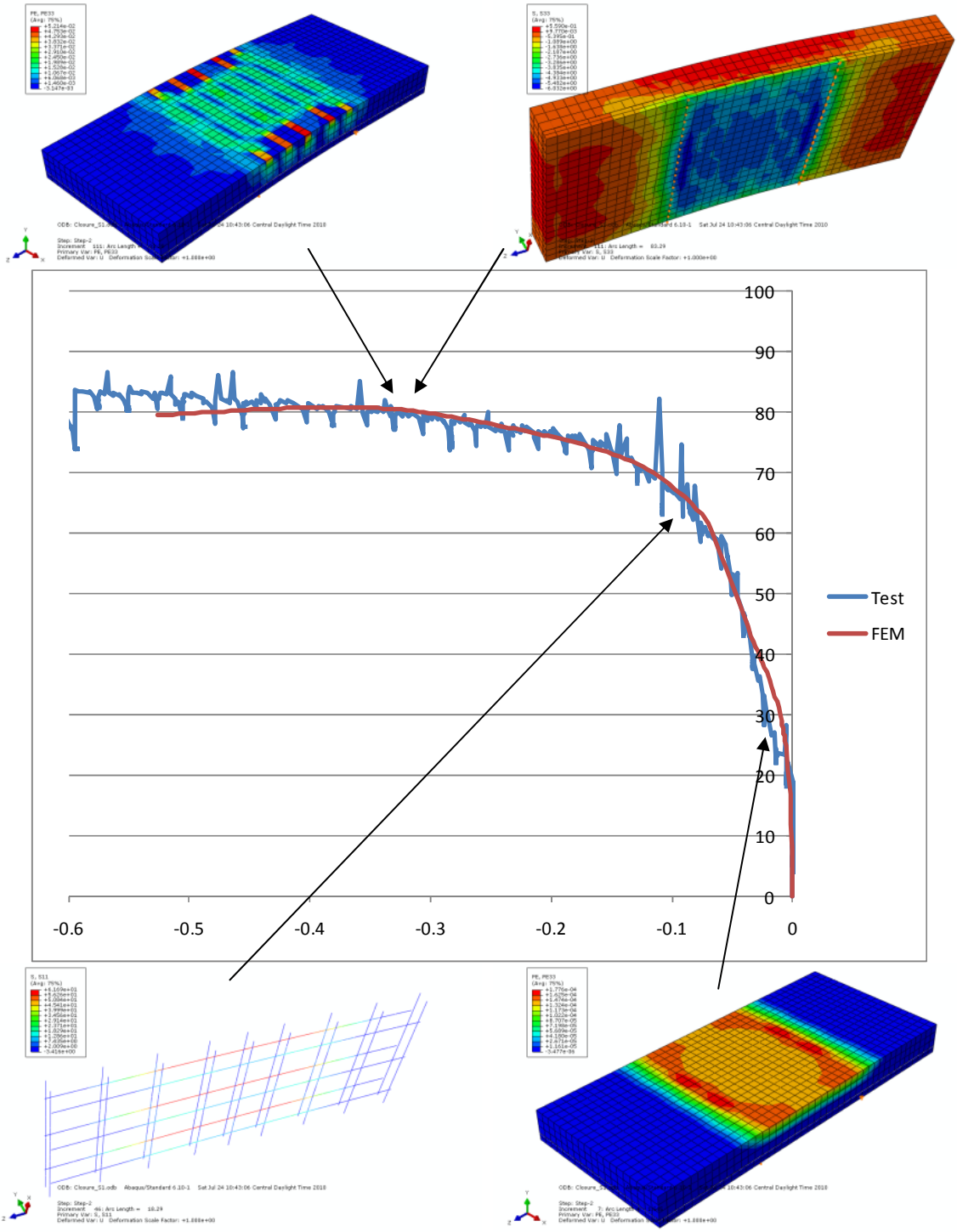

C) YIELDING OF TOP REINFORCEMENT AT 65 KSI

D) PLASTIC STRAIN IN CONCRETE (PREDICTION OF FIRST CRACKS) AT EARLIER LOAD STAGE

FIGURE 8-3: FINITE ELEMENT RESULTS FOR S2

8.2 Strength Tests for Slabs

Two sets of tests were performed on the slab specimens, positive moment testing and negative moment testing. The negative moment tests were performed first to observe the effectiveness of the concrete overlay. The positive moment tests were performed next to observe slab behavior in the traditional load case.

The figures showing deflection of the slabs in the following sections are compared to M/Mn. This ratio is used to eliminate the effect of differing yield strengths of steel between the specimens. The figure below shows the two beams which were used in the moment capacity calculations. The beam on the left was used for positive moment calculations and the beam on the right was used for negative moment calculations. The area of steel in the 12 in. wide sections was calculated by assuming three longitudinal bars over the 3.5 foot width of the slab. Table 8-1 shows the calculated moment capacities for each of the beams in kip-ft.

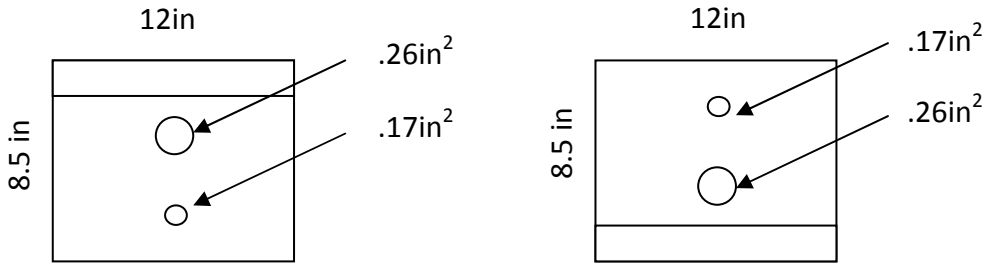

FIGURE 8-4: EQUIVALENT SECTION OF CONCRETE SLAB

TABLE 8-1: MOMENT CAPCITY OF EQUIVALENT BEAMS

[redacted]

8.3 Negative Moment Bending

Specimens S1,HD1, and H1 were tested for negative moment. The slab orientation and loading direction are shown below in Figure 8-5.

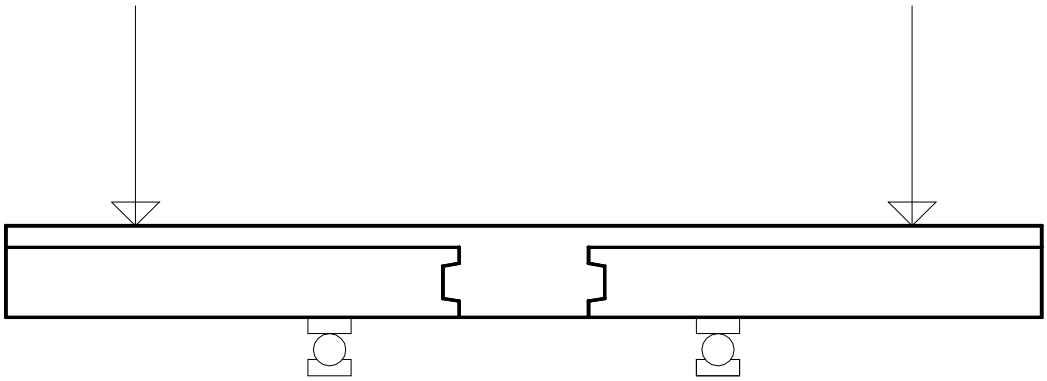

FIGURE 8-5: BENDING DIRECTION FOR FIRST ROUND OF TESTING

S1 is the control to which the subsequent tests will be compared. The deflections were found to be consistent across the width of the slab; this allows for each section to be represented by a single pot in each line. The pots chosen for analysis were pots 2 & 5 these are located at the mid-point of the width. Figure 8-7 and Figure 8-6 show the moment ratio vs. deflection for S1. Pot 2 is one of the pots located at the edge of the slab on the side containing 3 rebar. The side with three rebar consistently has slightly higher deflections than the other side. The slightly higher deflection values are due to the fact that the 3 rebar provide less stiffness. Pot 5 is located directly in the center of the slab.

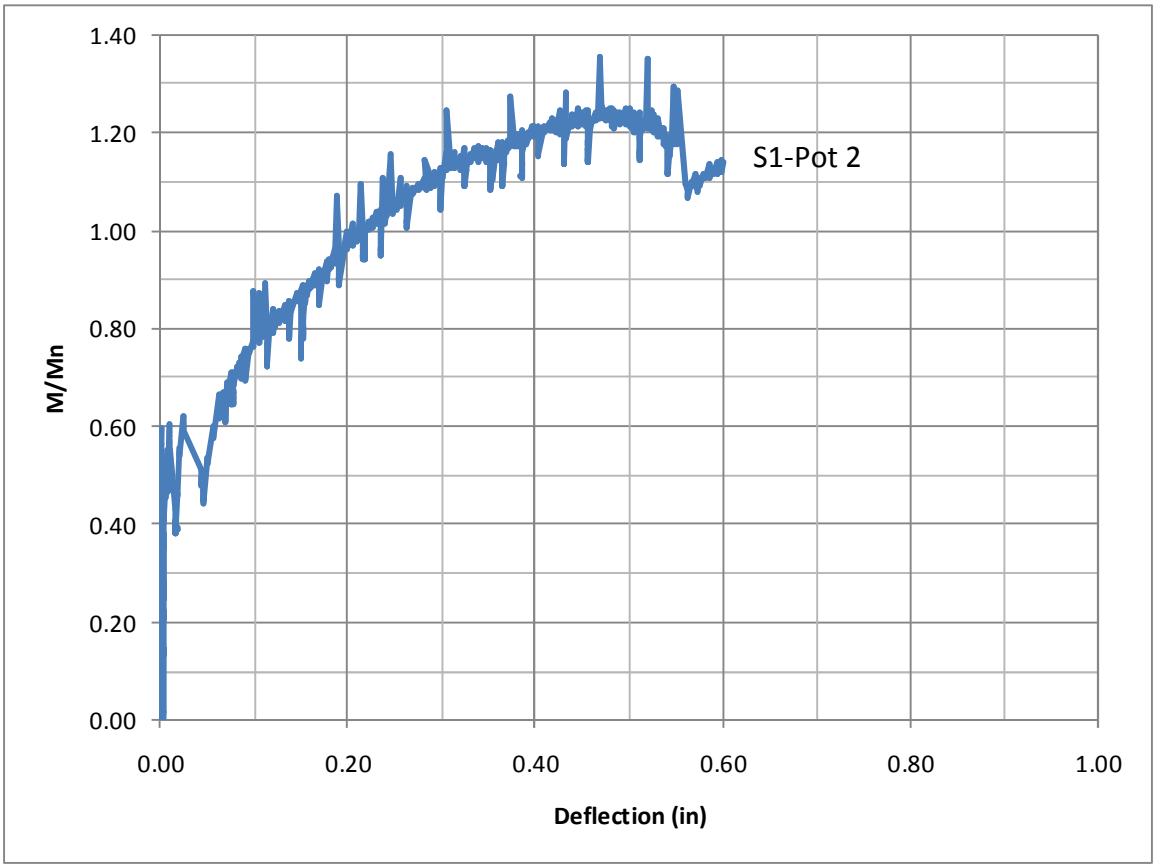

FIGURE 8-6: MOMENT VS. DEFLECTION FOR THE EDGE POT (POT 2) OF S1 (NEGATIVE MOMENT)

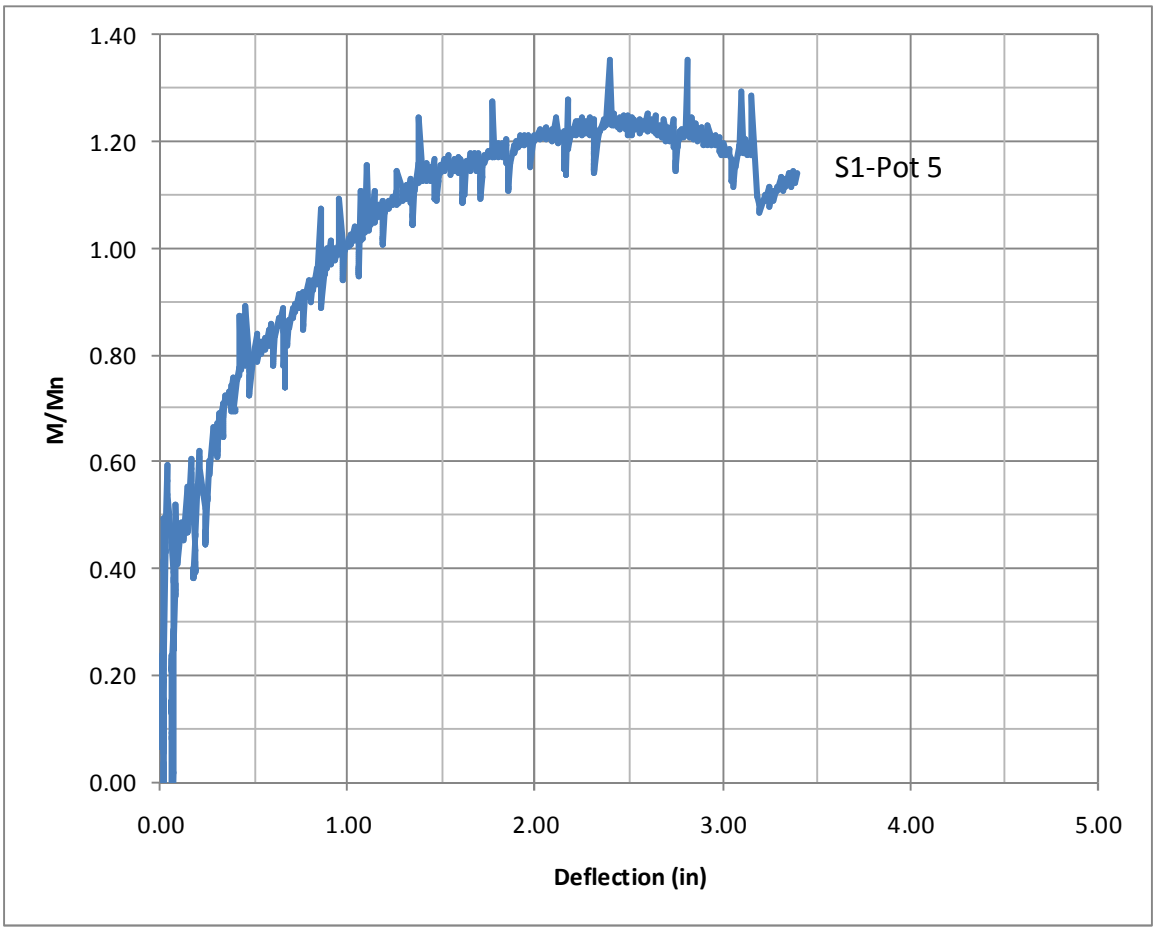

FIGURE 8-7: MOMENT VS. DEFLECTION FOR THE CENTER POT (POT 5) OF S1 (NEGATIVE MOMENT)

The next set of graphs is for the headed rebar (HD1). These specimens show the large crack occurring near the end of the test causing a drastic decrease in the load carrying capability of the slab.

Figure 8-9 & Figure 8-10 show the comparison between S1 and HD1. The figures show that the headed bar acts similarly to the straight bar up until major cracking occurs at approximately 28kips. The headed rebar still carries an acceptable amount of load, but does not reach the load carrying capacity which the straight bar does.

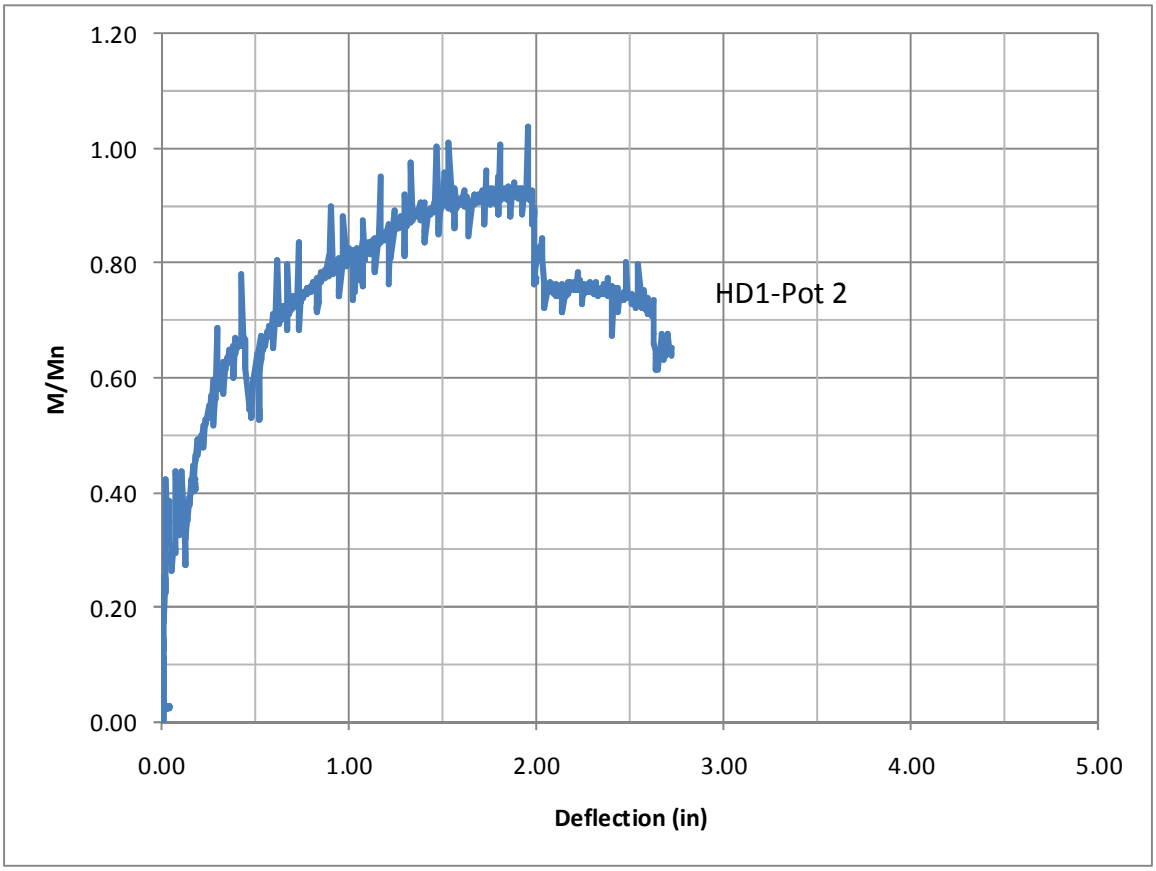

FIGURE 8-8: MOMENT VS. DEFLECTION FOR THE EDGE POT (POT 2) OF HD1 (NEGATIVE MOMENT)

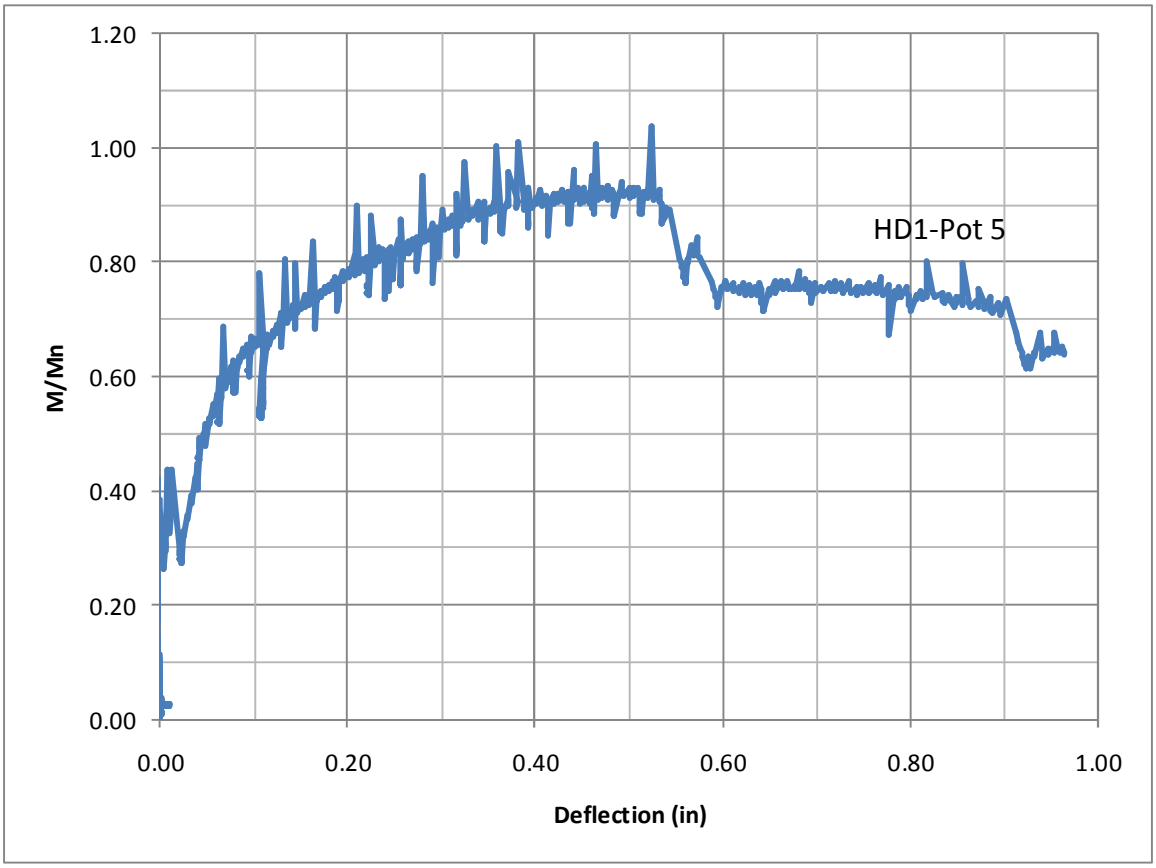

FIGURE 8-9: MOMENT VS. DEFLECTION FOR THE CENTER POT (POT 5) OF HD1 (NEGATIVE MOMENT)

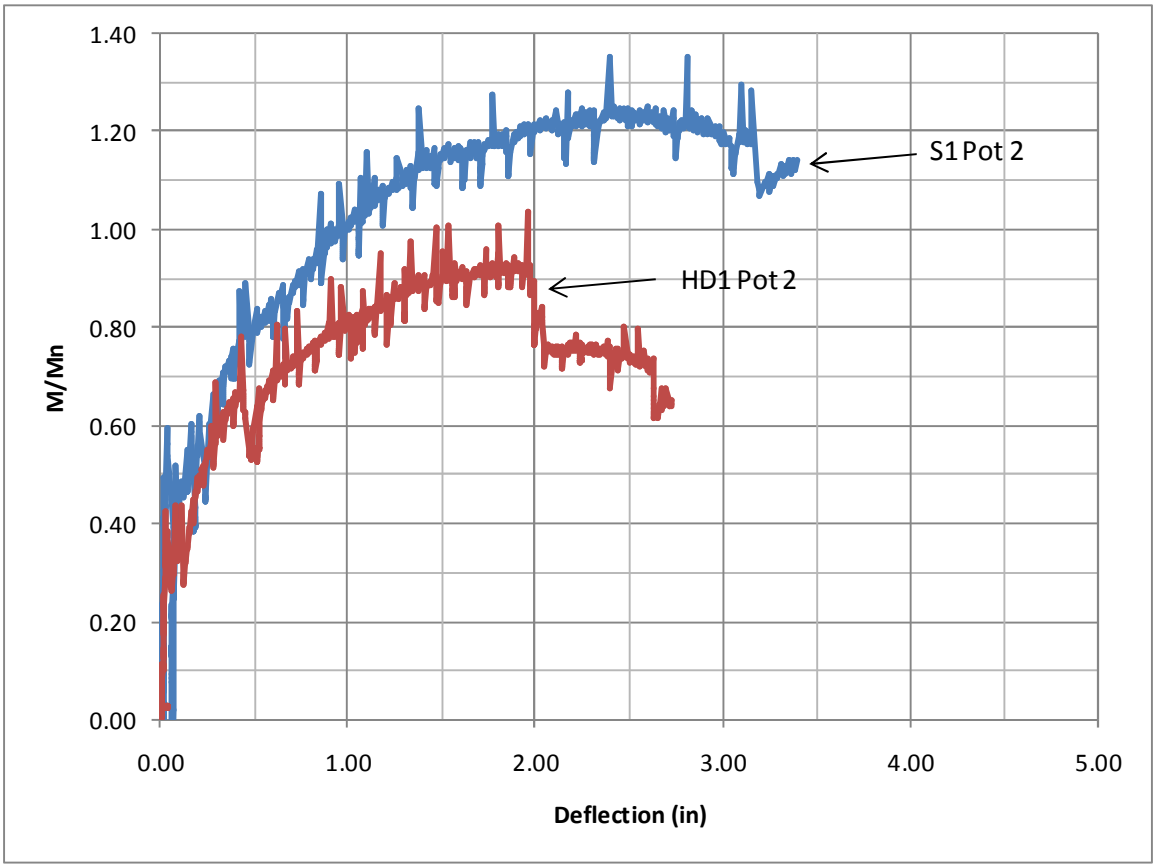

FIGURE 8-10: MOMENT VS. DEFLECTION FOR THE EDGE POT (POT 2) OF S 1 & HD1 (NEGATIVE MOMENT)

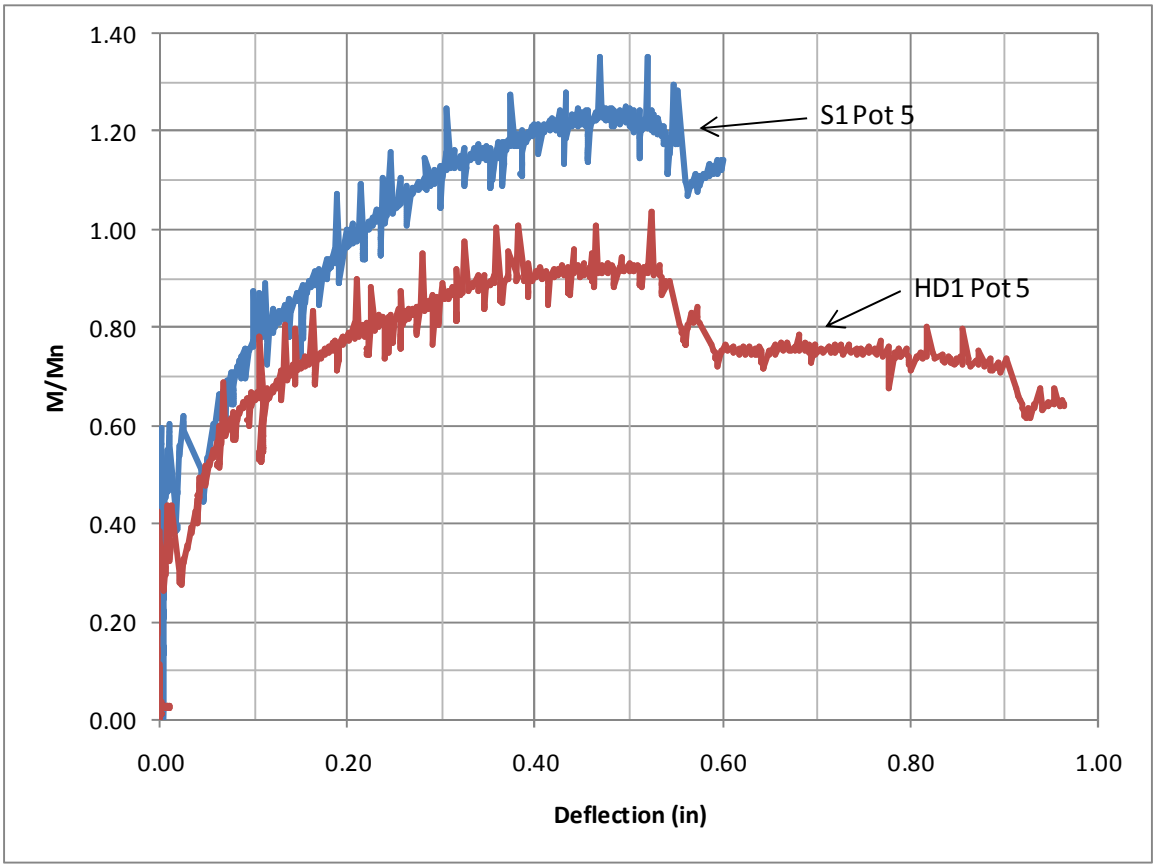

FIGURE 8-11: MOMENT VS. DEFLECTION FOR THE CENTER POT (POT 5) OF S 1 & HD1 (NEGATIVE MOMENT)

Figure 8-12 and Figure 8-13 show the moment ratio vs. deflection data for H1. In order to better observe the behavior of each of the rebar details comparisons are made between each. Figure 8-11 is the comparison to S1. As with HD1 the hooked specimen performs very similarly until the first major crack forms and the load deflection curve is shifted down slightly. When looking at the comparison between HD1 and H1 it can be seen that they both display very similar behavior. H1 shows slightly higher moment carrying capacity.

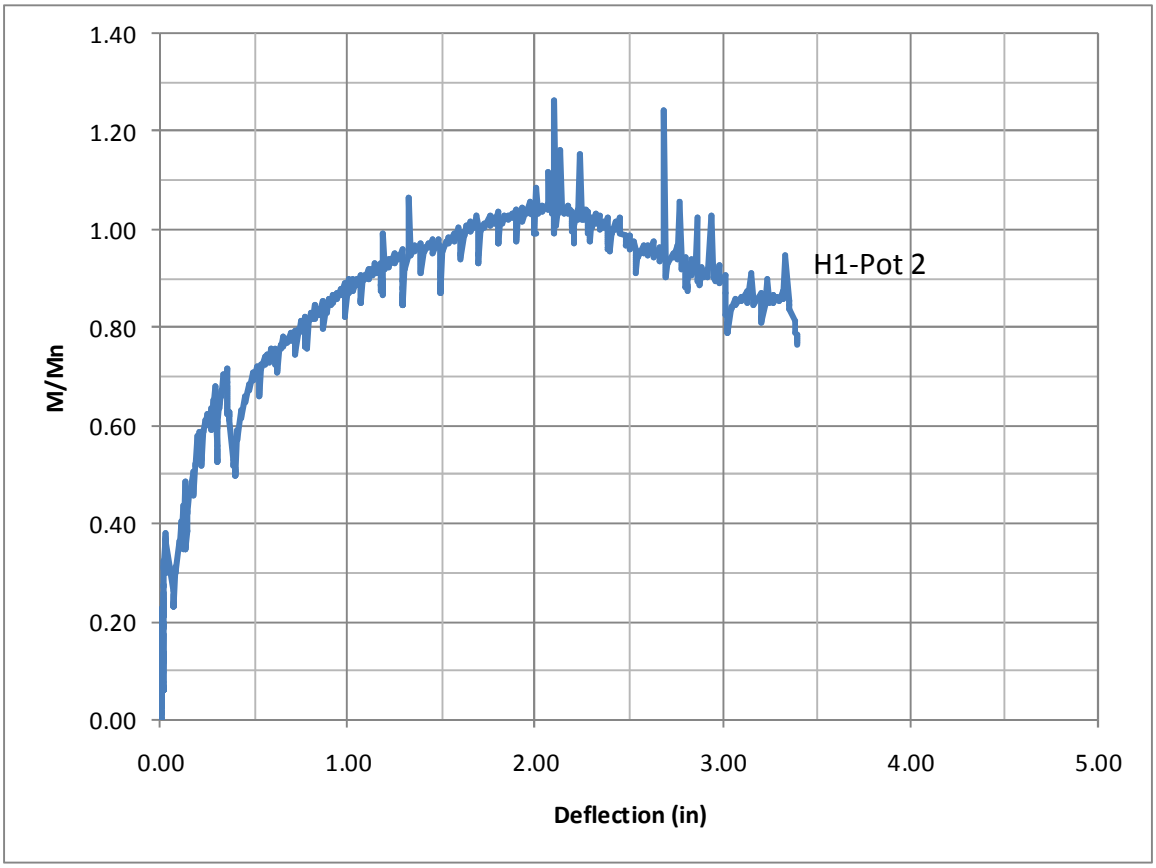

FIGURE 8-12: MOMENT VS. DEFLECTION FOR THE EDGE POT (POT 2) OF H1 (NEGATIVE MOMENT)

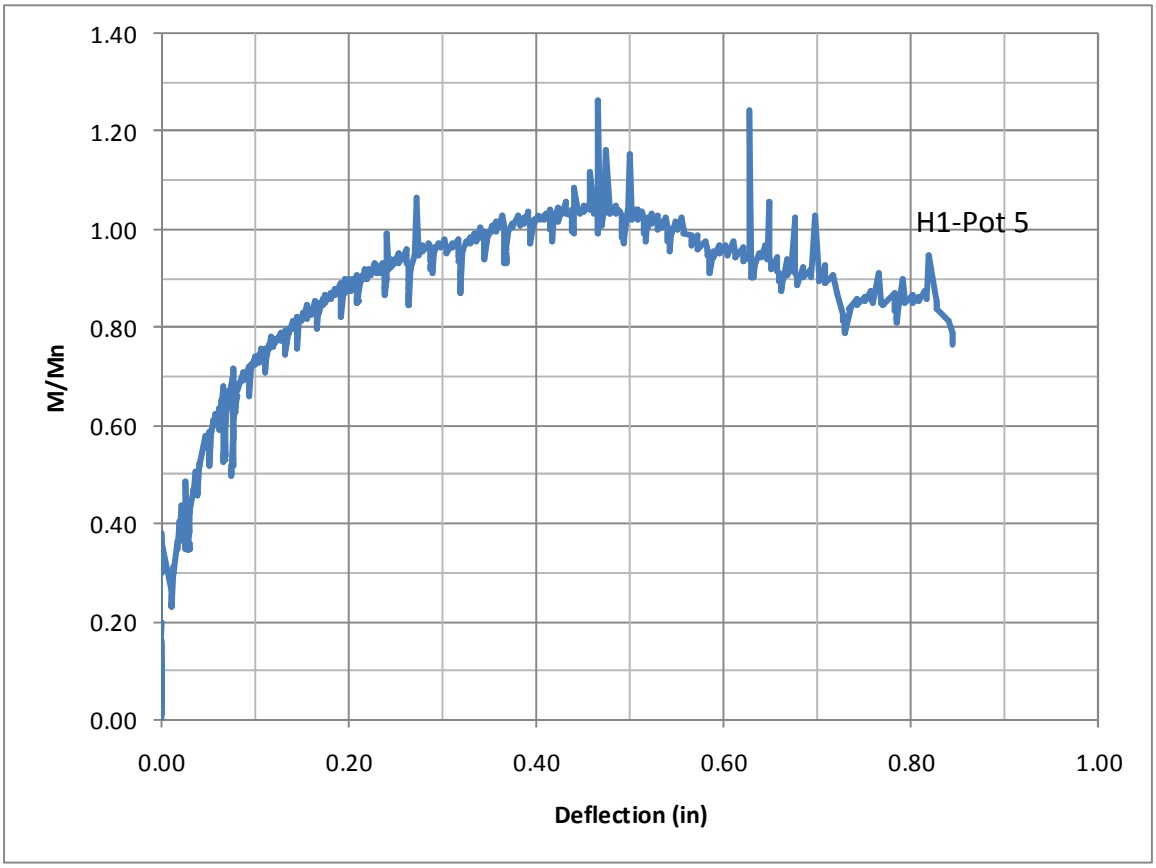

FIGURE 8-13: MOMENT VS. DEFLECTION FOR THE CENTER POT (POT 5) OF H1 (NEGATIVE MOMENT)

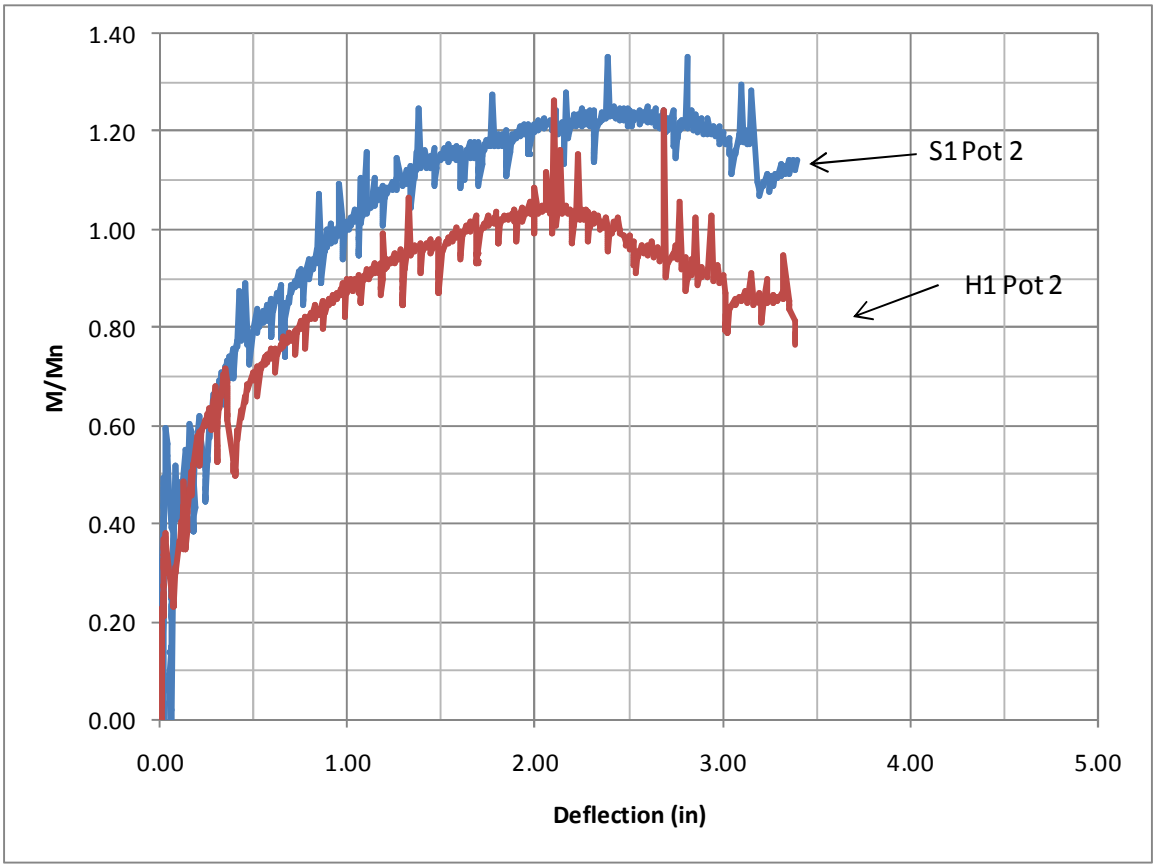

FIGURE 8-14: MOMENT VS. DEFLECTION FOR THE EDGE POT (POT 2) OF H1 & S1 (NEGATIVE MOMENT)

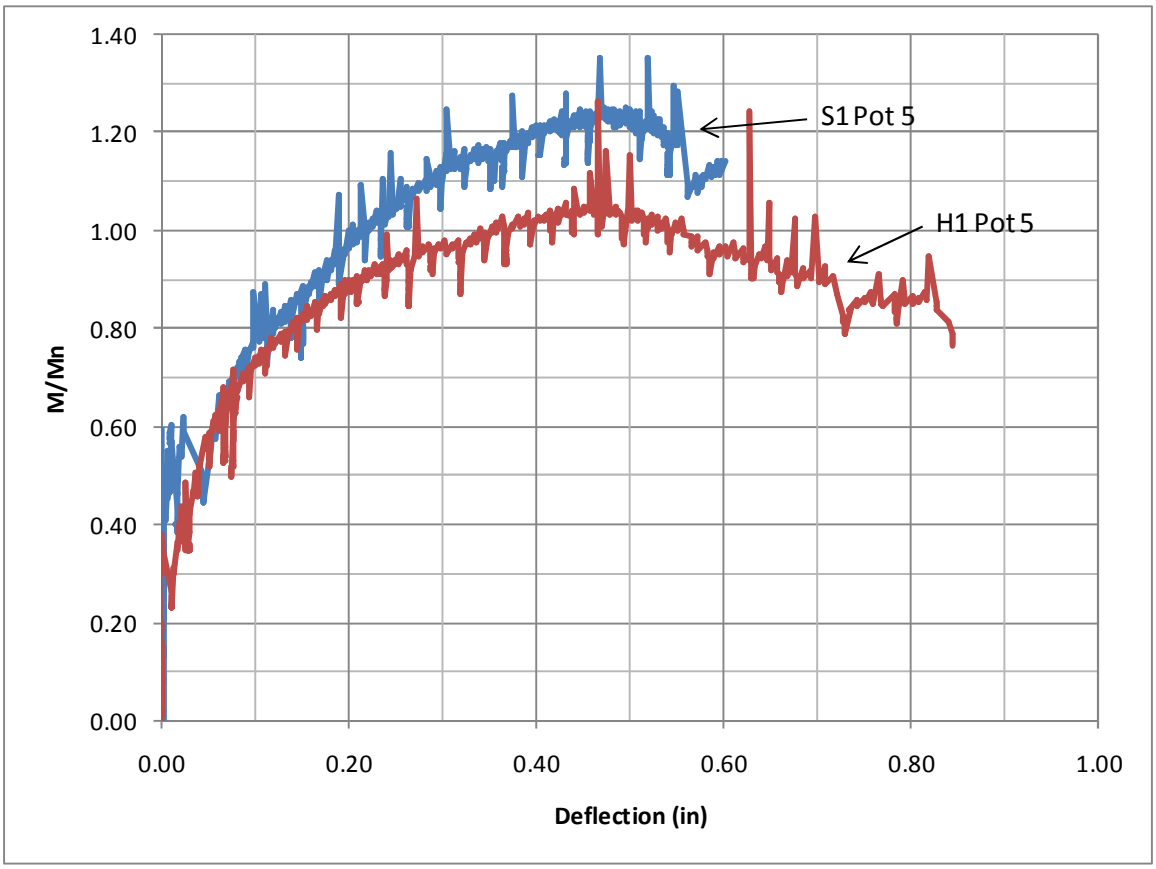

FIGURE 8-15: MOMENT VS. DEFLECTION FOR THE CENTER POT (POT 5) OF H1 & S1 (NEGATIVE MOMENT)

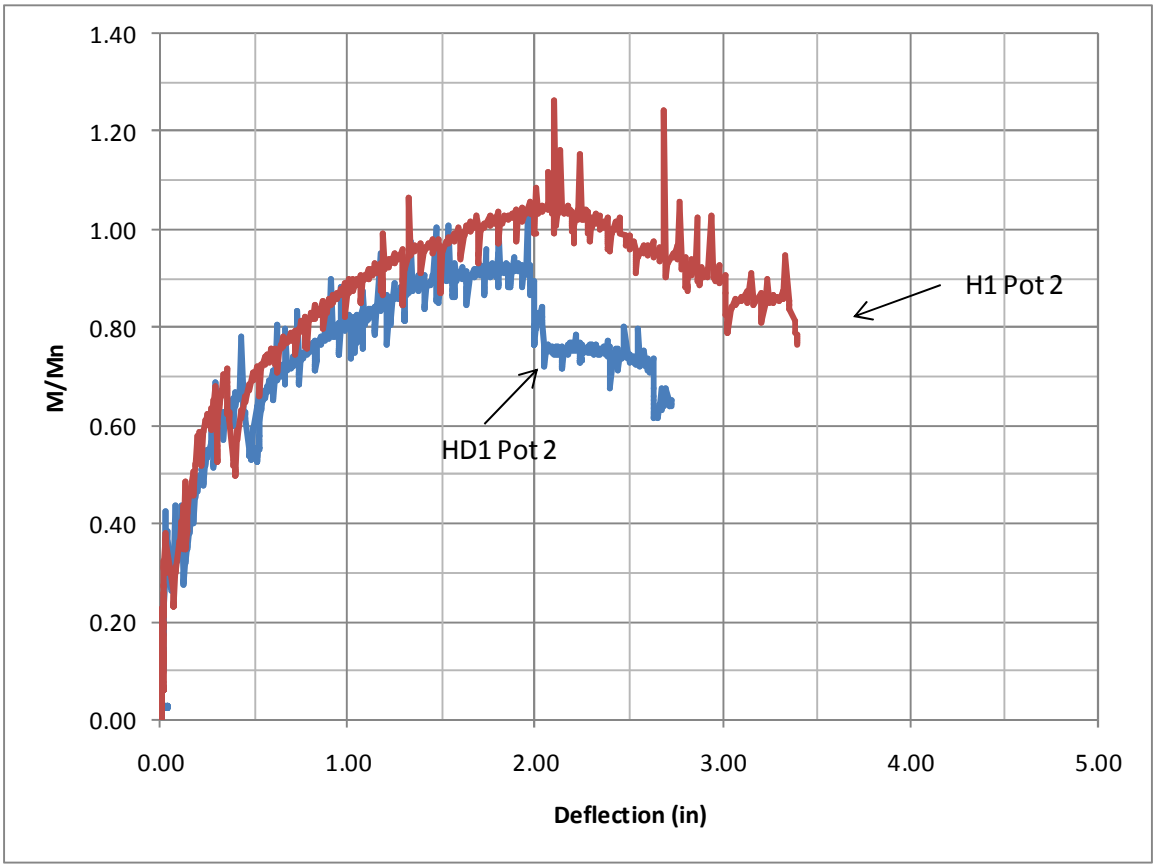

FIGURE 8-16: MOMENT VS. DEFLECTION FOR THE EDGE POT (POT 2) OF H1 & HD1 (NEGATIVE MOMENT)

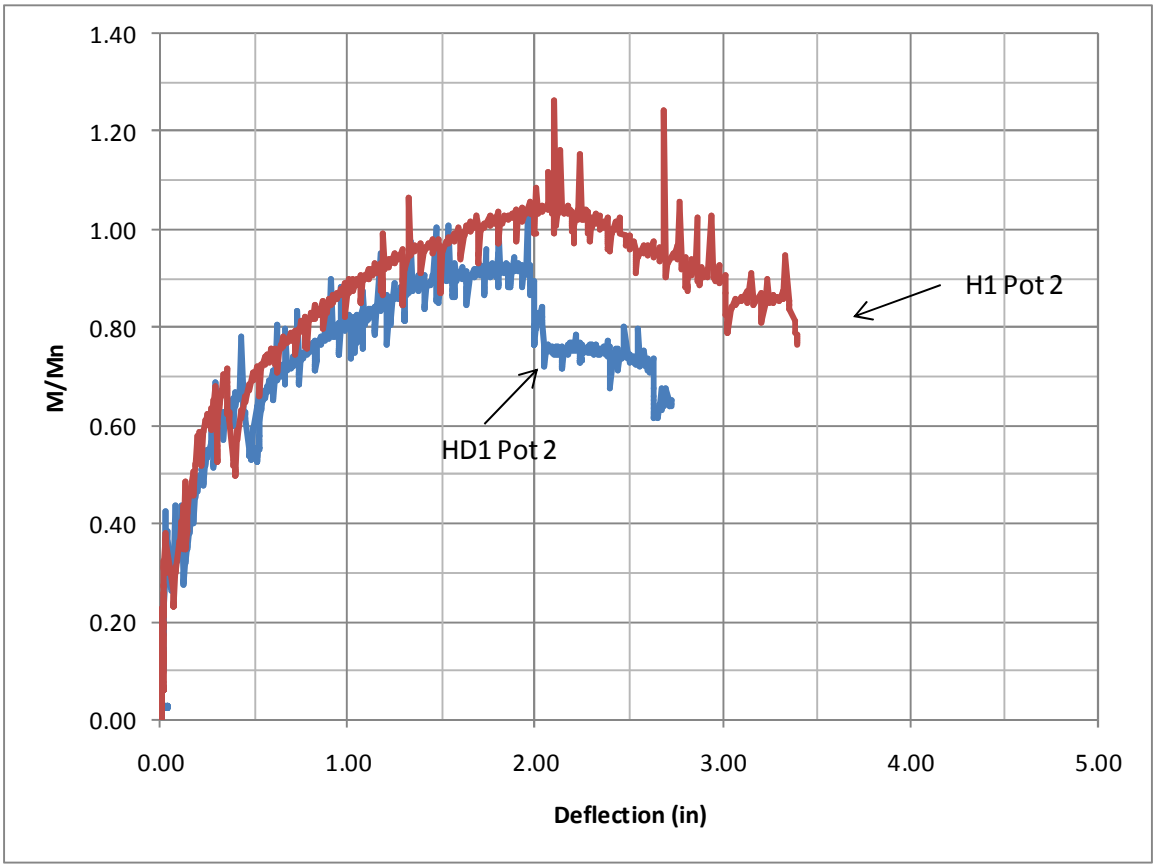

FIGURE 8-17: MOMENT VS. DEFLECTION FOR THE CENTER POT (POT 5) OF H1 & HD1 (NEGATIVE MOMENT)

The last two figures above show that the headed bar and hooked bar perform similarly under negative moment. This performance signifies that the hooked bar, for negative moment, is a viable substitute. Further testing into positive moment loading will verify if the hooked bar is a possibly alternative for previously recommended headed bars.

8.4 Positive Moment Bending

Once the concrete cover proved effective, the bottom face became critical. The small cover on the bottom face is of concern due to the primary load case having a positive moment where the bottom face is in tension. Figure 8-18 shows slab orientation and loading direction. As with the negative moment section the following figures will show the moment ratio vs. deflection of the slabs.

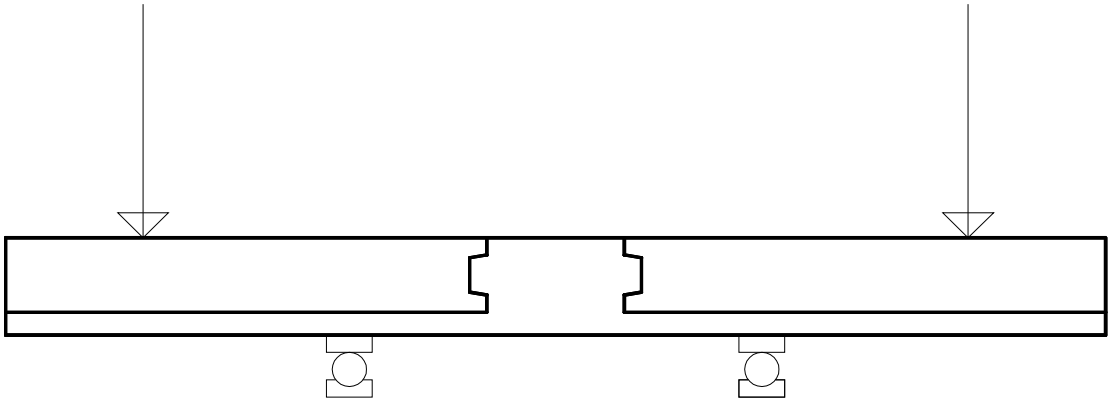

FIGURE 8-18: SLAB ORIENTATION AND LOAD DIRECTION FOR POSITIVE MOMENT TESTING

Figure 8-19 and Figure 8-20 show the results for S2. These results show that moment applied to the system reaches approximately 84% of the calculated moment capacity. The results for HD2 show that it does not reach the deflection limits which S2 does. A comparison of S2 and HD2 is plotted in order to better show the similarities.

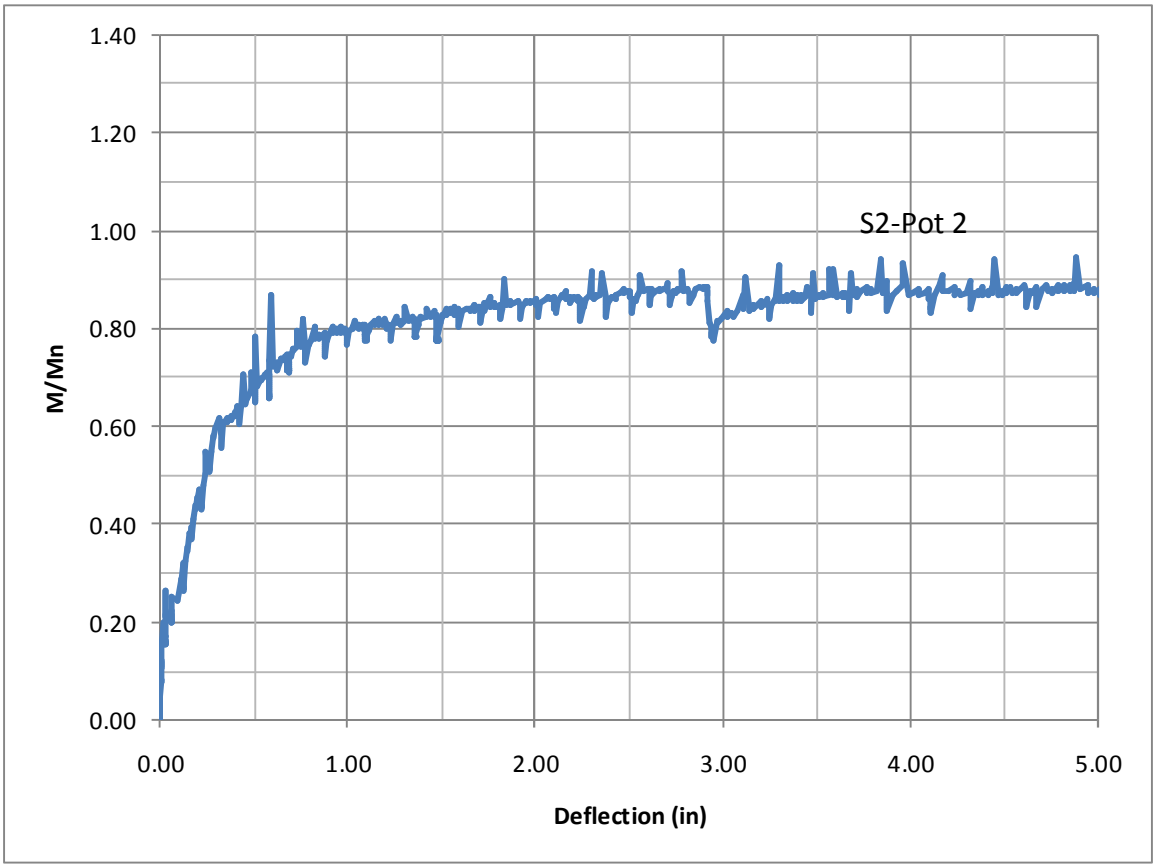

FIGURE 8-19: MOMENT VS. DEFLECTION FOR THE EDGE POT (POT 2) OF S2 (POSITIVE MOMENT)

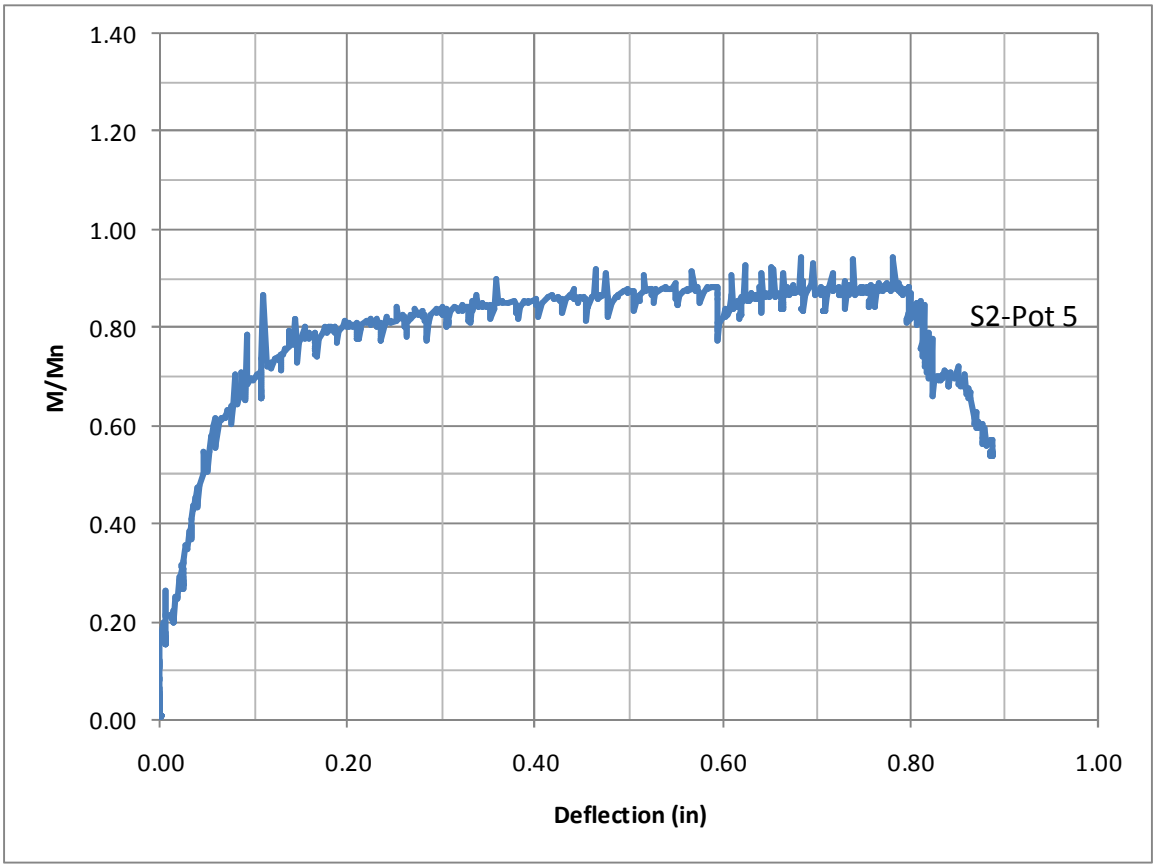

FIGURE 8-20: MOMENT VS. DEFLECTION FOR THE CENTER POT (POT 5) OF S2 (POSITIVE MOMENT)

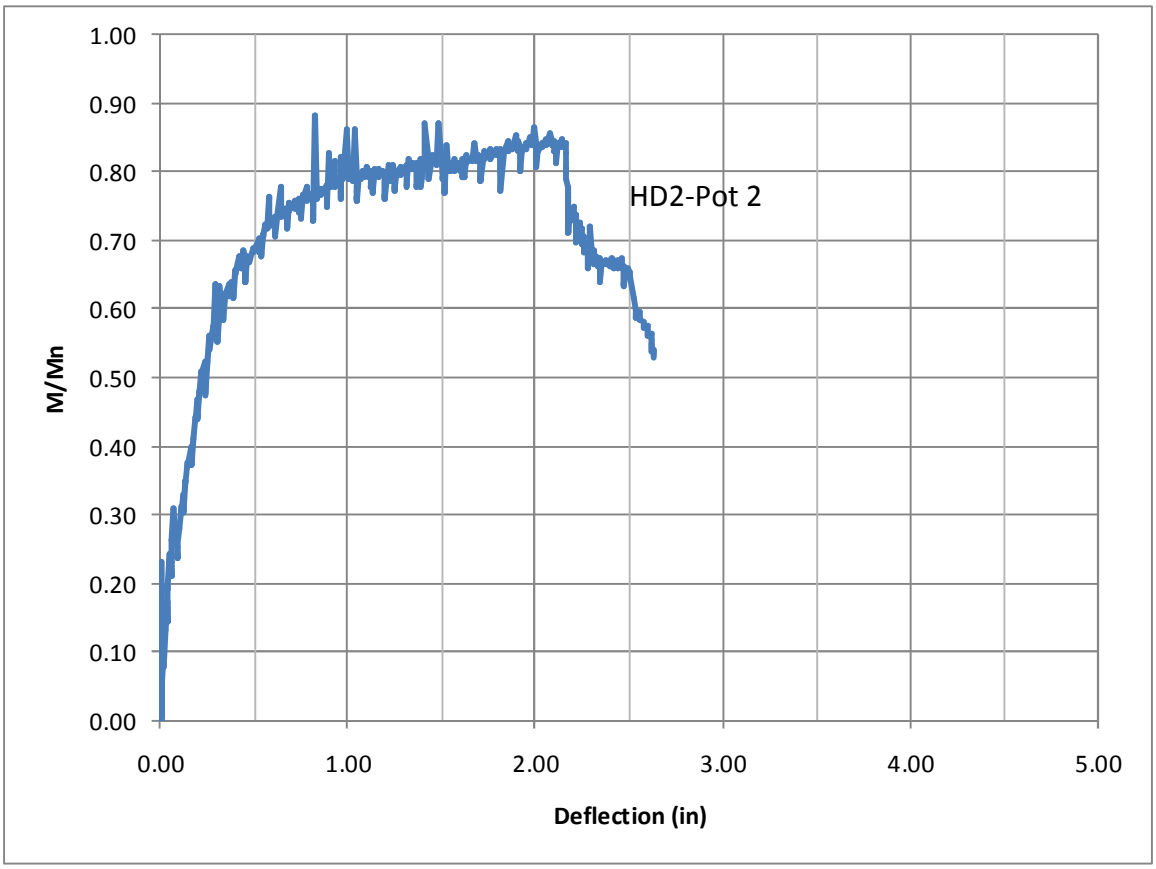

FIGURE 8-21: MOMENT VS. DEFLECTION FOR THE EDGE POT (POT 2) OF HD2 (POSITIVE MOMENT)

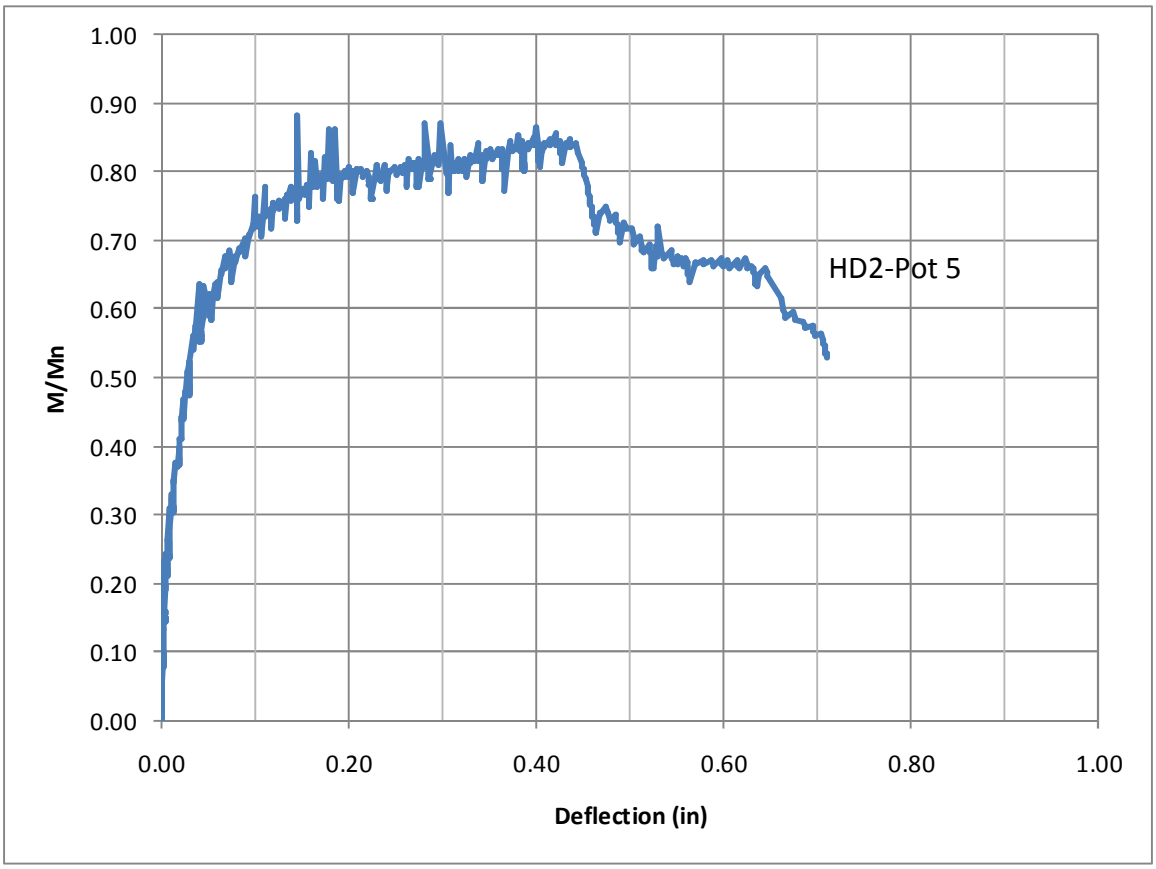

FIGURE 8-22: MOMENT VS. DEFLECTION FOR THE CENTER POT (POT 5) OF HD2 (POSITIVE MOMENT)

.

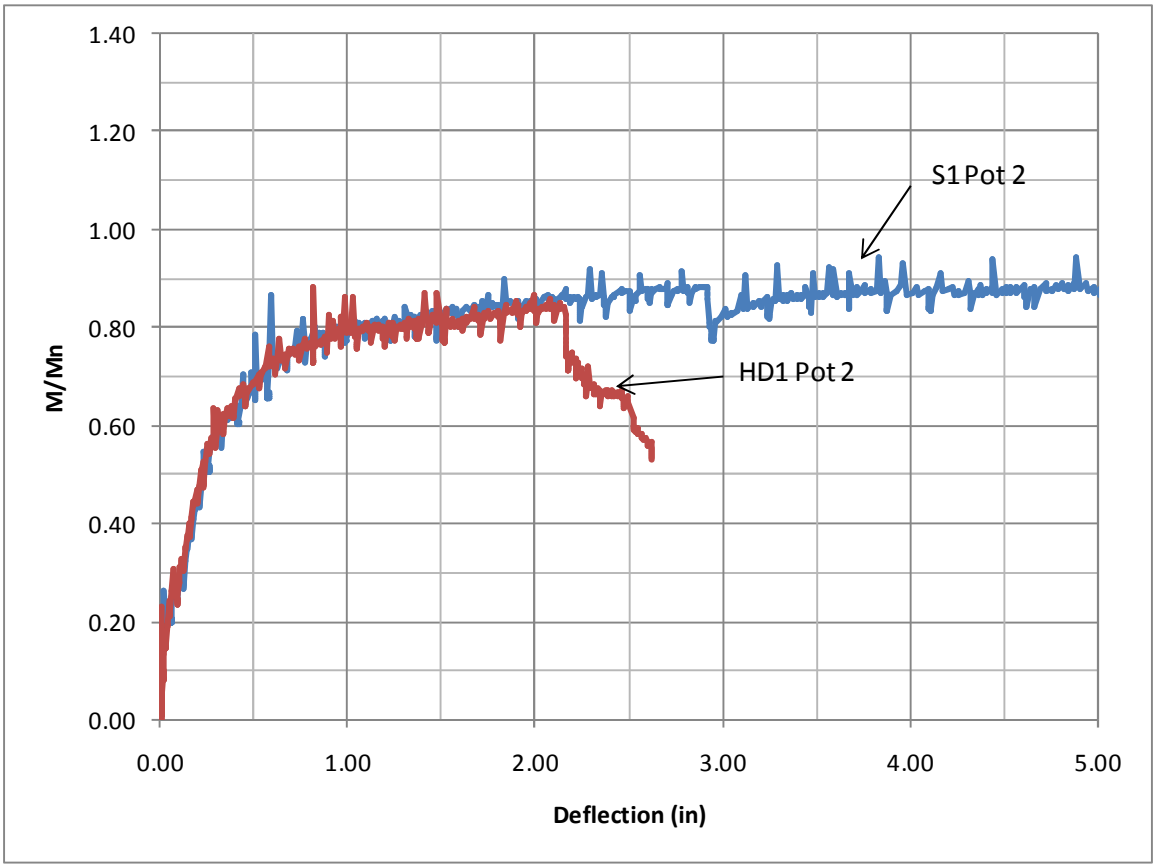

FIGURE 8-23: MOMENT VS. DEFLECTION FOR THE EDGE POT (POT 2) OF S2 & HD2 (POSITIVE MOMENT)

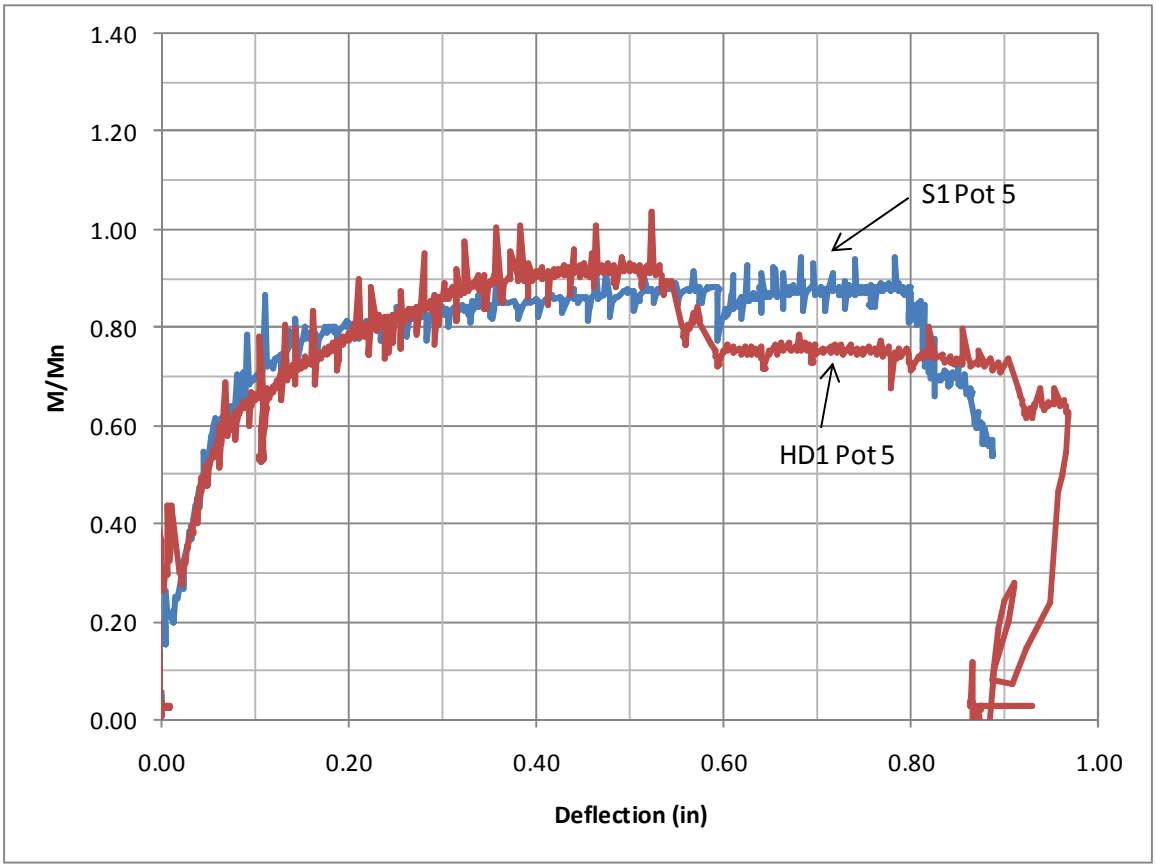

FIGURE 8-24: MOMENT VS. DEFLECTION FOR THE CENTER POT (POT 5) OF S2 & HD2 (POSITIVE MOMENT)

The comparison graphs above show that S2 and HD2 follow the same load path until their respective failures. The outside edges of HD2 do not experience the large deflections seen in S2. While the deflections are not as large, HD2 follows the same load path and displays sufficient ductility.

Figure 8-25 and Figure 8-26 show that the results from H2 show different behavior than the previous two specimens had shown. H2 shows a very ductile failure. While the previous two specimens would experience a crack with large drops in load carrying capacity, H2 experiences a smooth drop in load carrying capacity.

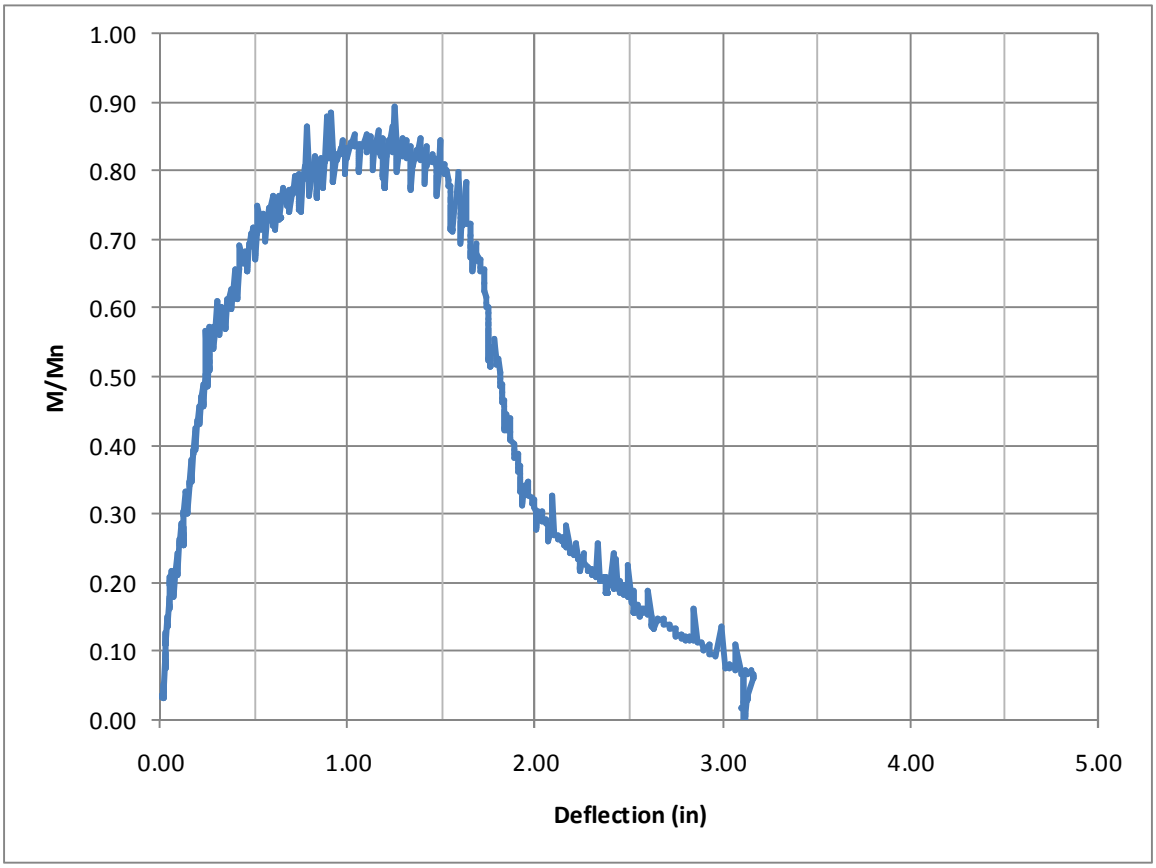

FIGURE 8-25: MOMENT VS. DEFLECTION FOR THE EDGE POT (POT 2) OF H2 (POSITIVE MOMENT)

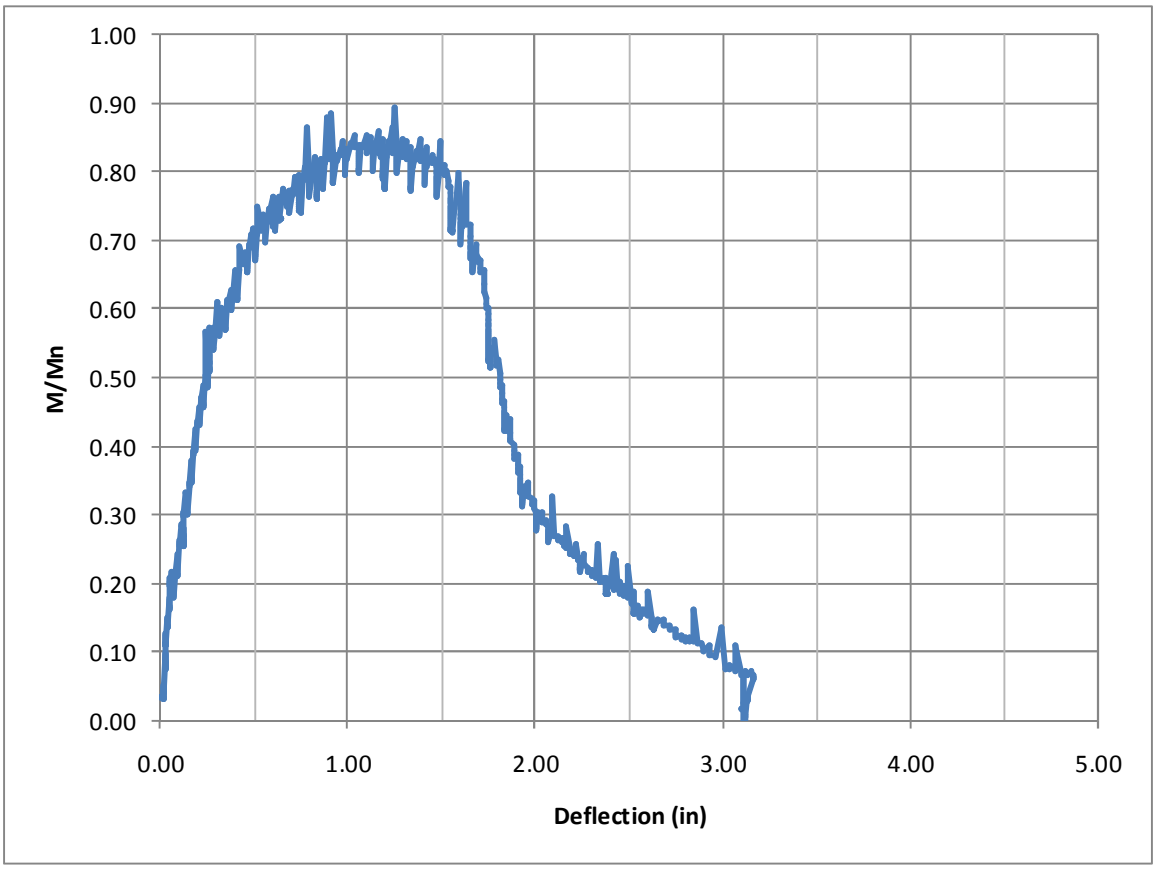

FIGURE 8-26: MOMENT VS. DEFLECTION FOR THE CENTER POT (POT 5) OF H2 (POSITIVE MOMENT)

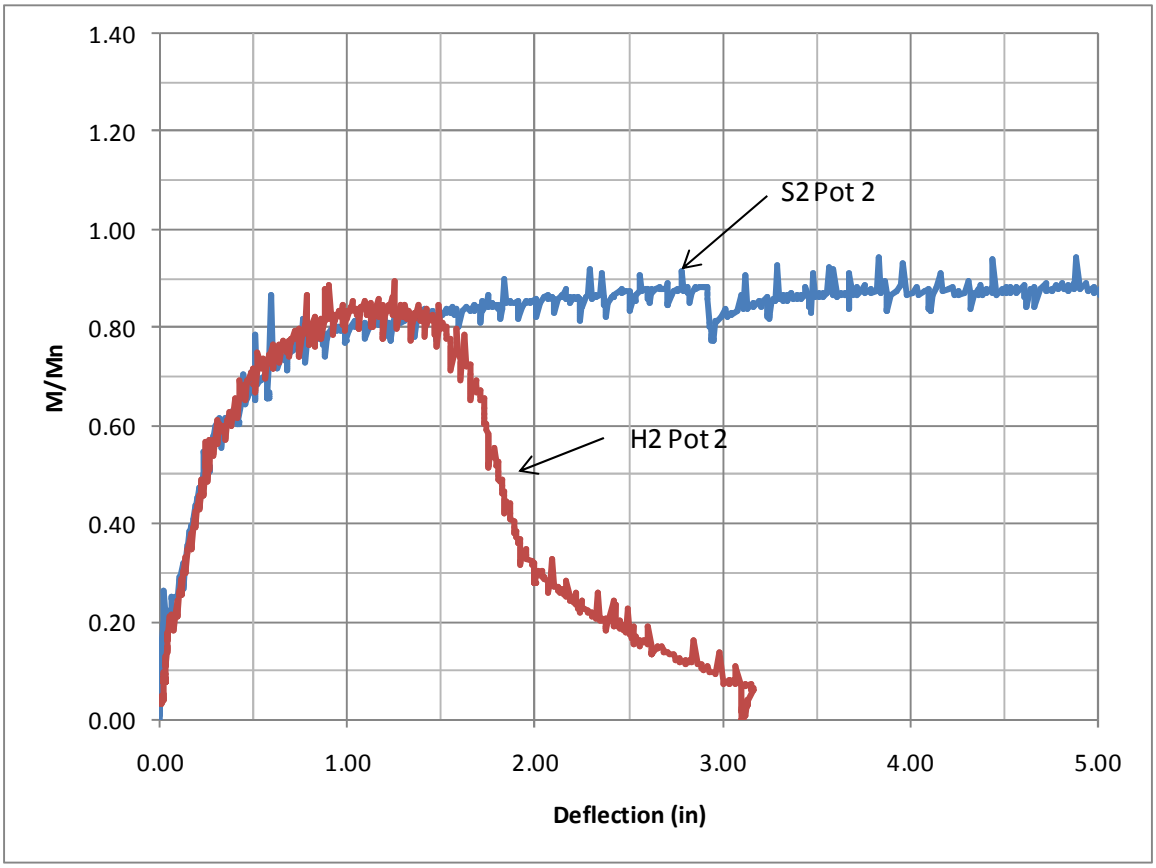

FIGURE 8-27: MOMENT VS. DEFLECTION FOR THE EDGE POT (POT 2) OF S2 & H2 (POSITIVE MOMENT)

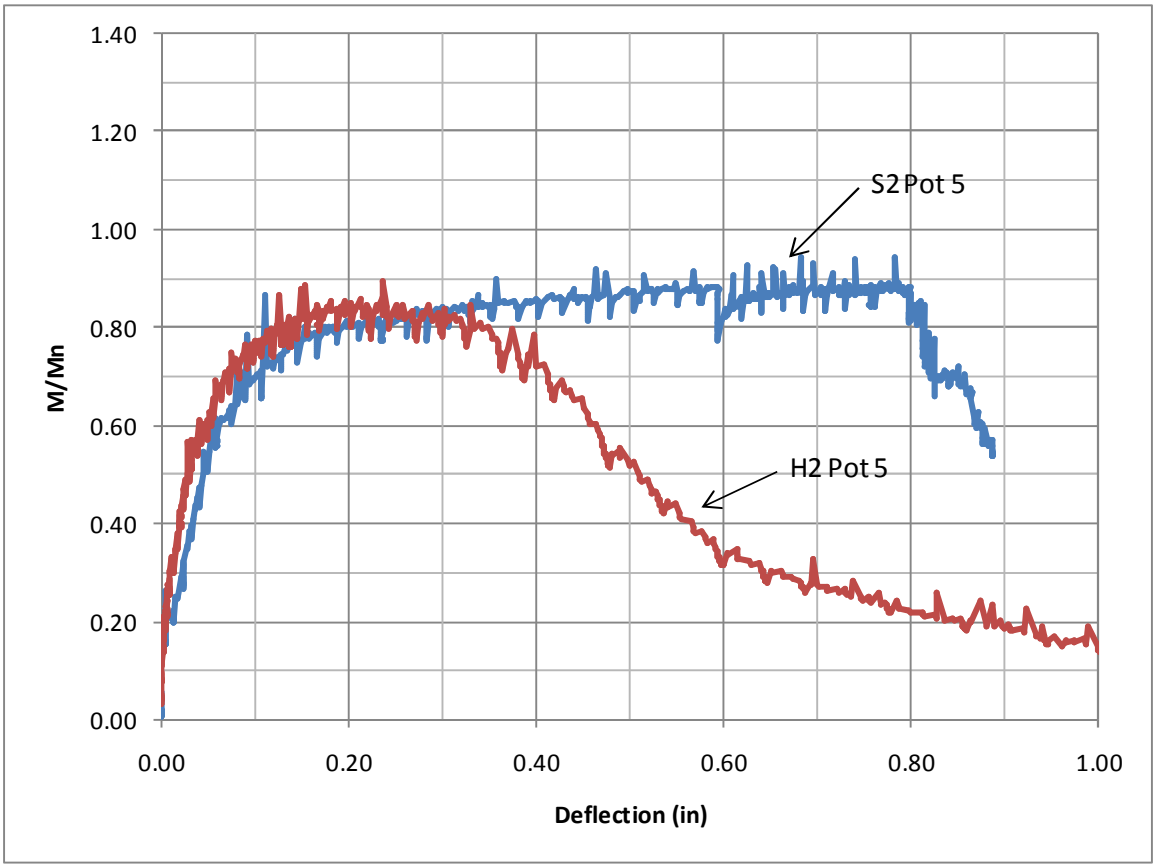

FIGURE 8-28: MOMENT VS. DEFLECTION FOR THE CENTER POT (POT 5) OF S2 & H2 (POSITIVE MOMENT)

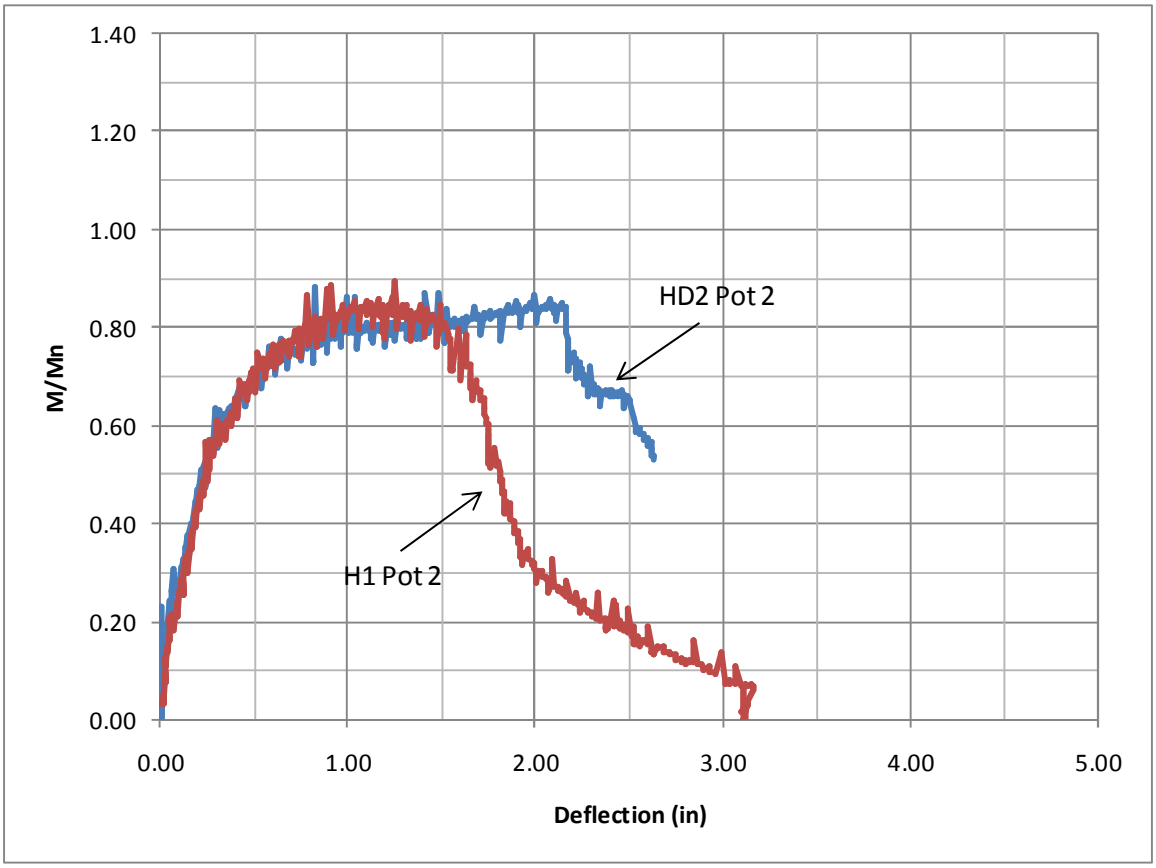

FIGURE 8-29: MOMENT VS. DEFLECTION FOR THE EDGE POT (POT 2) OF HD2 & H2 (POSITIVE MOMENT)

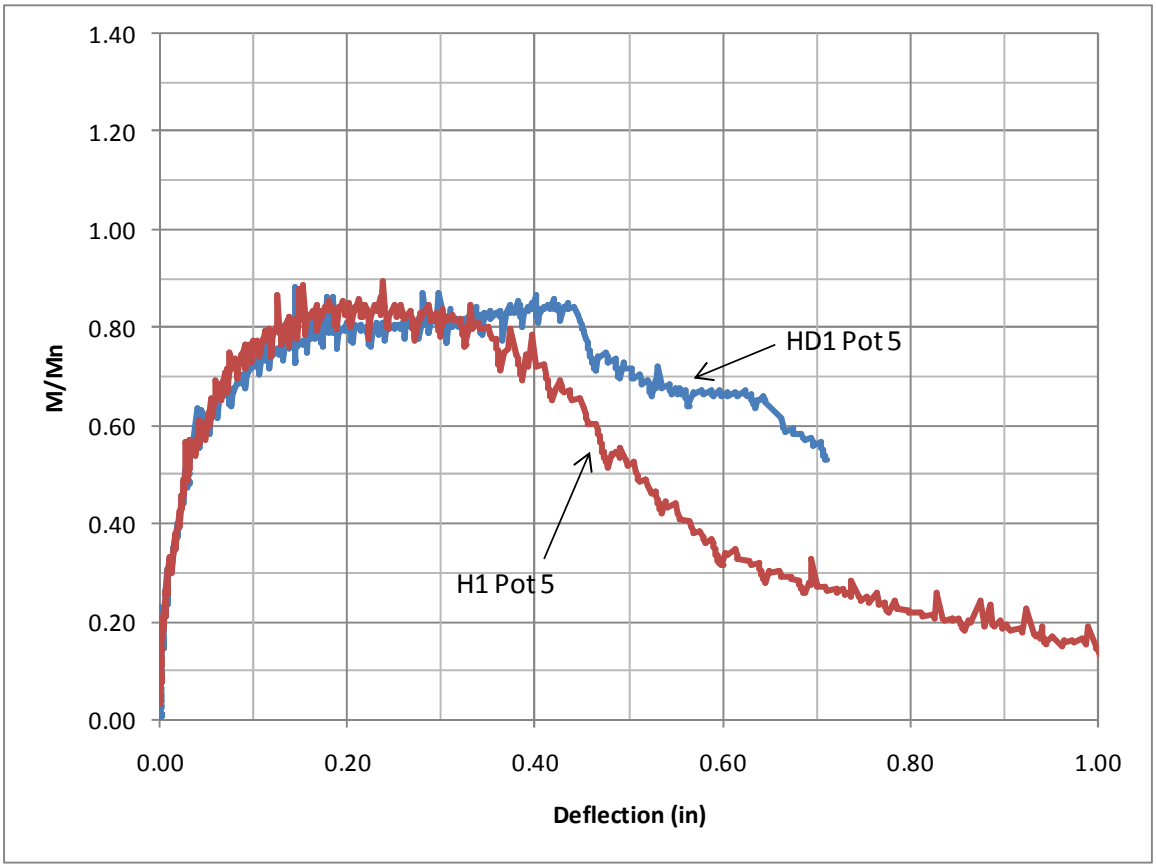

FIGURE 8-30: MOMENT VS. DEFLECTION FOR THE CENTER POT (POT 5) OF HD2 & H2 (POSITIVE MOMENT)

The comparison between HD2 and H2 show that H2 has a slightly higher moment carrying capacity with a lower stiffness resulting in larger deflection. The deflections seen in H2 occur after a considerable loss in moment carrying capcity.

The ultimate strength of the slabs was recorded and is shown in Table 8-2. The comparisons show that the greatest percent difference between any two specimens is 7%, corresponding to the difference between H1 & HD1. The difference between H2 & HD2 is only 0.25%. These values do not take into account the varying steel strengths as the figures above do.

Comparing the deflection at failure, the ductility of the specimens can vary as much as 2.5 inches. The differences in ductility are not an issue because all specimens reach an acceptable ductility for field application.

TABLE 8-2: ULTIMATE STRENGTH OF ALL SPECIMENS

	Ultimate Strength	
Specimen	**Positive**	**Negative**
Straight (S1, S2)	78,500 lbs.	44,600 lbs.
Headed (HD1, HD2)	78,800 lbs.	39,200 lbs.
Hooked (H1, H2)	73,400 lbs.	39,300 lbs.

8.5 Slab Cracks

During each of the tests cracks were mapped by tracing them on the slab. The mapping of the cracks was used to observe the order in which cracks formed. Once longitudinal cracks began forming mapping was ceased due to safety reasons. All remaining cracks were mapped upon the completion of testing.

8.5.1 Negative Moment Cracks

The following section provides test photos and explanations of the events during testing.

8.5.1.1 Specimen S1

Figure 8-31 shows the mapping of the cracks for S1. Cracks form on the East end of the specimen first and soon begin to develop symmetrically. The numbers next to each of the cracks correspond with the load stage at which they were mapped. Figure 8-31 e shows the crushing of the concrete near the support. Failure of S1 was due to concrete crushing near the supports. The final deflected shape of the slab may be seen in Figure 8-31 f. Partial de-lamination of the concrete topping occurred near mid-span. The crack

approximately 12” to the east of centerline followed the joint between slab and topping and connected with the crack traveling down the centerline of the slab, this can be seen in Figure 8-31 c.

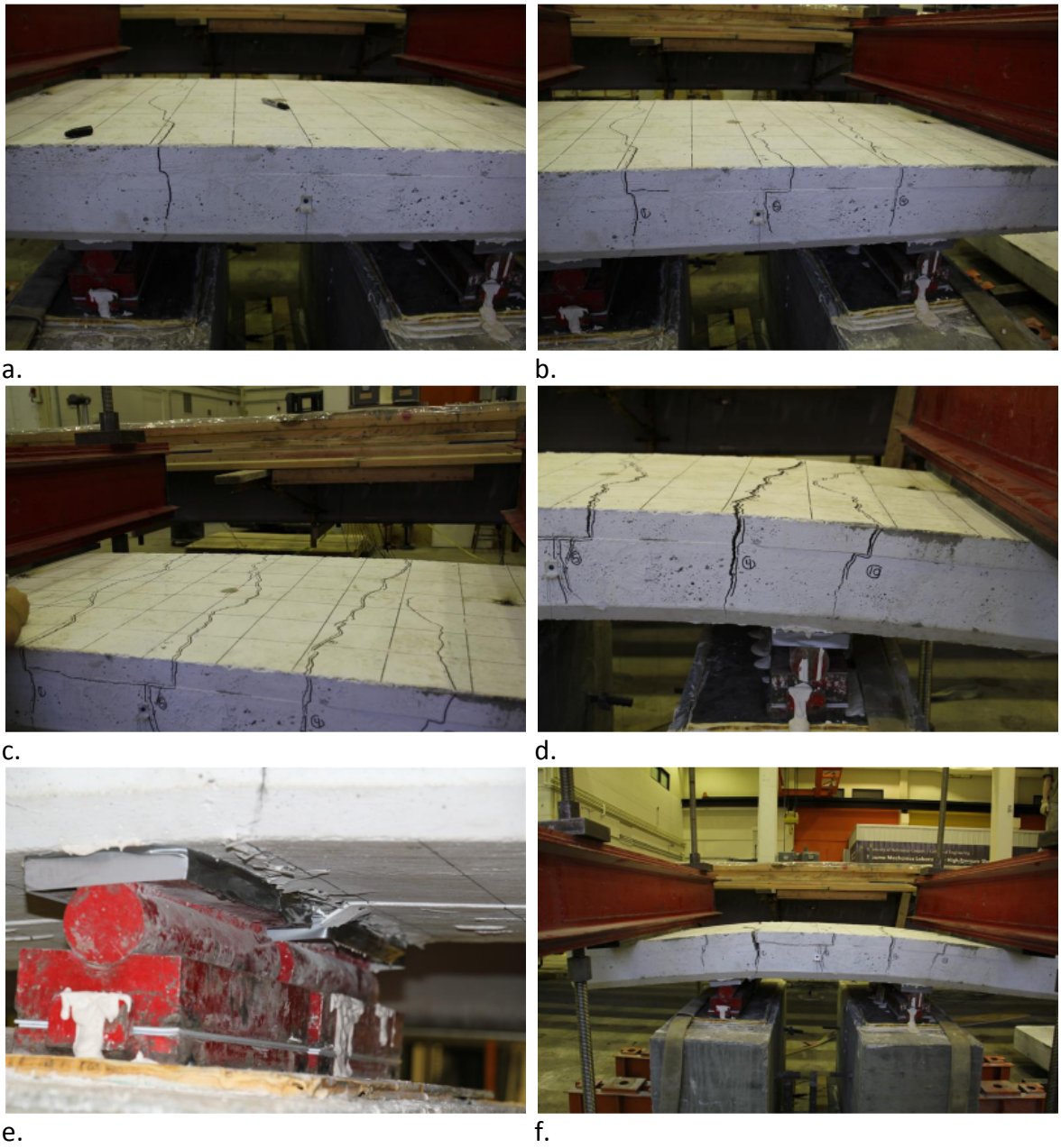

a. b. c. d. e. f.

FIGURE 8-31: TEST PHOTOS FROM SPECIMEN S1

8.5.1.2 SPECIMEN HD1

The second specimen tested, HD1, also began cracking approximately 12" East of the centerline. The rebar location is drawn in red in order to observe where the cracks are forming in relation to rebar location. The crack initiation in HD1 was symmetric as in S1. Cracks formed in close proximity to the cracks seen in S1. Figure 8-32 c shows the first longitudinal crack on this specimen. The longitudinal crack formed directly over one of the headed bars. This crack represents the lifting stress of the rebar on the slab. As load was increased the longitudinal cracks spread along each of the rebar towards the closure region. Concrete crush occurred approximately 6" to the inside of each of the supports, and controlled the ultimate behavior of the slabs. Figure 8-32 e & f show that the cracks on the West end of the specimen experienced more propagation than those on the East. The final crack width on the West was also much greater. This is due to the presence of 3 rebar and the increased deflections seen because of a reduced stiffness. The final cracked specimen is shown in Figure 8-32 f.

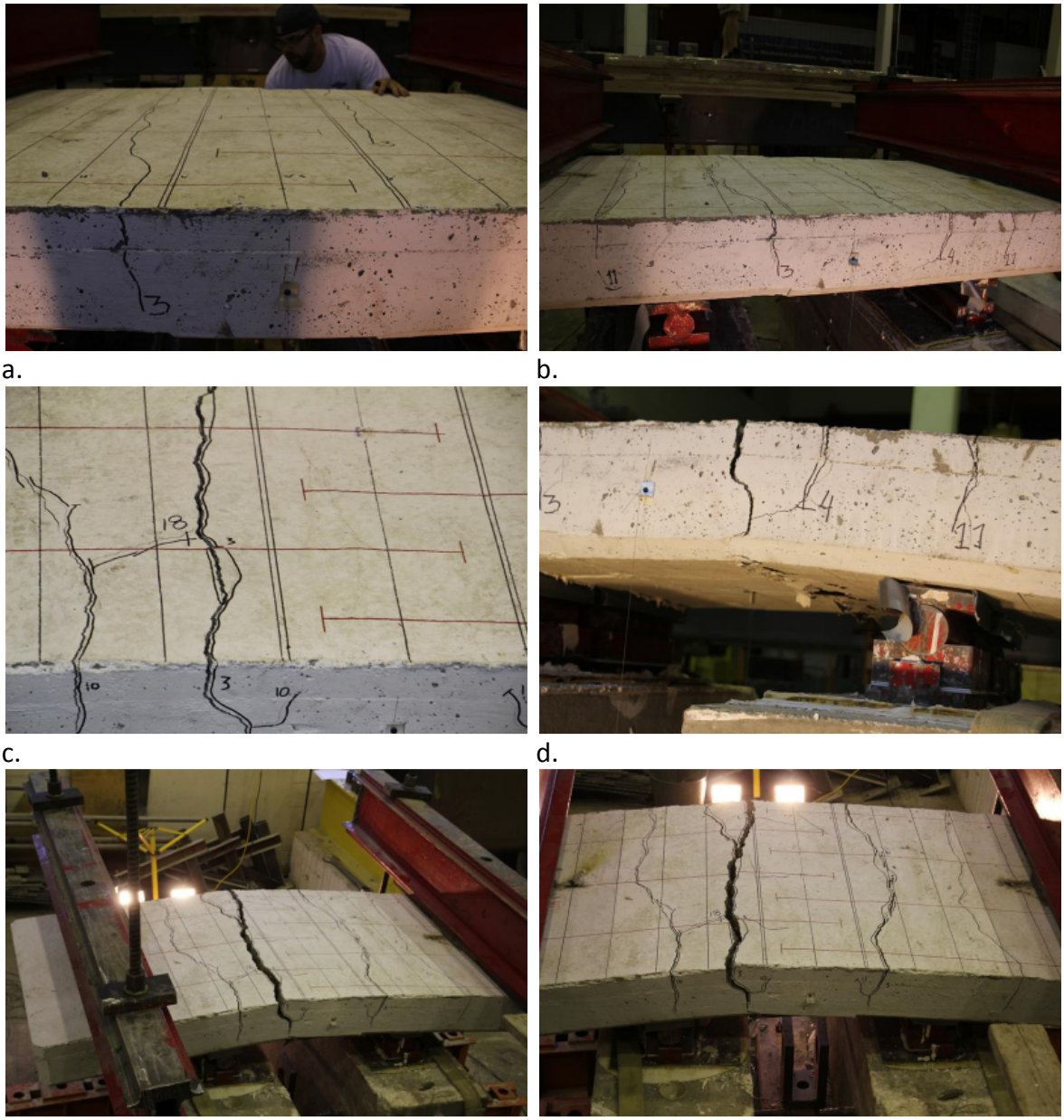

a. b. c. d. e. f.

FIGURE 8-32: TEST PHOTOS FROMSPECIMEN HD1

8.5.1.3 SPECIMEN H1

Specimen H1, the hooked bar, was the final specimen in this test series. Like the other two tests, H1 began cracking approximately 8-12" from the centerline of the slab. The cracks spread down the sides of the slab as load was increased. Longitudinal began forming and spreading towards the closure region of the test. The longitudinal cracks connected the crack 8" to the East of the centerline to a crack which formed along the closure region at 6" to the East of center. This caused a large portion of the overlay in that region to break completely loose. The large deflections causing larger cracks occurred on the side of the slab with 3 rebar as expected. Figure 8-33 e & f show the slab at ultimate load and after unladed respectively. In Figure 8-33 f the concrete which broke loose was removed in order to observe the condition beneath it. Once the concrete was top of the longitudinal bar could be seen, and separation of the concrete joint could be seen. Concrete crushing once again controlled the performance of the slab, the crushing can be seen in Figure 8-33 d.

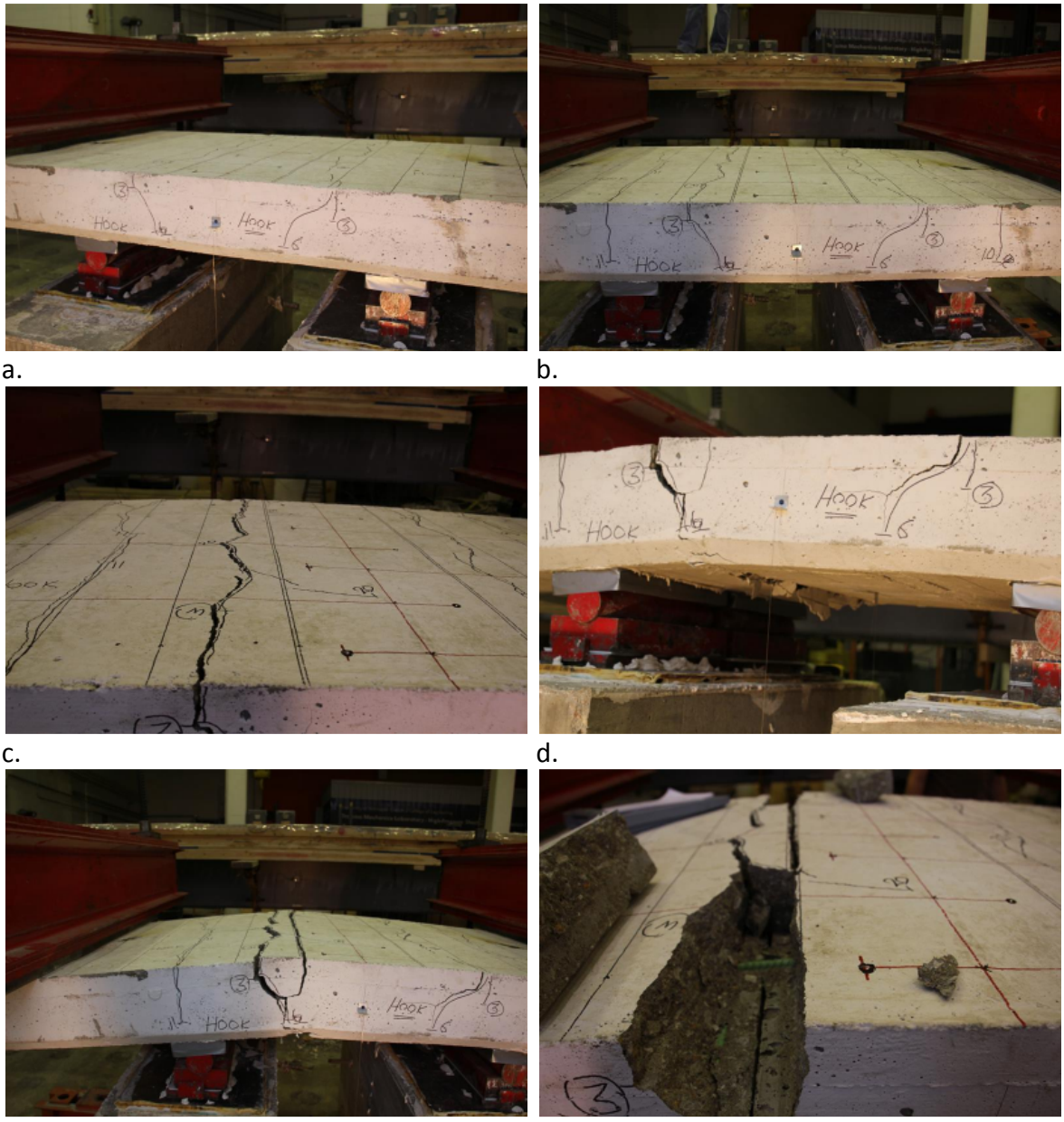

a. b.

c. d.

e. f.

FIGURE 8-33: TEST PHOTOS FROM SPECIMEN H1

8.5.1.4 Failure Comparison of Negative Moment Test Series

Once testing was completed for the first three specimens they were laid next to each other in order to observe the similarities in crack formation. As the figure below shows the largest cracks occur on the side with 3 rebar. All of these major cracks are 8-12" from the centerline of the specimen. The crack formation works its way out with the second set of cracks forming near 18" from centerline. With HD1 and H1 longitudinal cracks formed and spread towards the closure region along with a transverse crack down the centerline of the slab.

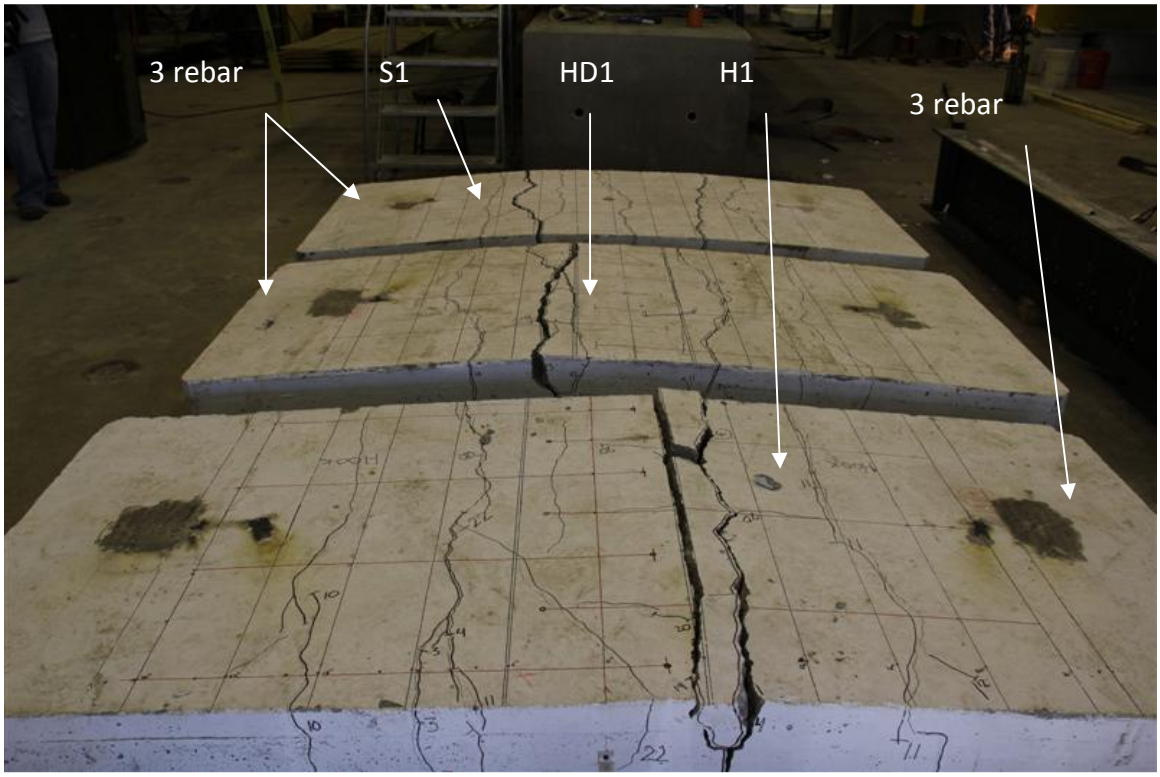

FIGURE 8-34: FINAL SLAB COMPARISON FOR NEGATIVE MOMENT

8.5.2 Positive Moment Cracks

The following section provides test photos and explanations of the events during testing.

8.5.2.1 Specimen S2

The first crack to form on S2 was directly down the centerline of the slab. As load increased cracks began forming further and further away from the centerline of the slab. The smaller cover on the positive moment specimens is resulting in more crack formation. The cracks begin forming on either side of the supports. Figure 8-35 d shows the cracks forming on either support. The cracks on the east support travel straight up the slab and join the transverse cracks, the cracks on the West side travel out towards the load point and connect with cracks near the load point. Longitudinal cracks formed and began breaking concrete loose. As in the previous tests, concrete crushed on the bottom face near the supports. At the final load stage large pieces of the slab had broken loose from both the tension and compression face of the slab. The straight bars caused the slab to deflect and fail in a symmetric manner.

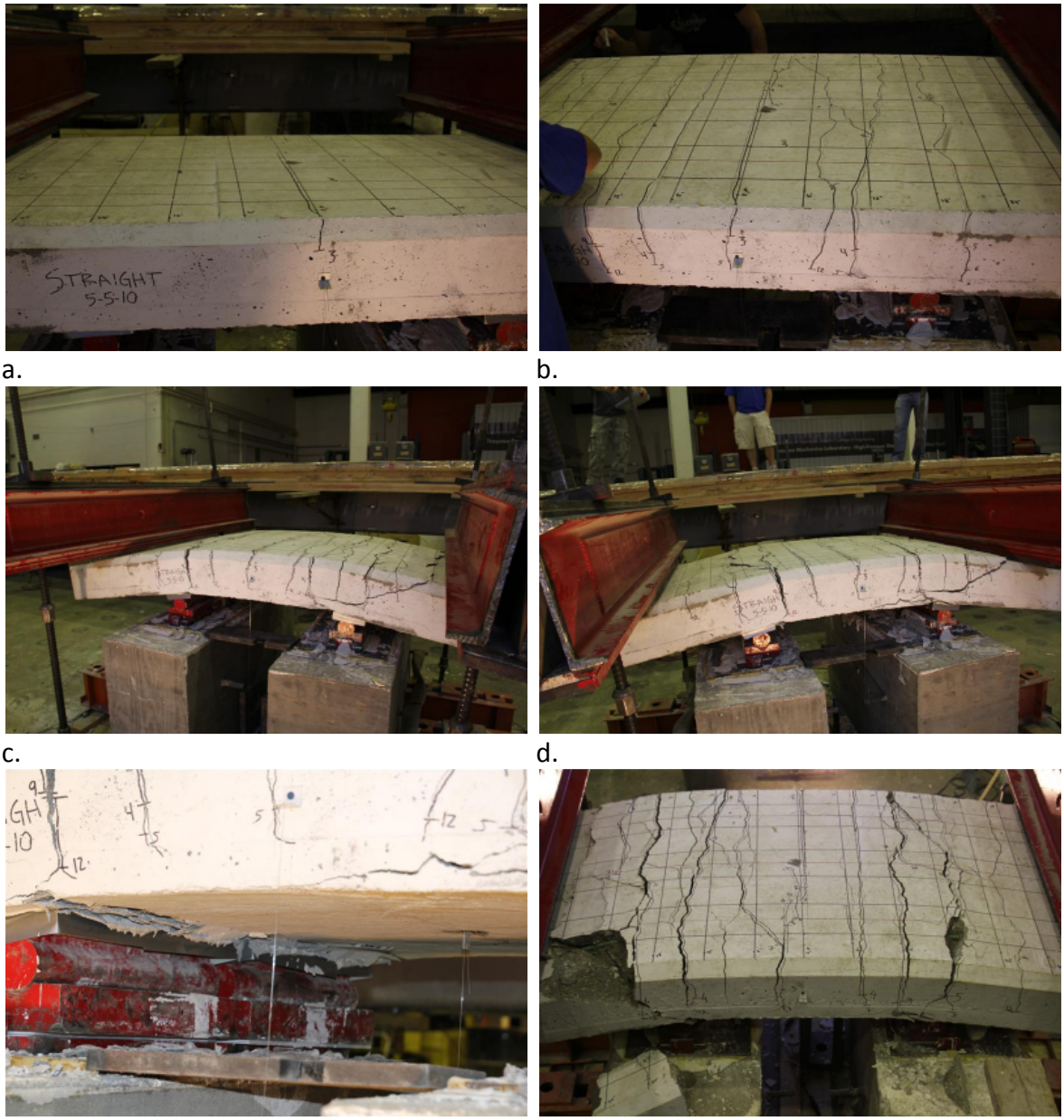

a. b.

c. d.

e. f.

FIGURE 8-35: TEST PHOTOS FROM SPECIMEN S2

8.5.2.2 SPECIMEN HD2

The first cracks for HD2 formed on either side of the closure region at the concrete joint. Cracks formed as they did in the other tests, moving outward as load increased. Cracks formed in the closure region starting at load stage 10 (47,100lbs), these cracks spread both transversely and longitudinally. Figure 8-36 c shows the initiation of the cracks in the closure region, and Figure 8-36 d show once the cracks have grown and begun to break apart the concrete. The sever breaking of the concrete on the surface made the top layer of rebar visible in some spots. Near the end of the tests a large piece of concrete fell from the north side of the test, this can be seen in Figure 8-36 e. Once the piece from the north side fell, the headed rebar was visible along with the broken apart concrete in the closure region. Concrete crushing and the tensile failure contributed to the failure of the headed rebar specimen.

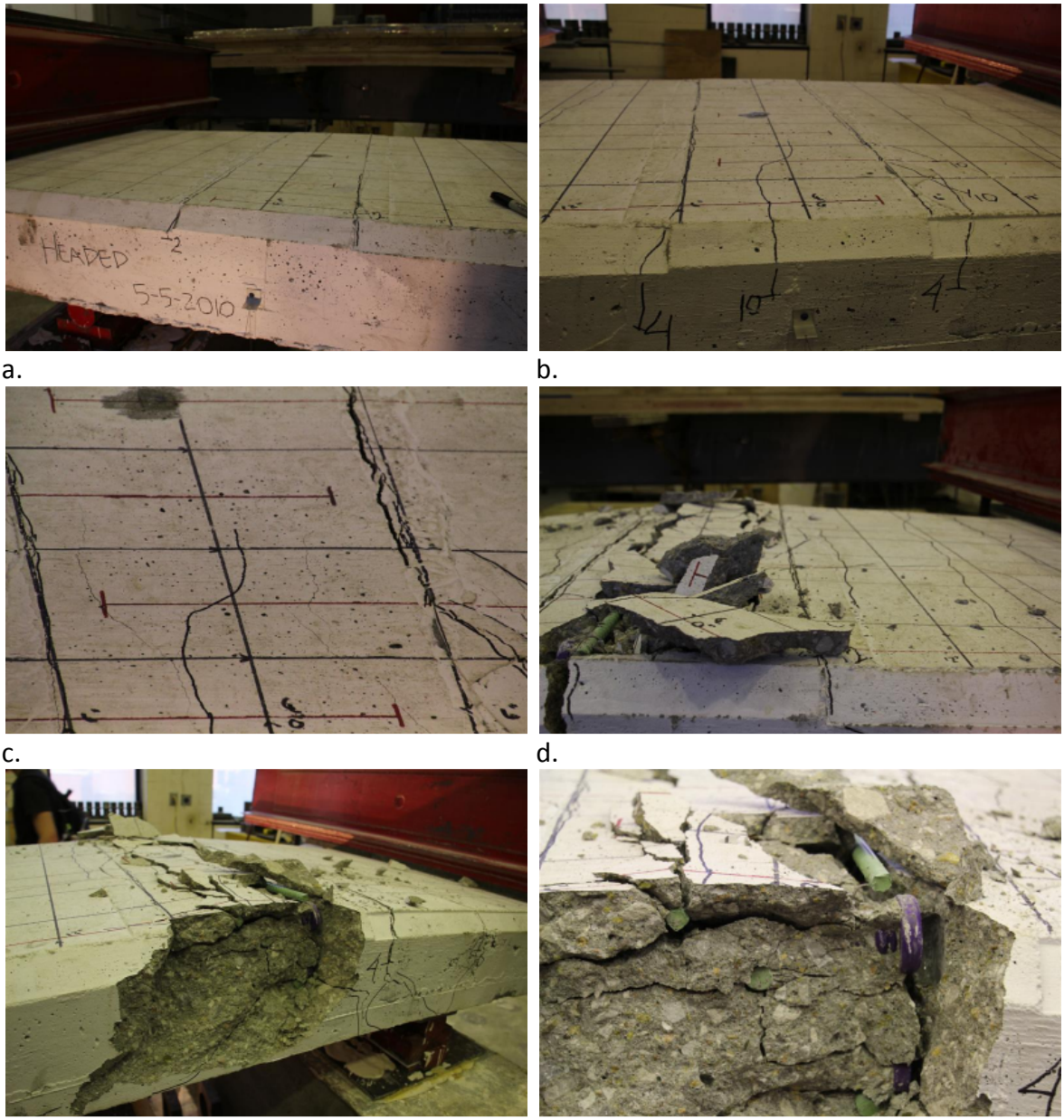

a. b. c. d. e. f.

FIGURE 8-36: TEST PHOTOS FROM SPECIMEN HD2

8.5.2.3 SPECIMEN H2

Specimen H2 began cracking just as HD2 did, with cracks along the closure region. As with all the other tests the second set of cracks were about 18" from the centerline of the slab. Starting with Figure 8-37 c the cracks can be seen spreading to the bottom of the slab and widening. The East side, containing 3 rebar, has a large crack which continues to grow wider. Figure 8-37 e shows the large crack on the east side along with the many transverse and longitudinal cracks in the closure region. The concrete breaks apart as load in increased just as it did with HD2. At the end of the test concrete had fallen off revealing the hooked bars at the north edge of the slab.

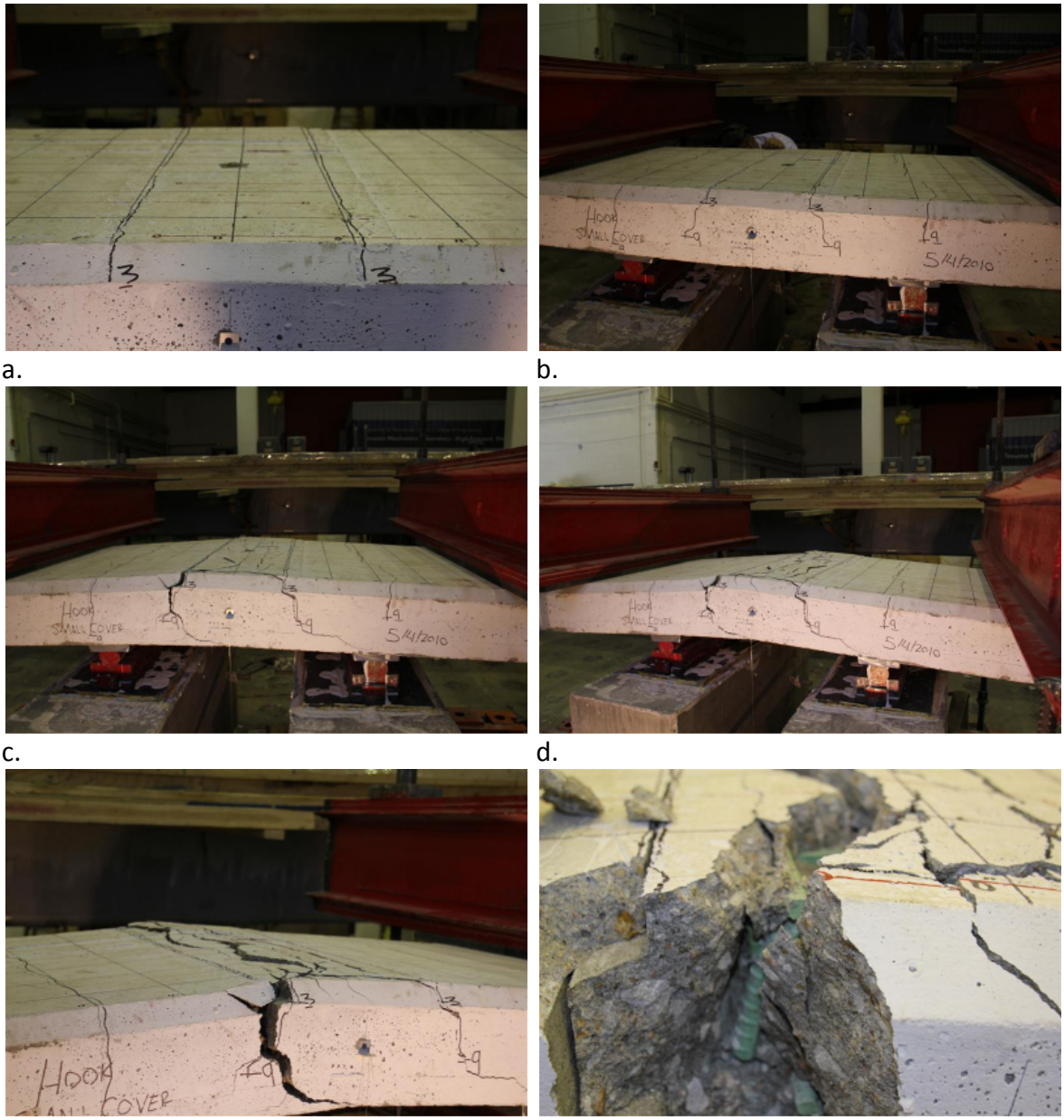

a. b.

c. d.

e. f.

FIGURE 8-37: TEST PHOTOS FROM SPECIMEN H2

8.5.2.4 Failure Comparison of Positive Moment Test Series

The slab comparisons show a small difference in the crack behavior between the 3. S2 cracked evenly across the width of the specimen with that largest crack being near the load point. HD2 and H2, containing the closure region, experienced the largest amount of cracking inside the closure region. The tension in the rebar in the closure region caused it to push against the concrete and break it apart. HD2 and H2 acted very similar, in that they both began cracking at the edge of the closure region followed by many transverse and longitudinal cracks connecting with one another in the closure.

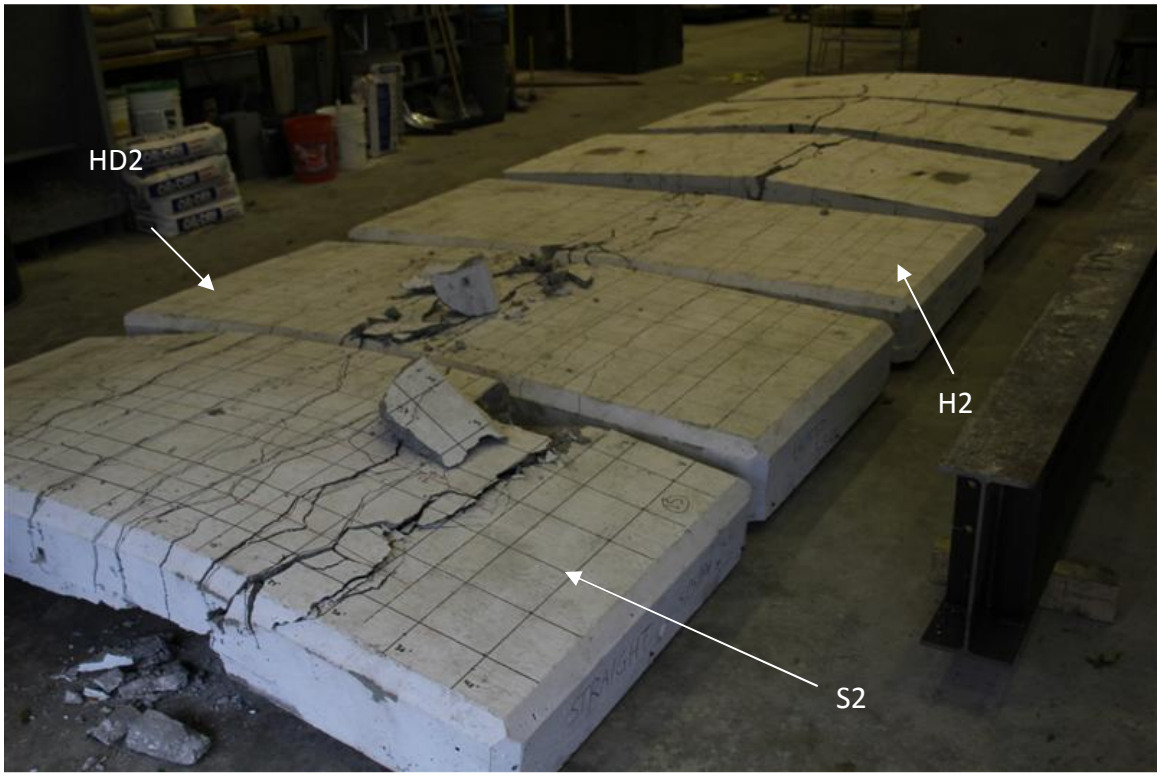

FIGURE 8-38: FINAL SLAB COMPARISON FOR POSITIVE MOMENT

9 CONCLUSIONS

The results from the FPG are part of an ongoing research project at the University of Nebraska which is developing the folded plate girder. Therefore the conclusion statements presented in this thesis are limited.

Based on the fatigue testing performed the following conclusions can be made about the FPG. The FPG can withstand the equivalent of 75 years of the physical maximum traffic without significant loss of stiffness. The strain distribution through the cross section of the girder does not change over the lifetime of the bridge. The bends in the steel, which contain residual stresses from the cold bending of the plate did not experience any changes in behavior throughout the test. After the equivalent of

219,000,000 cycles the FPG system showed no damage due to cyclic loading. The folded plate system provides a fatigue resistant system, which is both cost effective and provides ease of installation and implication.

The slab tests were used to in a comparative analysis between he headed bars and hooked bars. The headed bars provided sufficient strength and ductility when subjected to both positive and negative moment. The concrete failure mode provided an early warning of failure through concrete cracking and a drop in load. The small cover between the heads on the bar and the bottom face cause concrete failure in tension during loading. While the headed bars provide adequate strength and ductility, they cause issues with concrete cover. They are also difficult to obtain because of the specialized fabrication. The hooked bars also provided adequate strength and ductility for both positive and negative moment. The similar behavior of the hooked rebar to the headed rebar makes them both viable options for jointed slab construction. The hooked rebar provides a more cost effective option due to the fact that special considerations need not be taken for concrete cover. The hooked rebar requires no special fabrication, and may be obtained from local steel fabricators. The hooked bar detail has been shown to be a promising detail which provides a cost effective alternative to the higher strength headed bars previously used in adjacent slab joints.

10 REFERENCES

ACI Committee 318 (2008). Building Code Requirements for Structural Concrete Farmington Hills, MI: American Concrete Institute International.

AASHTO. (2007). *AASHTO LRFD Construction Manual,* 13th Ed., American Institute of Steel Construction,

AISC. *AISC LRFD Bridge Design Specifications,* 4th Ed., American Association of State Highway and Transportation Officials, Washington, D.C.

ASTM A 370-97 (1997). "Standard Test Methods and Definitions for Mechanical Testing of Steel Products." *1993 Annual Book of ASTM Standards,* Vol. 01.01, ASTM, Philadelphia, PA, pp. 164-182.

ASTM C 39-94 (1997). "Compressive Strength of Cylindrical Concrete Specimens." *1993 Annual Book of ASTM Standards,* Vol. 04.02, ASTM, Philadelphia, PA, pp. 17-21.

ASTM C 192-95 (1997). "Standard Practice for Making and Curing Concrete Test Specimens in the Laboratory." *1993 Annual Book of ASTM Standards,* Vol. 04.02, ASTM, Philadelphia, PA, pp. 111-117.

Lungui Li, Zhonggui Ma, Mary E. Griffey, Ralph G. Oesterle (2009) *Improved Longitudinal Joint Details in Decked Bulb Tees for Accelerated Bridge Construction: Concept Development,* Journal of Bridge Engineering August, 2009